Titre: Title:	MRI-Based Tumour Targeting Enhancement with Magnetotactic Bacterial Carriers
Auteur: Author:	Ouajdi Felfoul
Date:	2011
Type:	Mémoire ou thèse / Dissertation or Thesis
Référence: Citation:	Felfoul, O. (2011). MRI-Based Tumour Targeting Enhancement with Magnetotactic Bacterial Carriers [Ph.D. thesis, École Polytechnique de Montréal]. PolyPublie. https://publications.polymtl.ca/638/

URL de PolyPublie: PolyPublie URL:	https://publications.polymtl.ca/638/
Directeurs de recherche: Advisors:	Sylvain Martel
Programme: Program:	Génie biomédical

UNIVERSITÉ DE MONTRÉAL

MRI-BASED TUMOUR TARGETING ENHANCEMENT WITH MAGNETOTACTIC BACTERIAL CARRIERS

OUAJDI FELFOUL

INSTITUT DU GÉNIE BIOMÉDICAL

ÉCOLE POLYTECHNIQUE DE MONTRÉAL

THÈSE PRÉSENTÉE EN VUE DE L'OBTENTION

DU DIPLÔME DE PHILOSOPHAE DOCTOR (Ph. D.)

(GÉNIE BIOMÉDICAL)

JUILLET 2011

UNIVERSITÉ DE MONTRÉAL

ÉCOLE POLYTECHNIQUE DE MONTRÉAL

Cette thèse intitulée:

MRI-BASED TUMOUR TARGETING ENHANCEMENT WITH MAGNETOTACTIC BACTERIAL CARRIERS

présentée par: FELFOUL Ouajdi

en vue de l'obtention du diplôme de: Philosophae Doctor

a été dûment acceptée par le jury d'examen constitué de:

Mme CHERIET Farida, Ph.D., présidente

M. MARTEL Sylvain, Ph.D., membre et directeur de recherche

M. SYLVESTRE Michel, Ph.D., membre

M. FERREIRA Antoine, Ph.D., membre

ACKNOWLEDGMENT

The completion of this work has not been possible without the scientific, moral and human support that I received from several persons to whom I am very grateful. It remains certain that my supervisor, Professor Sylvain Martel, whose strategic vision and the human approach were able to help me to succeed. Professor Sylvain Martel, thank you for having opened the doors of your laboratory where I learned to do things differently and to try what others dare not explore.

I thank the jury: Prof. Cheriet, Prof. Ferreira, Prof. Sylvestre, and Prof. Henry for having agreed to evaluate this thesis. You honor me by evaluating this work. Please accept my respectful thanks.

A very special thought Dr. Mahmood Mohammadi, whose expertise was essential to the accomplishment of this work. With your magic fingers, we have undertaken great scientific discoveries.

I thank Dr. Louis Gaboury (UdeM), for the many tips in the analysis of histological sections, Micheline Fortin (UdeM), Julie Hinsinger (UdeM) and the team of histology (UdeM), for the preparation of tissue and interest in the project.

I thank Hakim Slimani, from the Institute Armand Frappier, and Hélène Ste-Croix, from MethylGene. Your support has enabled the implementation of in vivo tests that were a turning point in my work.

A very special tribute to the members of the laboratory Nanorobotics. It was a great pleasure to have attended over the years. Friendships were forged which I hope will last for years and years

to come. Neil Kaou, whose presence in the laboratory provides support, joy and organization. For Nasr, Dominic, Nisryn and Charles, for their friendship and continuous support.

I thank my family for their support during these long years of study and without which I would not be here today. To my family: mami and papi, Lahouma, Tata, Mahdouch, Halloula, Laysoun, Nanny, Nanna, Kimou, Mohsen Felfoul Junior, and Ammounatou you have been a continuous source of inspiration that has done much to help me get through requirements and the ups and downs of this thesis. Without you, I would probably have been discouraged by the difficulties associated with these academic activities.

The consecration of my studies and the culmination of many years dedicated to research coincided with the knowledge of the woman of my life, Besma that gived me a strong push at the end of the thesis.

This project is supported in part by a Canada Research Chair (CRC) in Micro/Nanosystem Development, Fabrication and Validation, the Canada Foundation for Innovation (CFI), the National Sciences and Engineering Research Council of Canada (NSERC), and the Fonds Québécois de Recherche sur la Nature et les Technologies (FQRNT). This work was also supported by US grant Number R21EB007506 from the National Institute Of Biomedical Imaging And Bioengineering. The content is solely the responsibility of the authors and does not necessarily represent the official views of the National Institute of Imaging And Bioengineering or the National Institutes of Health.

ABSTRACT

Magnetotactic Bacteria (MTB) are being explored as potential drug transporters to solid tumours. The MTB's active motility combined with magnetotaxism (their ability to swim following the direction of a magnetic field) offer new and potentially more accurate solutions in delivering drugs to tumours. In fact, the flagella bundles of the MC-1 bacteria (with an overall ideal cell diameter of approximately 50% the diameter of the tiniest human blood vessels) provide 4.0 to 4.7pN of thrust force for propulsion (roughly 10 times the value of many other well-known flagellated bacteria). Since there are no existing methods or technologies capable of inducing an equivalent force on a carrier of appropriate size for traveling inside a tumour's microvasculature, live microorganisms are considered as a viable option. Many of the parameters in a tumour microenvironment, such as malformed angiogenesis capillaries, heterogeneous blood flow, and high interstitial pressure, hinder the delivery of blood-borne drugs to the affected area. Active motility might prove to be helpful in bypassing these limitations and may facilitate the uniform distribution of the drug in the targeted area.

An MTB navigation technique that allows targeting without prior knowledge of the exact architecture of the vessels network has been developed. This navigation technique exploits both the ability of the MTB to swim following an imposed magnetic field and their random, continuous motion at low magnetic fields. Firstly, a focused magnetic field on the target sets the overall direction of the bacteria. Then, as the bacteria approach the targeted zone, the intensity of the magnetic field is decreased, which allows better bacteria repartition by exploiting their free motion. An additional approach that enhances MTB targeting relies on modulating the magnetic field direction in time, while keeping the magnetic field lines pointed toward the target. Navigation experiments in complex micro-channel networks highlight this process, where the successful targeting of bacteria is demonstrated when an appropriate magnetic field algorithm is applied, especially when it takes into account the nature of the channel network. Tridimensional control and navigation of MTB is also possible with the same technique through proper powering of the magnetic coils. In fact, by controlling their magnetic environment, it is possible to form a swarm of MTB, control its size and position within a given volume using a computer program.

MTB respond to magnetotaxis-based directional control since each cell contains internal structures known as magnetosomes. In the case of the MC-1 cells, these structures are composed of magnetite (Fe_3O_4) nanoparticles arranged in a chain that acts similarly to a magnetic nano-compass. The magnetosomes embedded in each MTB can be used to track the displacement of these bacteria using a Magnetic Resonance Imaging (MRI) system. These magnetosomes disturb the local magnetic field and affect the T_1 and T_2-relaxation times during MRI. Magnetic Resonance (MR) T_1- weighted and T_2-weighted images as well as T_2-relaxivity of MTB are studied in order to validate the possibility of monitoring MTB drug delivery operations using a clinical MR scanner. It is found that MC-1 MTB affect the T_2-relaxation much more than the T_1-relaxation rate and can be thought of as a negative contrast agent. The signal decay in the T_2-weighted images is found to change proportionally to the bacterial concentration. A minimum concentration of 2.2×10^7 cells/mL can be detected with a standard 1.5Tesla clinical MR system using a T_2-weigthed image. Furthermore, when the influence of the magnetosome's chain, the motility, and the bacterial cell of MC-1 MTB on the MRI contrast were studied, it was found that nanoparticles synthesized by MC-1 MTB were the predominant source of contrast in MRI.

In vivo studies, invastigating the ability of MC-1 MTB to reach the tumour, revealed the presence of these bacteria in the necrotic zone of solid tumours. The application of a magnetic field focused on the target, using a special magnetic system that was designed and built especially for these in vivo experiments, helped the accumulation of the bacteria in the tumour. In this paper we report on average, twice the number of bacteria found in the tumour when a magnetic field was applied using the 3D magnetic coils system over passive transport with the blood flow in the absence of any magnetic field. A second experience based on the comparison of tumours implanted in the same animal reported 10 times more bacteria in the targeted over the non-targeted tumour, which may suggest that the applied magnetic field may also be used to avoid a specific zone in the body.

RÉSUMÉ

Le cancer constitue la première cause de mortalité au Québec, avec 20,000 décès estimés par année. Parmi tous les patients atteints du cancer, une grande proportion pourrait profiter de l'avancement technologique en ce qui concerne le transport de médicaments. En effet, l'un des meilleurs moyens d'augmenter l'efficacité d'un médicament contre le cancer, tout en réduisant sa toxicité sur les cellules saines, est de le diriger vers la tumeur et de le maintenir à cet endroit jusqu'à ce qu'un effet thérapeutique se produise. Le transport ciblé de médicaments vers la tumeur peut considérablement améliorer l'efficacité thérapeutique, surtout si le transporteur est capable d'atteindre les zones nécrotiques et se répartir uniformément dans la zone à traiter. Les bactéries, de par leur motilité, sont d'excellents candidats pour une telle application, surtout qu'elles peuvent aussi être facilement fonctionnalisées. Ainsi, la recherche sur le traitement du cancer utilisant des bactéries s'est imposée comme une approche prometteuse surtout qu'elle pallie à une limitation majeure de la chimiothérapie et de la radiothérapie en permettant le traitement des zones anaérobies.

Alors que des laboratoires à travers le monde tentent de fabriquer des systèmes miniatures en se basant sur le modèle bactérien, nous avons opté pour l'utilisation des bactéries qui existent dans la nature. Notre stratégie a été de trouver un système biologique ayant les caractéristiques essentielles (e.x. diamètre total de moins de deux micromètres, force de poussée de plus de 4 pN, etc.) et de concentrer nos efforts à identifier une interface et une méthode permettant son contrôle pour des fins de ciblages thérapeutiques dans les lésions tumorales. Nous avons identifié les bactéries magnétotactiques de type MC-1 comme le meilleur transporteur potentiel de médicaments pour le ciblage du cancer.

Les MC-1 sont à la fois dirigeables par champs magnétiques et anaérobies, ce qui leur donne un grand avantage par rapport aux bactéries traditionnellement utilisées pour le ciblage du cancer. Le ciblage du cancer avec des bactéries exploite le plus souvent l'affinité des bactéries anaérobies à la région nécrotique faible en oxygène de la tumeur. Certes, ce ciblage manque de spécificité et un des problèmes le plus reconnu est la nécessité d'injecter une forte dose de bactéries pour assurer une croissance de celles-ci à l'intérieur de la tumeur. Ceci n'est pas le cas avec les MC-1 car elles sont à la fois anaérobies et magnétotactiques grâce à une chaîne de nanoparticules d'environ 70 nanomètres de diamètre, formant une sorte de « nano-boussole » magnétique à

l'intérieur de chaque bactérie, nous permettant de la diriger. Cette thèse étudie les différentes options de controle magnétique, et présente un système de contrôle magnétique programmable qui tient en compte d'une utilisation future chez les sujets humains.

De plus, la même chaîne de nanoparticules responsable du magnétotactisme, nano-cristaux d'oxyde de fer, constitue un agent de contraste en imagerie par résonance magnétique (IRM), qui est la modalité la plus efficace pour imager certains cancers tel que le cancer colorectal. Les MC-1, de par la taille de leur magnétosomes, engendrent une perte de cohérence du signal de résonance magnétique ce qui se traduit par une perte du signal sur l'image. L'étude des mécanismes de contrastes d'échantillons de MTBs révélent que les images en contraste T_2 (temps de relaxation transversal) sont beaucoup plus affectées que celles en contraste T_1 (temps de relaxation longitudinal) par la présence des MC-1. La quantité minimale qui peut être détectée avec un système standard d'IRM de 1.5Tesla est de 2.2×10^7 MC-1/mL utilisant un contraste T_2.

Nous avons aussi réalisé des expériences in vivo sur des souris porteuses de tumeurs afin de démontrer la capacité de transporter les MC-1 jusqu'à la tumeur. Les bactéries se sont retrouvées en grande quantité dans la partie nécrotique des tumeurs suite à une injection intraveineuse. L'application d'un champ magnétique focalisé sur la cible, en utilisant un système magnétique conçu et construit spécialement pour ces expériences in vivo, a permis d'accumuler les bactéries dans la tumeur. Dans cette thèse nous constatons, en moyenne, deux fois le nombre de bactéries quand un champ magnétique a été appliqué en utilisant un système de bobines 3D par rapport au transport passif avec le flux sanguin en l'absence de tout champ magnétique. Une deuxième expérience basée sur la comparaison de tumeurs implantées chez le même animal dévoile 10 fois plus de bactéries présentes dans la zone ciblée par rapport à celle non-ciblées, ce qui peut suggérer que le champ magnétique peut également être utilisé pour éviter une zone spécifique dans le corps, augmentant ainsi la specificité du traitement. Nous avons utilisé deux différents montages magnétiques pour le guidage des bactéries. Le premier montage, constitué principalement d'un électroaimant alimenté par une source de tension, est adéquat pour les tumeurs superficielles et accessibles. Le deuxième montage, constitué d'un ensemble de bobines tridimensionnel, permet un ciblage dans des sites profonds et inaccessibles permettant ainsi d'étendre l'application de l'utilisation des MC-1 pour le ciblage à plusieurs types de cancers dans le futur.

TABLE OF CONTENTS

LIST OF TABLES

LIST OF FIGURES

LIST OF ACRONYMS AND ABREVIATIONS

ABF	Artificial Bacterial Flagellum
COBALT	Combination Bacteriolytic Therapy
CPP	Cell Penetrating Peptide
FOV	Field of View
GRE	Gradient Echo
HCC	Hepatocellular Carcinoma
MNP	Magnetic Nanoparticles
MDT	Magnetic Drug Targeting
MMP	Magnetotactic Multicellular Prokaryote
MRI	Magnetic Resonance Imaging
MRP	Magnetic Resonance Propulsion
MTB	Magnetotactic bacteria
PBS	Phosphate Saline Buffer
PEI	Percutaneous Ethanol Injection
RF	Radiofrequency
SE	Spin Echo
SGC	Steering Gradient Coils
SMC	Steering Magnetic Coils
SPIO	Superparamagnetic Iron Oxides
TEM	Transmission Electron Microscopy
USPIO	Ultra-Small Superparamagnetic Iron Oxide

INTRODUCTION

Over the past two decades we have seen significant improvements in progression-free survival and reductions in morbidity for a number of cancer treatments, driven by the advent of biologically targeted therapies and more effective treatments. Many of these newer agents (e.g. Bevacizumab, Trastuzumab) actually sensitize tumours to the mainstay of anticancer therapy, cytotoxic chemotherapy. The latter is limited by significant acute and cumulative toxicities, such as myelosuppression and cardiac toxicity. While metastatic cancers most often require systemic therapy, there are specific contexts in which more effective localized therapy would have major impact on both quality of life and survival, including rectal and colorectal cancers, hepatocellular cancer, liver metastases from colorectal cancer and glioblastoma. **We propose to use MC-1 magnetotactic bacteria (MTB) as a drug delivery system for solid tumours.** MC-1 MTB use flagella for propulsion, while their swimming direction can be controlled by computer using an external directional magnetic field. This field induces a torque on a chain of nanoparticles that are naturally synthesized in the cell during cultivation. Like a compass needle, the swimming direction of the MTB is influenced through magnetotaxis. Furthermore, the MC-1 MTB spherical cells have a diameter of approximately 2μm, ideal for navigation in the smallest blood vessels, using an average swimming speed exceeding $200\mu m \cdot s^{-1}$. Although the final aim of this research is to treat cancer, the bacteria used are not drug-loaded yet and do not produce any therapeutic effect. We are developing the concept of guiding the bacteria to solid tumours, and we are confident that once the proof of concept is achieved, following research projects will transform the bacteria for a therapeutic effect to take place.

The research hypotheses were as follows:

Hypothesis 1: It is possible to control the motion of a MC-1 MTB swarm in a tridimenstional space under computer control.

Hypothesis 2: MC-1 MTB cause a significant magnetic resonance signal distortion making their targeting possible using clinical MRI systems.

Hypothesis 3: MC-1 MTB are able to reach the necrotic region of solid tumours.

We will address three main objectives in this thesis: **Objective 1: development of a programmable MC-1 MTB magnetic control system.** This system has to be designed for a human patient even though there are no planned human trials. **Objective 2: characterization of the contrast caused by the MC-1 MTB on magnetic resonance images.** The magnetic control system combined with the magnetic resonance imaging will form the future platform for MTB guidance. **Objective 3: assess and quantify the MC-1 distribution in tumour xenografts and evaluate the magnetic guidance advantage over passive targeting.**

Chapter 2 of this thesis studies the hydrodynamics of the MC-1 magnetotactic bacteria in high magnetic fields. It elaborates the influence of the magnetic torque on the overall motion of the bacteria and the consequences following application of a high magnetic field on a bacterial sample such the one found in MRI systems. Increasing the magnetic field leads to a decrease in speed of the MTB. During these observations, the magnetic field up to 1.27Tesla was used, which is quite similar to the one found in most MRI systems (1.5Tesla). Most importantly, MTB show a change in polarity when the field is released; for example, if a sample of 100% north-seeking bacteria is submitted to a 1 Tesla field, the MTB will be divided into 50% north seeking and 50% south seeking bacteria once the field is released. This observation greatly impacts the targeting method as we have suggested at the beginning of the project to use the MRI image as a feedback to correct the magnetic field used to control the bacteria. In fact, we can conclude that doing this will change the bacteria's behavior, which will have a negative impact on controllability during *in vivo* drug delivery applications. A mathematical model describing the interaction between the magnetosome chain and the magnetic field and how it affects motion is presented along with a an explanation on what causes the bacteria to change polarity when they hit an obstacle.

Chapter 3 covers the different MTB control techniques that are suitable for *in vivo* drug delivery applications. After several iterations, designs and much experimentation, we found that the coil structure providing the best results for MTB navigation was a mix of 3-axis Helmholtz coils and 3-axis Maxwell coils. The Maxwell configuration traps the MTB that follow the magnetic field lines in the center of the coils. Controlling the motion of the bacteria then becomes possible using the computer-controlled Helmholtz coils. The current flowing in the Helmholtz coils and the position of the zero fields generated from the Maxwell coils are linearly related.

In **chapter 4,** we characterize the swimming of MTB *in vitro* by mimicking different situations they could encounter in an *in vivo* environment. The goal was to be able to predict the MTB behavior in a complex microvasculature and to choose the correct magnetic field algorithm to optimize targeting. In fact, as the MTB follow the magnetic field, they could easily get stuck on obstacles, especially in very complex capillary networks such as the tumour angiogenesis. Consequently, changing the direction of the field is necessary to guide the bacteria. The problem is a lack of visual information on the route and obstacles that the bacteria face.

Since we lack this information, we must achieve blind control knowing only the starting position of the bacteria (the injection site) and their final destination (the center of the tumour). As a simple example to help understand the problem and the way we propose to solve it, we used a microchannel design consisting of multiple U-channel shapes. The bacteria were injected into two tanks connected to the network through a small capillary. The magnetic field was set to a target location. We measured the number of bacteria that reached the target as time passed.

We show in this paper that a magnetic field algorithm is very important in order to navigate the bacteria accurately and that it can be generalized to complex geometries. Taking into account the geometry of the channels, the bacteria's speeds and behavior for a given magnetic field, we can optimize targeting with the appropriate magnetic field. Modeling and simulation can play an important role in this case. In fact, using the typical architecture of angiogenesis found in scientific literature in addition to the characterization of bacteria when submitted to different environmental parameters, we can predict and engineer a magnetic field algorithm that would optimize targeting. The direction, intensity and duration of the magnetic field are the three parameters to consider for MTB guidance. Changing the direction of the magnetic field allows the MTB to bypass obstacles while modulation of its intensity will give more or less freedom to the MTB to deviate depending on oxygen or other physical entities.

The paper presented in **chapter 5** extends the usage of the magnetic control method presented in chapter 5 to a three-dimensional space and presents the required time multiplexing of coil powering in order to achieve bacterial swarm control in 3D. The notion of a magnetic monopole does not exist in nature and it is impossible to reproduce in laboratory. In fact, the magnetic field that converges in a two-dimensional space exits from the third dimension. We propose in this paper a method that allows us to retain a swarm of bacteria in a target location.

Chapter 6 presents the *in vivo* results of MTB delivered to a tumour xenograft implanted on a mouse. Two different magnetic setups were used for the delivery of MTB to the tumour following their intravenous injection. The first setup consists of an electromagnet placed as near as possible to the tumour, while the second involves the use of the tridimensional-coil system described in chapters 4 and 5. Since MTB have a life span of 30-45 minutes at body temperature, the duration of the experiment was set to 30 minutes during which the magnetic field was applied to the tumour. Following the experiment, the animal was euthanized and the tumour extracted for analysis. Histochemical staining allowed identification of the bacteria on the histology slide.

CHAPTER 1 LITERATURE REVIEW

This literature review is comprised of four parts. The first part covers the main cancer therapy methods as well as the major physiological barriers that drugs encounter on their way to targeted tissues. The goal of the first part of this review is to bring to the reader's attention the importance of developing a tool that deliver the active drug directly to tumours. The second part discusses methods of delivery, namely the magnetic drug targeting approach and the Magnetic Resonance Propulsion (MRP) method that was first proposed and developed by the NanoRobotics laboratory of the Ecole Polytechnique de Montreal. The third part covers the use of bacteria in cancer treatment and focuses on their application clinical applications. Finally, the last part of the review presents the MC-1 magnetotactic bacteria (MTB) and discusses particularities of the MTB that are accessible in the literature.

1.1 Cancer Therapy Approach

Cancer, as well as the therapy undergone following its diagnosis, is classified depending on where it develops in the body. For example, patients with colorectal cancer[1] will undergo integrated surgery and chemotherapy whereas in the case of patients with rectal cancer, additional radiation therapy is used. On the other hand, hepatocellular carcinoma[2] (HCC) requires resection, liver transplantation, and percutaneous ablation (percutaneous ethanol injection (PEI) and radiofrequency (RF)) that can only be used on 30-40% of the patients. Meanwhile, chemoembolization is the only alternative therapeutic strategy capable of improving survival for the majority of patients. Chemoembolization combines arterial administration of drugs with a form of arterial occlusion in the liver by an embolizing agent. Systemic therapies, which affect the entire body, are used for the treatment of almost all type of cancer.

---

[1] Colorectal cancer is the third most prevalent malignancy worldwide and the second leading cause of cancer death in Canada based on Canadian Cancer Statistics 2009.

[2] Liver cancer is a leading cause of cancer deaths worldwide based on The American Cancer Society.

1.1.1 Systemic therapies

The most common systemic therapies are radiotherapy, chemotherapy, immunotherapy, and gene therapy. **Radiotherapy** involves irradiation of the tumour by ionization radiation that damages the DNA of cancerous cells. It is used for patients who are not permissible for surgery, or as a complementary treatment. The source of radiation can be external or internal, which mainly depends on the affected organ. Image-guided radiotherapy accounts for the body motion, such as respiration and internal organs motion, through the use of advanced imaging modalities. The efficiency of radiotherapy is however hindered by the hypoxic nature of the center of solid tumours that poses a limitation since the cells in this region are 2 to 3 times more resistant to radiation than normal cells [1, 2]. This region of the tumour also decreases the efficacy of **Chemotherapy**, which relies on systemic blood circulation to transport drugs. Chemotherapy acts by killing rapidly dividing cells such cancerous ones, and as a matter of fact, quiescent cells, which are far from the vasculature, are hardly affected [3]. In order to reduce its side effects, the active agent is encapsulated inside particles that attach to certain proteins present on cancerous cells and are subsequently actively targeted at tumours [4]. Active targeting is not to be confused with direct delivery, which encompasses methods that physically transport the active agent to the tumour. **Immunotherapy** enhances the way the immune system deals with cancerous cells by inducing a response against the antigen they express [5]. It consists of injecting lymphocyte cells that are "trained" to recognize and destroy specific cancer cells. **Gene therapy** uses a vector, usually a virus, to transport and inject healthy human genes inside cancerous cells. The short circulation time of vectors as well as their toxicity, immune system responses, gene control and targeting issues all prevent successful medical application of this technique [6]. The success of the techniques mentioned above depends on the efficacy of the active agent in killing cancerous cells as well as the quantity that reaches the tumour. The injected dose is limited by the tolerance of the body since systemic therapies affect cancerous cells as well as healthy cells [7, 8]. Moreover, tumours induce many physiological barriers that hinder the drugs from reaching the target.

1.1.2 Physiological barriers

The systemic therapies described in the previous section rely on transporting particles, molecules or cells to the tumour. For the therapy to be successful, the active agent must reach the tumour in

sufficient quantity. First, the active agent has to reach the main blood vessels that lead to the tumour; second, it must extravagate in the interstitial space of the tumour, and then migrate so as to be in direct contact with the cancerous cells [9-15]. The heterogeneous blood flow of the tumour and the high interstitial pressure are the major obstacles that drugs need to surmount to reach the target [16-20].

1.1.2.1 Tumour blood supply and transvascular transportation in tumours

The rapid growth of the tumour generates a lack of oxygen and nutrients and triggers the creation of new blood vessels, which is known as angiogenesis [21, 22]. Blood vessels thus created are different from healthy ones, and are characterised by leakiness, ill formation, and inhomogeneities [23-25]. In fact, large pores exist in tumour blood vessels [26]. The pore size depends on the tumour itself as well as nearby organs [14, 15, 19, 20, 24], it can range from a nanometer, as is the case with human glioblastoma (HGL21) transplanted in the cranial windows of a mouse [27], to 2000nm for the mammary adenocarcinoma of a mouse (MCalV) transplanted into the dorsal skinfold chamber [28]. Moreover, tumour angiogenesis blood vessels have dead ends, ramifications and an irregular size [11, 12, 16-18]. Heterogeneities characterise transvascular transport in tumours, as shown experimentally in [15], where fluorescent liposomes that were injected in tumour-bearing mice accumulated in some regions of the tumours but not in others. These characteristic particularities of tumour blood supply dictate the way drug molecules reach the tumour cells. In addition, systemic therapies have different therapeutic effects depending on the perfusion of the tumour. In fact, there are four distinct regions where the treatment is perceived differently as depicted by Figure 1.1. The first region is a hypoxic necrotic one, the second is a semi-necrotic region, the third is a stabilized microcirculation region, and the fourth is an advancing front [10, 29].

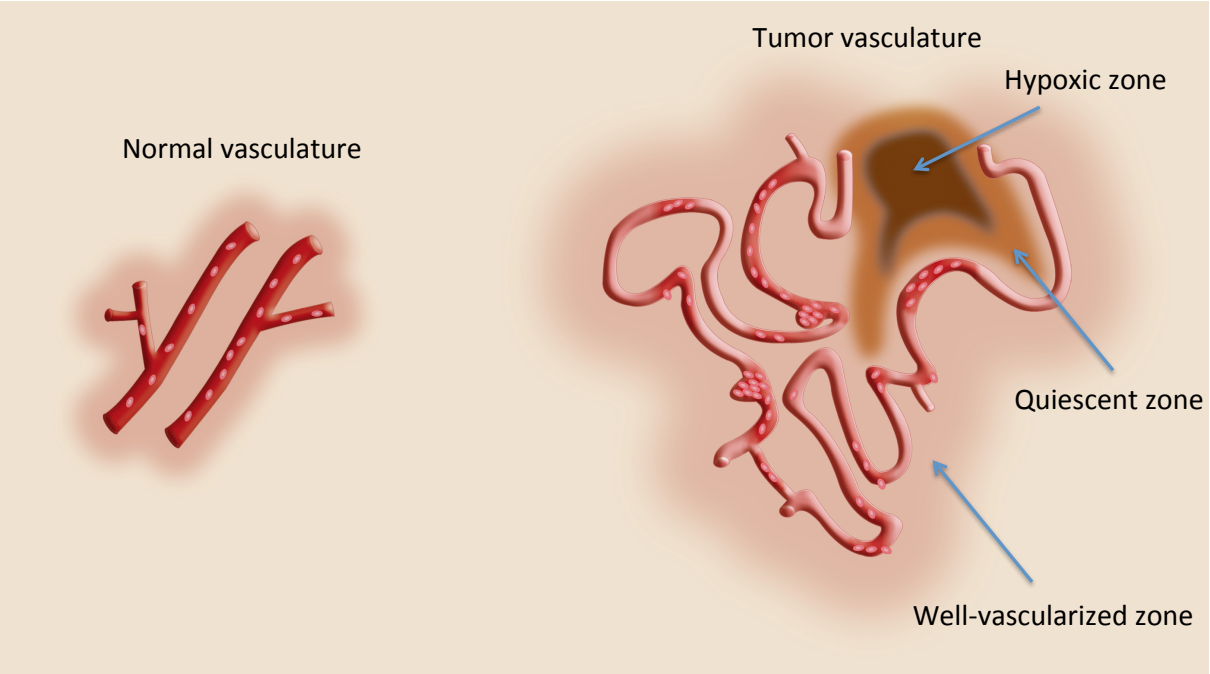

Figure 1.1. Differences between normal vasculature and one found in tumours. While normal vessels are regular and supply a homogenous blood flow to surrounding tissues, tumour angiogenesis blood vessels have dead ends, ramifications and an irregular size. Four distinct regions are noticeable where the treatment is perceived differently. The first region is a hypoxic necrotic one, the second is a semi-necrotic region, the third is a stabilized microcirculation region, and the fourth is an advancing front. Adapted from [30]

1.1.2.2 Interstitial transport in tumours

Molecules or particles that successfully cross the vascular wall will encounter a second major obstacle before reaching cancerous cells. Transport through interstitial space poses a real challenge for passive particles because of the high interstitial pressure inside the tumour and the lack of functional lymphatic vessels [31]. However, when the interstitial space of tumours is evaluated, it is found that it is much larger than those found in normal tissue [32, 33]. While this observation might suggest that transporting molecules and particles should be easier in tumour tissue than in normal tissue, experimental data shows the opposite. In fact, the interstitial hydrostatic pressure is high in the center of the tumour and low in the periphery. Therefore, interstitial fluid motion is expected to move from the center of the tumour to the periphery. Various studies show that 1-14% of plasma entering the tumour leaves through the periphery

[34]. The outward fluid velocity resulting from this leakage is estimated to be 0.1-0.2 μm/s at the periphery of 1 cm of tissue-isolated tumour [9]. Thus, particles or molecules must counter this fluid motion in order to reach the interior of the tumour.

Diffusion and convection govern passive transportation of molecules in the interstitial space. Furthermore, because of micro and macroscopic heterogeneities in tumours, the magnitude of these two parameters varies inside the same tumour and over time as well as from one tumour to another [35]. Active transport, such as the use of micro-engineered systems, magnetic particles steered by magnetic fields, or bacteria may enhance the transportation of drugs in transvascular and interstitial spaces, as will be discussed in the next section.

1.2 Direct drug delivery to tumours

Transportation of untethered microcarriers bearing therapeutic agents through the vascular network of a human body to a target requires an appropriate propulsion and steering system. The development of such propulsion and steering system can be a real technical challenge especially when the dimensions of these microcarriers must be reduced to a diameter of approximately 2μm to allow them to operate efficiently in the narrowest blood vessels of the microvasculature. An entirely synthetic approach that does not rely on an external source of induced propulsion force is beyond the limit of current technology. In fact, approaches that do rely on an external source for propulsion are still facing many technological challenges when designed to operate in the human microvascular networks. The major limitation consists of difficulties in miniaturising the power source that allows efficient autonomy of the microcarrier.

1.2.1 Synthetic systems

Flagellae and cilia, nanomotor-like mechanisms by which most microorganisms move, have inspired researchers in the design of modern engineering tools. Artificial Bacterial Flagellum (ABF) made from a helical tail, resembling a natural flagellum, and a soft-magnetic material head was fabricated in [36], based on a principle that was theoretically described in [37]. Under the action of an alternating magnetic field, the ABF was successful in reproducing the bacterial motion using a synthetic system [38, 39] as depicted by Figure 1.2. However, profiting from the existing flagella of microorganisms such as bacteria appeared more advantageous [40-44]. Successful on/off motion control of the bacteria by adjusting the chemical composition of their

medium was demonstrated in [45]. In addition, bacteria have shown to possess sufficient thrust force to move micro-objects from one location to another [46], and to build more complex structures under the conjoint action of a swarm of microorganisms [47].

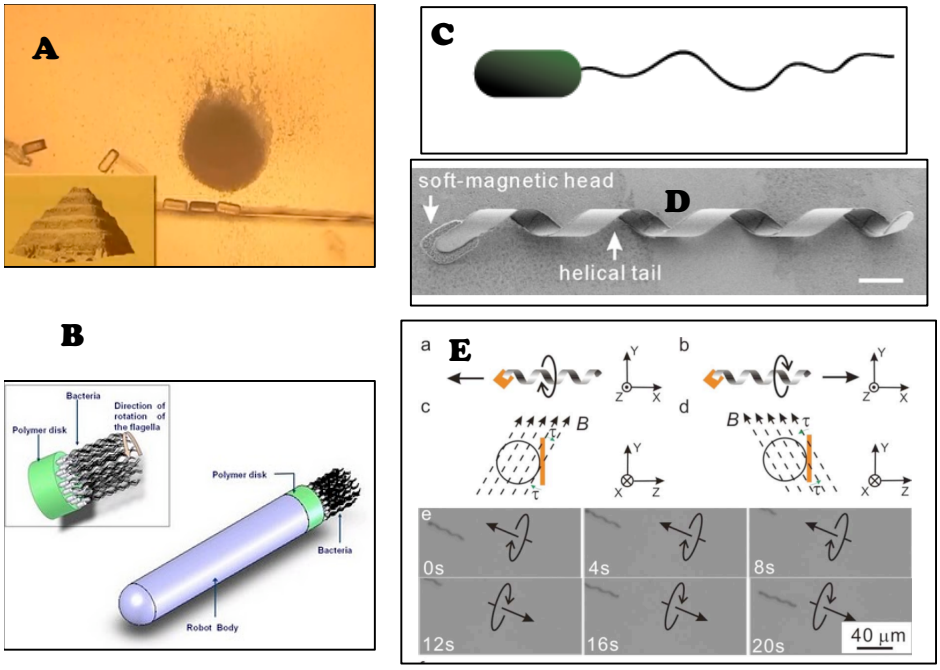

Figure 1.2. A computer controlled swarm of Magnetotactic bacteria was able to build a tiny pyramid made of SU-5 material blocks as depicted in A [47]. In B a scheme of a hybrid system made from synthetic material and propelled by the conjoint action of several bacteria attached to its end [42]. Scheme of a bacterium showing its body and an attached helical structure called flagella responsible of the bacterial motion through its spinning. The bacterial motion was reproduced by a synthetic system made from soft magnetic material head and a helical tail as shown in D [36]. Motion of this artificial flagella is granted through application of an alternating magnetic field generating a torque on the structure's magnetic head as depicted in E [36].

1.2.2 Magnetic drug targeting

Magnetic Drug Targeting (MDT) is a technique that magnetically concentrates drugs at the tumour site in order to reduce secondary toxicity effects that follow common therapies in cancer treatment [48-52]. Currently, MDT consists of loading drugs into magnetic particles that carry this complex in the vicinity of a tumour using an external applied magnetic gradient as described by the Figure 1.3. Moreover, lack of navigational control when combined with complex

microvascular networks near a tumour contributes further in lowering the efficacy of such targeting.

Present implementations for magnetic targeting of tumours rely on an external permanent or an electro-magnet located near and above the tumour. In this method, a catheter is typically used to release the magnetic nanoparticles as close as possible to the target. However, due to higher field intensity towards the external magnet [53], targeting is mostly restricted to superficial tumours near the skin. Because of higher magnetic gradient intensity towards the external magnet, targeting efficacy is higher for tumours located near the magnet and decreases substantially when the tumour is located deeper in the body.

Therefore, as the targets get deeper in the body, significant reduction of targeting efficacy is anticipated with this technique. Furthermore, this approach relies on trapping the particles without any further navigation or trajectory control over pre-planned pathways towards the tumour; thus, the distance between the nanoparticles releasing site and the tumour significantly affects targeting effectiveness. The dimensions and the technology of the available catheterization will always limit the efficacy of this technique to reach a desired site in the complex microvasculature. Deep organ targeting has been improved through the use of magnet tipped catheter, magnetic needles, wires or stents [48, 54-56], but still, the non-linear geometry of the induced field and the resulting distribution of the particles remain uncontrolled.

When tumours near the surface are considered, such as head, neck and skin carcinomas, experimental data showed complete remission of the tumour after one treatment using magnetic particles. This significant achievement lead to better efficacy with only one-fifth the medication that would otherwise conventionally be needed. Combining MDT with hyperthermia is yet another approach to enhance efficacy of a well-established tumour treatment. Involvement of big companies such Siemens provide a positive outlook for the clinical future of this technique.

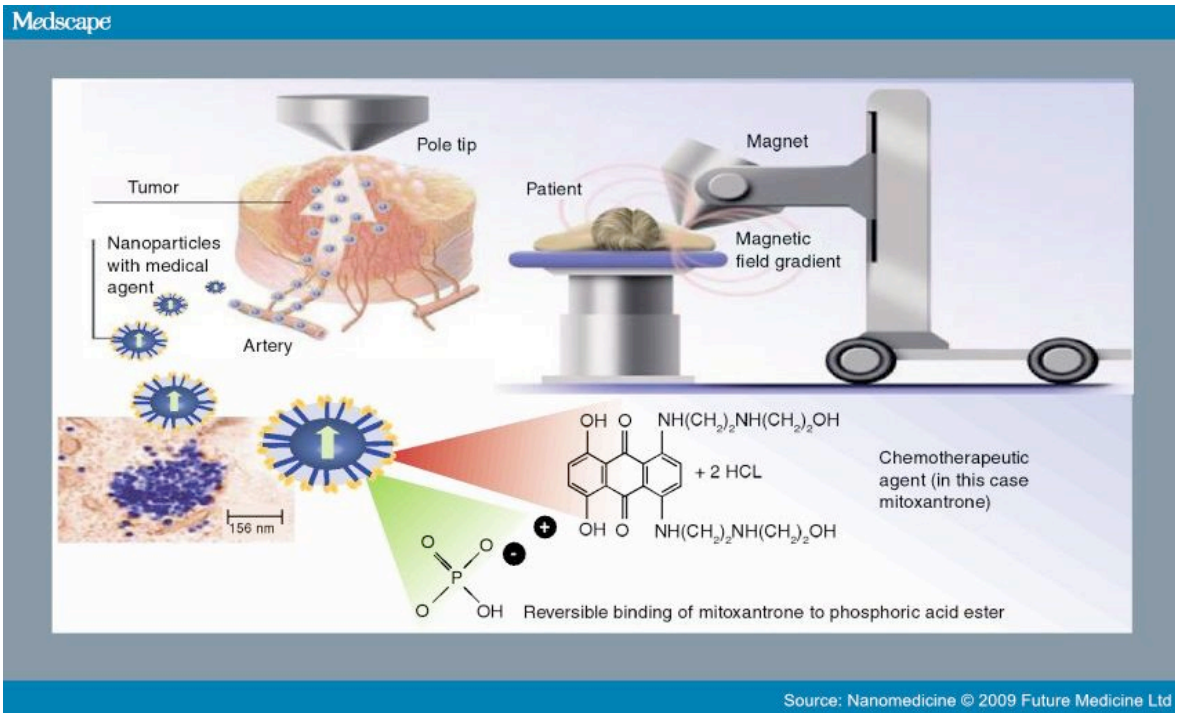

Figure 1.3. Principles of the magnetic drug targeting method. An active anticancer agent is encapsulated with a magnetic material forming a magnetoliposomes. Following an intravenous injection, retention of the magnetic particles that contain the drugs is achieved through the application of a strong magnetic field generated by an external source [57].

1.2.3 Magnetic Resonance Propulsion (MRP)

In order to improve targeting efficacy for tumours located deeper in the body, a new method has been proposed. This method relies on an induced propulsion force on magnetic materials (with sufficient magnetization saturation) generated by the three orthogonal coils used for image encoding in conventional clinical Magnetic Resonance Imaging (MRI) systems. [58-64] Using the tracking information provided by the imaging modality of the MRI, a closed-loop computer controlled displacement of a ferromagnetic bead along a pre-planned pathway in the vasculature of a living animal was demonstrated. The experiment was conducted in the carotid artery of a living swine and the results illustrated that this technology was able to adapt the navigation of magnetic microparticles through the microvasculature for future therapeutic applications beyond the limits of modern catheterization. This experiment also ensured that using MRI as an imaging modality would not only be advantageous for the purpose of tracking of the magnetic

microparticles, but also for real-time monitoring of therapeutic efficiency during such interventions [61].

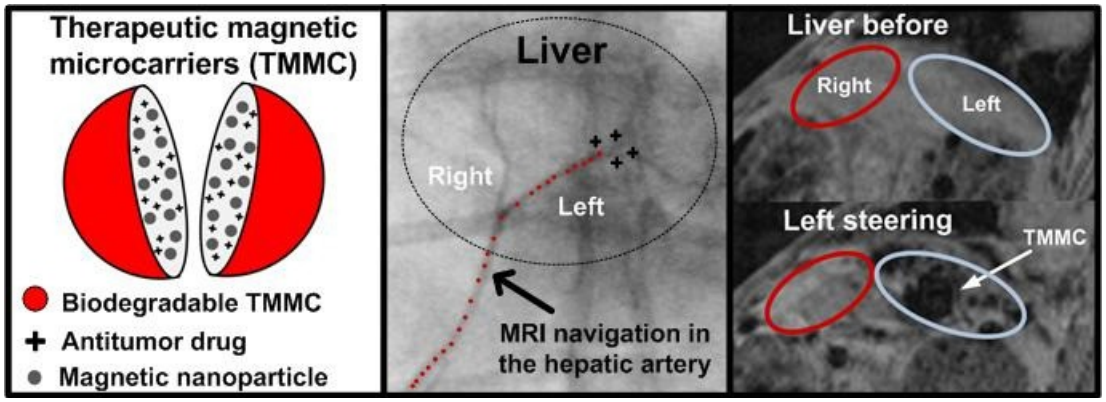

Figure 1.4. Successful MRI-based navigation, targeting, and controlled release of a cancer drug in a pre-defined lobe in the liver of a live rabbit [64].

Inducing sufficient force on nanoparticles would require magnetic gradients with amplitudes that are beyond today's technological advances when operating at the human scale. This is due in great part to the very small volume of the magnetic materials involved. Even if such high amplitude gradient field was achievable, there are physiological limitations to the gradient field amplitude that have previously been pointed out. One possible solution when operating in the microvasculature is to encapsulate such magnetic nanoparticles with therapeutic agents within polymeric microcarriers [64] as shown in Figure 1.4. With this approach, a higher effective volume of magnetic material can be achieved while retaining the advantages offered by the properties of magnetic nanoparticles for MR-target applications. However, tumour lesions are typically accessible by transiting through anarchic arteriocapillar networks stimulated by tumour angiogenesis. These capillaries are as small as 4-5µm in diameter. As such, this environment restricts the overall maximum diameter of each magnetic microcarrier for efficient navigation to approximately 2µm. Although at such a scale, the blood flow would typically be used for propulsion, sufficient magnetic gradient must still be generated to steer such microcarriers efficiently, especially at vessel bifurcations. Preliminary studies showed that additional gradient steering coils could provide maximum gradients sufficient for larger microcarriers used for target chemo-embolization but may prove to be insufficient for enhanced targeting inside a tumour.

One approach proposed by our group is to eliminate the need for such gradient coils when operating in the microvasculature and to replace it by the propulsion force provided by flagellated

bacteria. Since steering control is also required for target interventions, special types of cells referred to as Magnetotactic Bacteria (MTB) are considered by our group for such applications.

1.3 Bacterial cancer therapy

Bacteria that are present in the human body outnumber human cells by a factor of 10 to 1 [65]. Relying on complex mechanisms for their motion, sensory apparatus and communication, they play important roles in many aspects of the body's operation. Ever since a patient accidentally infected by bacteria recovered from cancer in 1891 [66], many researchers have focused on the use of bacteria as a potential treatment for cancer [6, 67-74]. The phenomenon by which the bacteria helped the patient to recover from cancer remains unknown, though many researchers believe that their ability to proliferate in the center of a solid tumour, and their production of toxins figure as key factors. Among the tremendous number of bacteria available in nature, the anaerobic ones (i.e. bacteria that live in the absence of oxygen) have been the primary consideration for most researchers that have tried to reproduce the accidental success witnessed by Dr. Coley [66, 73]. Figure 1.5 shows an example of an application for the bacterial cancer therapy.

1.3.1 Principle of bacterial therapy

Bacteria are believed to be more specific when targeting hypoxic regions of the body that are characteristic of solid tumours [68]. The commonly used bacteria belong to the *Clostridia*, *Salmonella* and *Bifidobacterium* strains [75]. They can be genetically modified to express a certain gene that can have an antitumour effect or supress certain genes to make the bacteria better tolerated by the body. The therapeutic effects come from the bacteria thriving from consuming necrotic cancerous tissue, or through products of bacterial activity such as endotoxins, which can be used for tumour destruction. Bacteria can also be used as delivery agents for anticancer drugs, and as vectors for gene therapy.

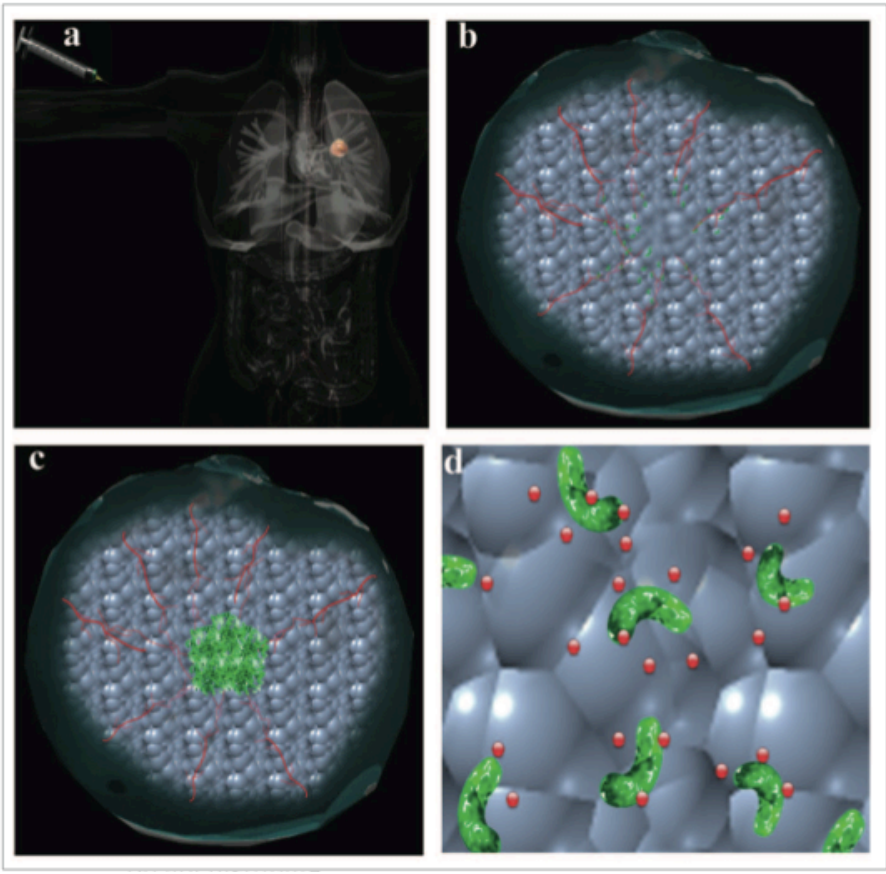

Figure 1.5. Anaerobe bacteria colonize the necrotic central regions of solid tumours following an intravenous injection. The bacteria can be engineered to produce toxins that cause the death of cancer cells once in a poorly vascularized zone [67].

1.3.2 Tumour-colonizing bacteria

It was found through animal model experiments that, following an intravenous injection, anaerobic bacteria found an appropriate environment for their proliferation in the hypoxic region of solid tumours as shown in an histology slide in Figure 1.6. The presence of pathogenic anaerobic clostridia species resulted even in tumour regression, but caused a severe toxicity, which resulted in either death or illness of the host animal [76, 77]. Non-pathogenic strains of *Clostridium* were also able to colonize the hypoxic zone of solid tumours, yet they did not cause tumour regression as the pathogenic strain did [78]. An attenuated strain, the C. novyi-NT, which was obtained after deleting gene coding for lethal toxin, caused tumour regression, but the

quantity that was necessary for a therapeutic effect to take place still produced toxicity. However, when the bacteria were administered in combination with chemotherapy, extensive hemorrhagic necrosis of the tumours resulted in significant and prolonged antitumour effects, which is best known as combination bacteriolytic therapy (COBALT) [69].

1.3.3 Combination bacteriolytic therapy (COBALT)

There are two main motivations behind the combination of bacteria therapy and existing treatment. Firstly, the bacteria are unable to consume living cancerous cells at the tumour. So, while the bacteria consume the tumour from the inside out, a chemotherapeutic agent would treat cancer cells in the well-perfused periphery that is accessible through the vasculature region. Therefore, combining both techniques could bypass major limitations in bacterial therapy and chemotherapy, which are the inability of chemotherapy to reach the necrotic zone and the inability of bacteria to proliferate in the wee-perfused tumour region. Furthermore, C. novyi has been tested to make the necrotic region of the tumour accessible to drug, or to enhance the release of liposome-encapsulated drugs [79]. *Salmonella typhimurium* was also investigated through the VNP20009 strain after deletion of two genes encoding endotoxins. Since the VNP20009 is a facultative anaerobe, it was successful in targeting small tumours that lacked a necrotic zone. Its specificity in growing in tumours was established through making its growth depending on an external source of purine, which is a compound that is available in tumours and not in organs such as liver or spleen. Not only has chemotherapy been combined with bacterial therapy, C. novyi has also been investigated in conjunction with radiotherapy in experimental tumour models [68, 80]. Phase I clinical trials in cancer patients has been conducted for the VNP20009 [81]. It has been demonstrated that the VNP20009 strain of Salmonella typhimurium can be safely administered to patients. At the highest tolerated dose, some tumour colonization was observed, yet no antitumour effects were seen.

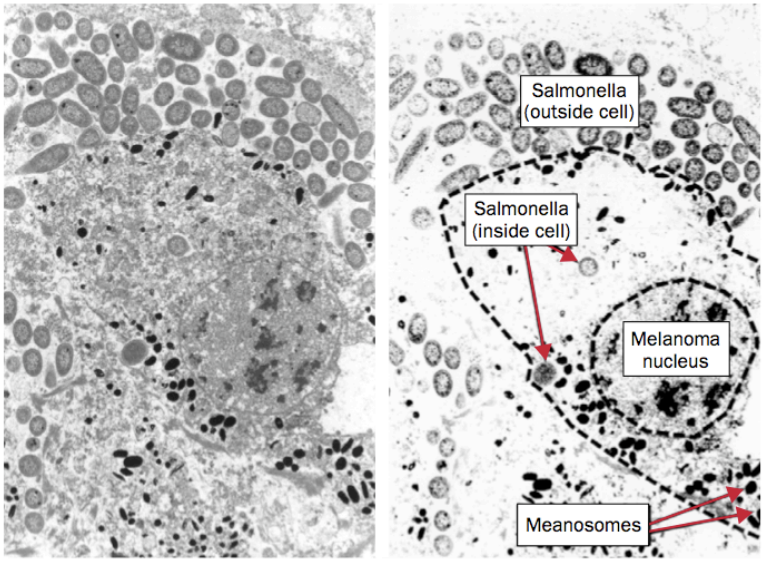

Figure 1.6. Histology slide showing the presence of Salmonella inside a solid tumour [74].

1.3.4 Problems associated with bacterial therapy

The risk of infection and the mitigated success have made many researchers concentrate their work on using the toxins produced by these bacteria rather than using live cells for treatment. Even though the preferential replication and accumulation of many bacteria in tumours was proven since then, bacteria cancer therapy faces many challenges before it becomes clinically effective. The first major limitation is the necessary high dose required to induce a significant therapeutic effect, which is most of the time associated to severe toxicities. The inefficiency of bacteria to target small tumours, where a hypoxic zone is not formed yet, constitutes the second major limitation. In addition, combining bacterial therapy with other conventional methods, such as chemotherapy or radiotherapy, is mandatory in most cases for complete tumour consumption.

These bacteria could reach tumoural lesions by means that are not compatible with electronic computer such as chemotaxis. Although there are efforts to control the motion of chemotaxis-based bacteria in an aqueous medium [45], the use of bacteria being influenced by magnetotaxis is more appropriate and efficient for computer-based navigation such as target interventions in microvasculature [82-84]. Furthermore, the use of MTB can not only enhance targeting through

flagellated propulsion and directional control from an external system, but can also be tracked for feedback control by MRI due to the chain of magnetosomes in the cell that causes a local field heterogeneity detectable by MRI.

1.4 Magnetotactic bacteria

1.4.1 General description

A photograph of a MC-1 MTB is depicted Figure 1.7. From an engineering point-of-view, this bacterium can be considered as a micro-robot possessing an efficient molecular motor, sensory and actuation capabilities as well as an embedded remote control interface. MC-1 is a cocci bacterium and measures approximately 2 micrometers (µm) in diameter. Each cell has two flagella providing a thrust force exceeding 4 picoNewtons (pN). This value is relatively high compared to other flagellated bacteria with a typical thrust force in the range of 0.3-0.5pN. This allows the MC-1 bacteria to swim in water at room temperature and without load at speeds often exceeding 200µm/s. This is a very high speed when we know that the swimming speeds of most flagellated bacteria in the same conditions are ~30µm/s.

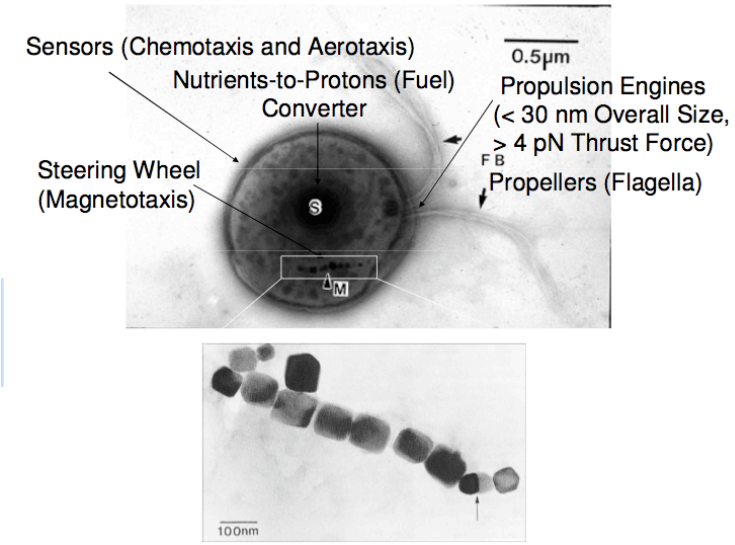

Figure 1.7. Electron scan microscopy images of MC-1 magnetotactic bacteria showing the round shaped cell with its internal organelle magnetosomes assembled into a chain. The MC-1 cells possess also two bundle sets of flagella. The magnetosome size range between 30-80nm [44].

Unlike most bacteria that base their motility and detection of nutrients on chemotaxis, the direction of displacement of MTB, although also influenced by chemotaxis and aerotaxis, is also influenced by magnetotaxis through their chain of magnetosomes, which are membrane-based nanoparticles of a magnetic iron [84]. When subjected to a magnetic field slightly higher than the earth's magnetic field of 0.5 Gauss, the directional motions of these MTB become mainly influenced by magnetotaxis and therefore fully controllable by electronics and computers [44, 46].

1.4.2 Choice of MTB

Although several types of MTB exist and can be found all over the world [85-88], the selection process for the type of MTB to be used as a drug delivery vehicle is still constrained since only a few types can be cultured in artificial or laboratory conditions. Most cultured strains belong to the genus Magnetospirillum (M.) and include species such as M. magnetotactium strain MS-1 [89], M. magneticum strain AMB-1 [87], M. gryphiswaldense [85]; the marine vibrios strains MV-1 and MV-2 [88]; a marine coccus, strain MC-1 [46]; a marine spirillum strain MMS-1 (formerly MV-4) [86]; and sulfate-reducing rod-shaped MTB known as Defulfovibrio magneticus strain RS-1 [88].

Table 1.1. Summary characteristics of some MTB

MTB NAME	CELL MORPHOLOGY	Mean Speed ($\mu m \cdot s^{-1}$)	WIDTH (OR DIAMETER) (μm)	LENGTH (μm)
MC-1 [44]	Coccoid	200	2	-
Magnetospirillum gryphiswaldense [85]	Helical	50	0.2–0.7	1-20
AMB-1 [86]	Helical	49	0.5	3-10
MV-1 and MV-2 [87]	Vibroid to Helical	- *	0.2–0.5	1-5
MMP (Many celled Magnetotactic bacteria)[87]	Sphere (a cluster of 10-30 Coccoid cells)	105	3-12	-
Magnetobacterium bavaricum [87]	Rod-shaped	40	1–1.5	6–9
RS-1[87]	Helical to Rod-shaped	- *	0.9–1.5	3-5
Magnetospirillum magnetotacticum (MMS–1) [88]	Spirillum	40	0.5	5

* - Missng data

For drug delivery applications, higher swimming speeds typically become one of the key factors for selecting the right MTB. In general, the magnetotactic spirilla are at the slower end (<100μm/s) while the magnetotactic cocci are at the faster end at >100μm/s. As such, the MC-1 strain seems to be a good choice and has been selected in this particular study. If the size of the MTB is an important aspect to consider, the MV-4 bacterium is the smallest with a length of ~0.5μm compared to ~2μm for the MC-1, but the choice for a smaller cell is done at the cost of slower swimming speeds (range of ~30-80μm/s). Both previous types have two bundles of flagella on one side of the cell and they are classified as polar MTB. Polar MTB swim persistently in one direction along the magnetic field. Polar MTB unlike axial MTB are generally more suitable for drug delivery applications since they are usually more predictable when controlling their swimming directions. For instance, some cells have two bundles of flagella on both ends. These MTB swim in both north and south directions with unpredictable reversals. Generally, the proportion of polar bacteria swimming in each direction is same, while for MC-1 cells the proportion is 80%-20%.

CHAPTER 2 DYNAMICS OF MC-1 MAGNETOTACTIC BACTERIA AT HIGH MAGNETIC FIELDS

2.1 Introduction

Applications involving Magnetotactic bacteria are continually increasing since their discovery by Blackmore in 1975 [82]. Besides being the simplest microorganisms known that uses the Earth's magnetic field for guidance, their swimming direction can be controlled through computer interface using magnetic coils or magnets [46]. The direction of movement of the bacteria is controlled by applying magnetic fields that influence the orientation of a chain of nano-scale organelles named magnetosomes. From systems on chips [90], to magnetic resonance contrast agents [91], MTB are being integrated in many engineering applications and even investigated as a drug-targeting vehicle for cancer treatment [43, 44, 60].

Few studies focus on the dynamics of MTB at high magnetic fields. The motion of MTB has been studied mostly at relatively low fields, more specifically around the Earth's 0.5 Gauss magnetic field. With the emergence of new applications, such as those involving magnetic resonance imaging systems, the MTB are subjected to extremely high fields, equalling 30,000 times the Earth's field. The dynamics of MTB at high magnetic fields differs from that at low fields. We expect these differences to be caused by the physical interaction of the magnetosome chain with the external magnetic field.

Similar phenomena involving other strains of MTB are reported in the literature, which may be caused by the same physical principles than those reported in this paper. The increase in the pitch angle of MTB helical motion at high magnetic fields has been observed with uncultivated magnetotactic enriched coccus from Lake Miyun near Beijing, China [92]. However, the magnetic fields used in [92] to study the helical motion, range from 1 to 15 Gauss while the ones used in this paper range from 0 to 600 Gauss. Furthermore, excursions opposite to the magnetic field direction after collision with the edge of the water droplet have been observed with a Magnetotactic Multicellular Prokaryote (MMP) [93]. Further studies [94] suggested that this "ping-pong" motion might result from the magnetoreceptive capability of the MMP since it could not be explained by conventional magnetotaxis. MC-1 also exhibits excursions in the direction opposite to a high magnetic field followed by a continuous "ping-pong" motion as long as the

field remains applied. Contrary to the MMP, and due to the relatively simpler model of the MC-1 bacteria, an explanation using conventional magnetism is possible especially when using the chain of spheres model for polarity reversal [95].

For the purpose of this paper we used MC-1 MTB that are polar coccus gram negative bacteria having one magnetosomes chain made up of 10-15 Fe_3O_4 nanoparticles. These bacteria move using two bundles of flagella located in one extremity of the cell body. The speed of this bacterium can reach up to 300μm·s^{-1} making their flagella very effective at low Reynolds number flows. Interaction between the magnetosome chain and the external magnetic field is probably the cause of the bacteria's change in motion when the magnetic field is increased, as can be demonstrated using a simplified mathematical model based on previous work done by Noguiera and Lins De Barros [96].

2.2 Materials and Methods

2.2.1 Bacterial growth and preparation

Magnetococcus sp. (MC-1) was grown in a chemoheterolithotrophic liquid medium under microaerobic conditions. Iron-enrichment of the medium was done using 50μM of ferrous sulfate heptahydrate $FeSO_4 \cdot 7H_2O$ (F8048, Sigma-Aldrich). The bacteria were used at day seven, which corresponds to the end of their exponential growth phase.

2.2.2 Motion observation

Magnetotactic bacteria motion has been observed under a phase-contrast capable Zeiss optical microscope. It was possible to record the helical motion of the MTB by increasing the shutter speed of the Sony camera used to transfer video recordings to a computer. Images were investigated for the measurement of the helical motion pitch angle θ_p, the longitudinal speed v_3 and the transverse speed v_{12} using MATLAB (The MathWorks, Natick, MA).

2.2.3 Magnetic field

A 30×15×10mm neodymium (NdFeB) rare earth magnet was used to generate a strong magnetic field of 600 Gauss. The drawback associated with the use of a rare earth magnet is that the

resulting magnetic field gradient can induce a force on the magnetosome chain. This force is given by,

$$\vec{F}_{mag} = (\vec{m} \cdot \nabla)\vec{B} = V \cdot (\vec{M} \cdot \nabla)\vec{B} \quad (2.1)$$

where $\vec{F}_{mag}$ is the magnetic force (N), $\vec{m}$ is the magnetic moment of the ferromagnetic body $(A \cdot m^2)$, $\vec{M}$ is the magnetization of the material (A / m), V is the volume of the magnetosome chain (m^3), $\vec{B}$ is the magnetic field (T), and $\nabla\vec{B}$ is the gradient or spatial variation of the magnetic field (T / m). Whether the magnetic gradient field affects the dynamic of magnetotactic bacteria or not is unknown, however for the purposes of this paper we discard its influence based on the two following assumptions. First, the magnetic force is proportional to the volume of the magnetic particle. The MC-1 bacteria are made up of a single magnetosome chain comprised of 10 to 15 magnetosomes, which have a mean diameter of 50nm as depicted in Figure 2.1. Hence, the magnetic force is expected to be quite small, particularly in the case of MC-1 MTB. Secondly, the gradient is a spatial variation of the magnetic field. The smaller the field of view, the smaller the variation of the magnetic field.

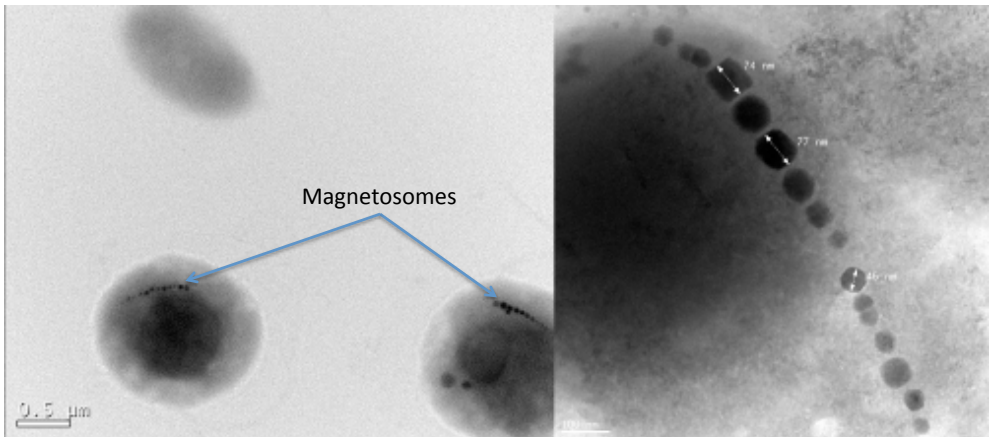

Figure 2.1. Bright-field transmission electron micrograph (TEM) of a negatively stained cell of MC-1. The cell contains a single chain of magnetosomes and possesses two bundles of flagellae (not visible on the image). There are 10-15 magnetosomes per bacteria, having an approximate mean size of 50nm.

2.2.4 Mathematical model

Noguira and Lins De Barros [96] have developed a mathematical model for the hydrodynamics of MTB describing their motion with six degrees of freedom. They considered the most common

approximation for a bacterium being propelled by a bundle of flagella, which is represented by a sphere being pushed at a point *p* on its surface. This paper examines the dynamics of the body of the bacteria in a two dimensional plane, focusing on the rotation of the cell body caused by the tangential component of the flagellum's force along with the magnetic torque. In fact, considering a flagellum with a non-integer number of turns, which is essential to model the helical motion of the bacteria [97], the force $\vec{F}$ acting on the cell body will be given by:

$$\vec{F} = F_{12}(cos(\omega t)\vec{e}_1 + sin(\omega t)\vec{e}_2) + F_3\vec{e}_3 \tag{2.2}$$

where ω is the angular frequency of the flagellum relative to the cell body, and F_{12} and F_3 are the tangential and longitudinal force. The tangential force F_{12} (see Figure 2.2 for the reference system) will induce a torque on the cell body given by:

$$N_{12} = R \cdot F_{12} \tag{2.3}$$

where R is the radius of the bacteria's body. Considering a low Reynolds number regime where the hydrodynamic force is approximated as a pseudo-steady stokes drag, v_{12} and v_3 are given by:

$$v_{12} = \frac{F_{12}}{6\pi\eta R} \tag{2.4}$$

$$v_3 = \frac{F_3}{6\pi\eta R} \tag{2.5}$$

where η is the dynamic viscosity of the medium (for the purpose of this paper, we consider the viscosity of water to be 1.002 Pa•s).

Due to v_{12} and v_3, the bacteria's swimming path will follow a helical motion with a pitch angle θ_p given by:

$$tan(\theta_p) = \frac{v_{12}}{v_3} \tag{2.6}$$

eqs 4 and 5 into eq. 3, the torque N_{12} on the bacteria's body caused by the force F_{12} can be written as:

$$N_{12} = 6\pi\eta R^2 v_3 tan(\theta_p) \quad (2.7)$$

The second torque that the bacterium's body is subjected to is the torque caused by the externally applied magnetic field, which is given by

$$N_m = m \times B = m \cdot B \cdot sin(\theta) \quad (2.8)$$

Where m is the magnetic moment of a bacterium, B is the external field and θ is the angle between them. This torque is generally considered negligible once the bacteria are aligned with the external field due to the small angle θ. In fact, it is clear that this torque can be ignored at low field levels due to its insignificance compared to the hydrodynamic torque caused by the tangential force F_{12}. However, at very high field levels, the magnetic torque increases to the same magnitude, if not greater, than the hydrodynamic torque.

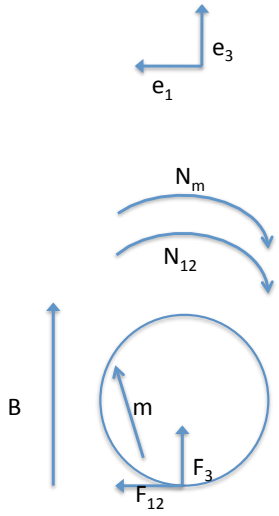

Figure 2.2. Reference system for the simplified model describing the dynamics of a magnetotactic bacteria. The magnetic torque results from the angle between the magnetosomes chain and the external field while the hydrodynamic torque is produced by the movement of the flagella on the cell body. The cell body is represented by a sphere.

2.2.5 Motion study

The torque N_{12} caused by the flagella rotation can be estimated by measuring the pitch angle θ_p and the migration velocity v_3 at a zero gauss magnetic field, which balances the magnetic torque. Two pairs of orthogonal magnetic coils powered with opposite current provided the zero gauss magnetic field. Mean value for the MTB radius, as well as the magnetosomes dimensions were obtained from electronic microscopy. The pitch angle and the migration velocity were estimated for different magnetic field values ranging from 1 Gauss to 600 Gauss.

2.3 Results and discussion

2.3.1 Motion

Magnetic field values above 200 Gauss cause observable changes to the motion of MC-1 under optical microscopy. As depicted in Figure 2.3, the application of a high magnetic field causes a decrease in the speed of MC-1 and an increase of the pitch angle of the spiral that describes the trajectory of the bacterium. This change is likely to be caused as a consequence of the magnetic torque being applied to the motion of the bacterium. In order to compare the magnetic torque to the hydrodynamic torque, we measured the longitudinal v_{12} and the tangential speed v_3 in the absence of a magnetic field and calculated the hydrodynamic torque using Equation 2.7. At a magnetic field of zero, as depicted in Figure 2.4, the MC-1 bacteria swim in circles confirming the negligible effect of the action of the magnetosome chain since non-magnetic bacteria have tendency of swimming in circles near boundaries [98, 99]. We established an approximate value of $1 \cdot e^{-17} N \cdot m$ for the hydrodynamic torque. At geomagnetic field values, the magnetic torque is approximated by $1 \cdot e^{-19} N \cdot m$, which, in terms of magnitude, is 100 times smaller than the hydrodynamic torque. However, at 600 Gauss, the magnetic torque increases to $1 \cdot e^{-16} N \cdot m$, which is higher than the hydrodynamic torque.

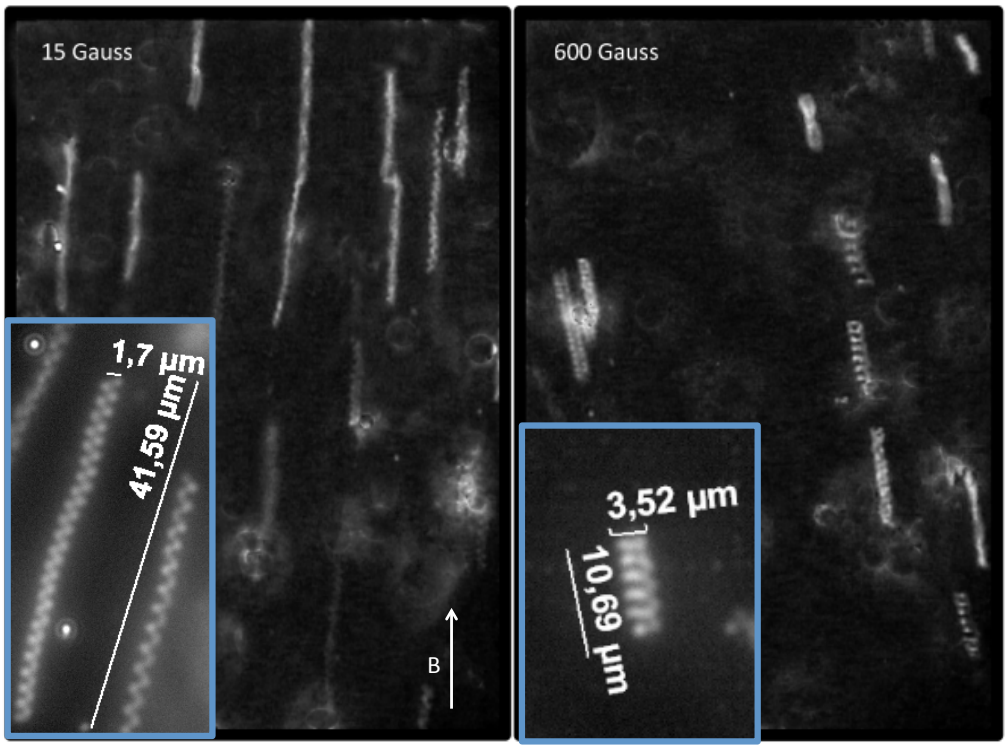

Figure 2.3. Representation of MC-1 in a 15 Gauss and 600 Gauss magnetic field. When subjected to a strong magnetic field, the angle of pitch of the helical motion increases causing the longitudinal speed of the bacteria to decrease. It was possible to record the helical motion of MTB by increasing the shutter speed of the Sony camera used to transfer video recordings to a computer.

The v_3 speed of MC-1 is always negatively affected by a high magnetic field, which suggests that the magnetic torque always adds to the hydrodynamic torque thus increasing the pitch angle of the helical motion. In order for this to happen, the orientation of the magnetosome chain within the bacteria must be coherent with the bacterial population, otherwise the pitch angle will decrease. Figure 2.5 shows three possible orientations of the bacteria's internal magnetosome chain for a fixed hydrodynamic torque direction. In cases a and b, we can expect a decrease in the pitch angle which causes an increase in the v_3 speed, while configuration c will be the only one to cause an increase in the pitch angle and a decrease in bacterial speed. This simplified model does not account for the precession of the bacterial body nor for the difference in frequency between the rotation of the flagella and the cell body, it only suggests a relationship between the orientation of the magnetosome chain and the flagella axis.

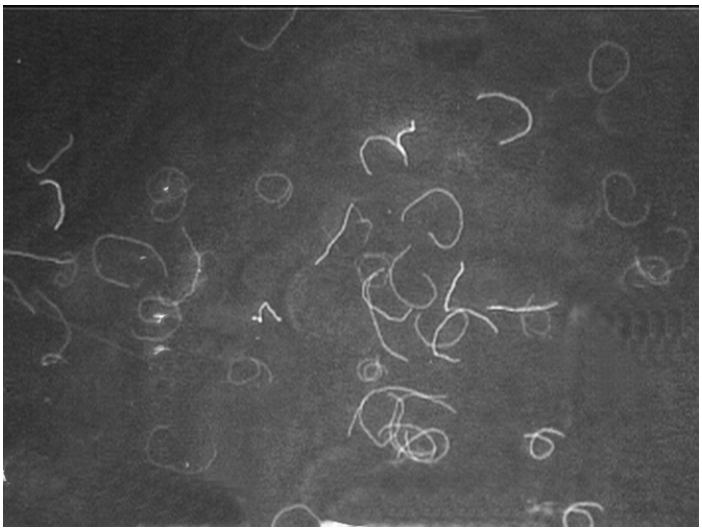

Figure 2.4. In the absence of a magnetic field, MC-1 travels in a circular motion that is characteristic of non-magnetic bacteria swimming near boundaries. The zero magnetic fields were obtained by activating two pairs of magnetic coils with opposing current. In such a context, since the magnetic torque caused by the interaction of the magnetosomes chain with the external field is null, the hydrodynamic torque can be estimated with more accuracy.

2.3.2 Magnetization reversal

MC-1 change polarity when submitted to a high magnetic field. The change of polarity occurs only when the bacteria come in contact with a physical obstacle, such as the edge of the droplet. The polarity reversal is permanent. MC-1 sample normally contains 90% north seeking and 10% south seeking bacteria. After being submitted to a 600 Gauss field, 50% of the bacteria in that same sample become North seeking and the other half south seeking.

This phenomenon can be explained using the model of the chain of spheres that describes the mechanism by which aligned spherical magnetic particles reverse polarity when the external field is reversed. The model was first introduced by Jacobs and Bean [95], in which they show that less energy is required for the spheres to reverse following a fanning mechanism than a coherent one. Jacobs and Bean, approximated the coercive force of a chain of 10 single domain nanoparticles reversing polarity following a fanning mechanism to a value of 2270Oe. The presence of imperfections in a chain of spheres causes the coercive force to decrease. This may explains why the change of polarity for MTB does not occur at the same magnetic field for all the bacteria in the sample.

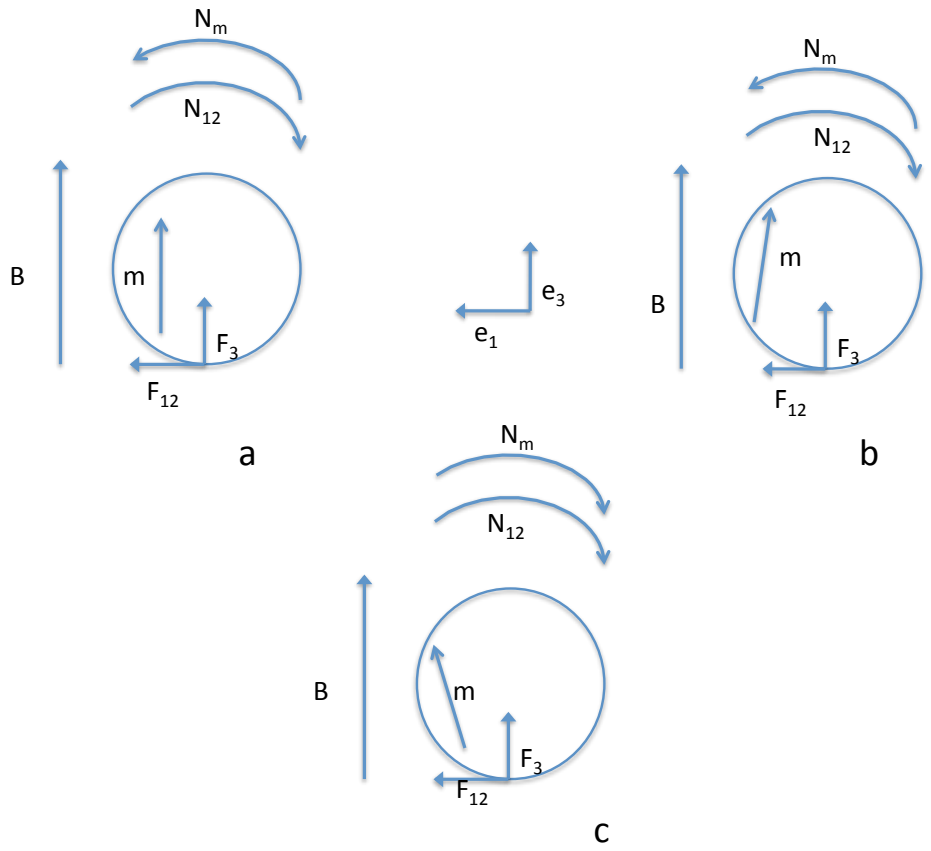

Figure 2.5. Representation of three different configurations for the orientation of the magnetosomes chain influenced by an external field. A and B are the only possible configurations where the magnetic torque adds to the hydrodynamic torque.

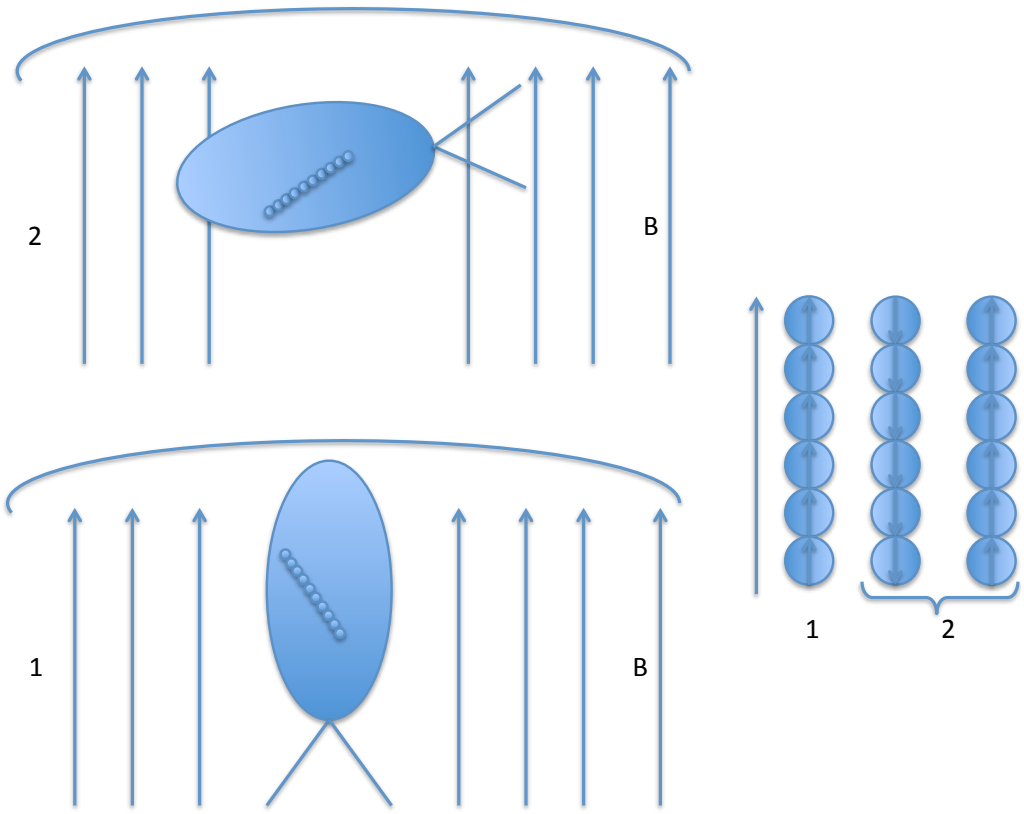

Figure 2.6. Artistic view of polarity reversal once a bacterium hits the edge of a droplet. Because of the constant movement of the flagella when the edge is reached, the magnetosomes chain can be orientated in the opposite direction to the magnetic field. Single domain spheres assembled in a chain change polarity when submitted to an opposing magnetic field stronger than its coercive field.

Figure 2.6 shows what we think happens to the bacteria prior to reversing direction as we apply a high magnetic field. First, the bacteria line up with the magnetic field and swim toward the edge of the droplet with a high pitch angle helical motion resulting from the high magnetic field. When the bacteria are near the edge of the droplet, the hydrodynamic interaction with the boundaries causes the bacteria to trace out round trajectories. Figure 2.7 shows a picture of MTB motion near the edge of the droplet for a magnetic field of 10 Gauss. The motion of the MTB is not aligned with the magnetic field anymore and a bacterium can swim for a short time against the magnetic field. For a very brief moment, the magnetosome chain will be subjected to an opposing strong magnetic field that will reverse the magnetosome chain polarity placing the flagella on the reverse side of the starting direction. Bacteria containing less or non-uniform magnetosomes will

be more susceptible to the reversal of polarity than bacteria with a greater number of uniform magnetosomes.

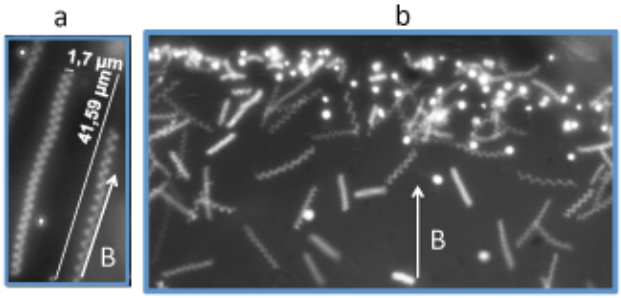

Figure 2.7. Magnetotactic bacteria swim by means of flagella. Helical motion is a consequence of the non-integer number of turns of the flagella spire. MTB follow the magnetic field direction as in (a), however, near boundaries and obstacles, their motion forms an angle with the magnetic field.

The polarity reversal can be used to homogenize a bacterial sample so that it only contains either a north seeking or a south seeking population. In order to do so, four strong permanent magnets are positioned to face each other (North or South) in pairs in an orthogonal pattern. Figure 2.8 illustrates how each population conducts itself in the sample. South-seeking bacteria will tend to gravitate toward and remain in the center while North-seeking ones will be attracted to the edge of the setup then reverse direction due to the polarity reversal caused by the high magnetic field at the magnet's surface and finally settle in a neutral midpoint where force fields are neutralized.

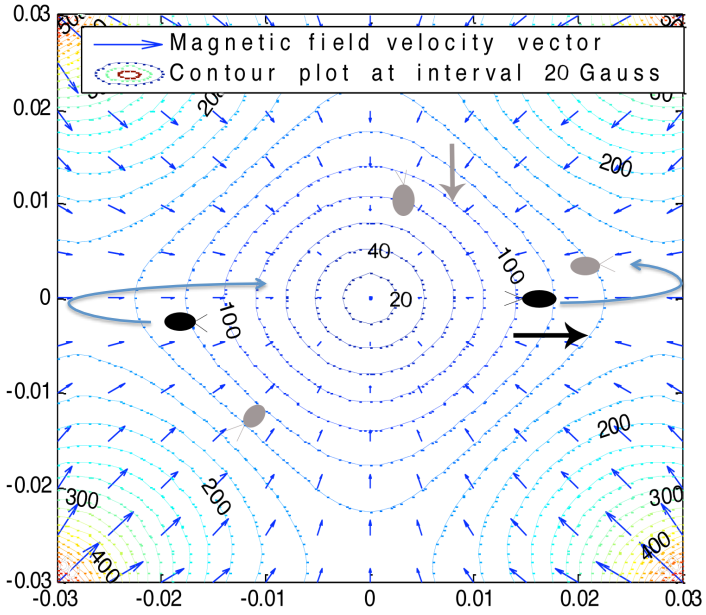

Figure 2.8. Polarity selection magnetic setup. A sample containing both north-seeking and south-seeking bacteria will be transformed into a homogenous sample containing only one population using this magnetic setup. The setup is guided by four permanent magnets arranged so that two positive magnets face each other and two negative magnets also face each other North-seeking bacteria will be directed to the center and will stay there. South-seeking bacteria will be directed to the edge of the setup and reverse direction due to the high magnetic field near the magnet surface, and will head to the center where the field is null. Since polarity reversal is permanent, only one population will remain.

CHAPTER 3 A Magnetic Guidance System for Magnetotactic Bacteria Targeting Tumours

3.1 Introduction

A novel drug delivery technique using MC-1 Magnetotactic bacteria (MTB) is considered in this paper. MTB align and swim along the direction of an external applied field using flagella and an induced magnetic torque on a chain of nanoparticles called magnetosomes embedded in each bacterium [82, 100]. MTB possess all the needed components for effective targeting in the human vasculature, such as a flagellum, an internal magnetic sensor, an appropriate size and enough thrust [46]. The magnetosomes chain embedded in the cell makes the bacteria very sensitive even to weak magnetic fields. Besides the intrinsic characteristics of MTB, many gains can be achieved by using these microorganisms in drug targeting applications. First, MTB can help to uniformly distribute a drug into the tumour because of their active motility. Second, they could enhance embolization procedure since they don't require blood flow in order to move in the vasculature and can reach cancerous cells even in the absence of flow. Third, the bacteria can be easily functionalized through antibody bond, or by the use of cell penetrating peptide (CPP) to name just a few methods.

Close-loop control of MTB in targeting applications requires a tracking system, an external magnetic guidance system, and a control algorithm that adjust the direction of the magnetic fields according to the actual and the desired position. Since the Fe_3O_4 magnetic nanoparticles embedded in each bacterium are similar to the nanoparticles used as MRI contrast agents, tracking and *in vivo* imaging of MTB is possible using a clinical Magnetic Resonance Imaging (MRI) system [101]. Furthermore, the MRI also offers an environment for the real-time integration of the different modules required for the targeting procedure. A demonstration of the real-time navigation of ferromagnetic microdevices in the vascular system of a living animal was presented in [59, 61-63]. The same architecture could be used for MTB navigation, using an external magnetic field instead of the MRI internal gradient fields. In fact, the high static magnetic fields of 1.5 Tesla or higher inside the MRI bore prevent the navigation of MTB and

constraint their motion to the direction of the main field.

Many options are available for MTB navigation; however, a special care is to be made in order to build a system compatible with the MRI machine since the magnetic guidance system will be placed as close as possible to the MRI bore. A sliding table will connect the interior of the MRI with the magnetic guidance system as in XMR-suite where a sliding table connects together the MRI scanner with an X-ray system [102]. We opted for magnetic coils instead of permanent magnets in order to minimize interference with the MRI machine since the magnetic coils can be turned off during the imaging phase, which is not possible with permanent magnet.

3.2 Method

3.2.1 Magnetotactic bacteria characteristics

MC-1 magnetotactic bacteria are used in this experiment. MC-1 MTB are characterized by a high swimming speed (we recorded a peak speed of 300μm·s^{-1} in our laboratory), spherical shape and a typical size of 2μm of diameter. There is approximately 12 to 15 nanoparticles per cell having an approximate size of 70nm. The samples used for the experiments contain pre-selected bacteria. The pre-selection step aims to split the north seeking from the south seeking population and to select the most active ones. This is done by applying a homogenous magnetic field on the entire sample in the z-direction. The north seeking and south seeking bacteria go to the top and the bottom of a container respectively. We invert then the magnetic field and took a sample at a few centimeters from the top in order to get the fastest ones. The amount of bacteria was quantified using a Zeiss Imager.Z1 microscope. For this first characterization experiments, the bacteria was kept in their growth medium.

3.2.2 Magnetotactic bacteria motion

MTB moves due to their flagellar motion with the constant speed v_0. The direction of motion is dictated by the external applied magnetic field $\boldsymbol{H}$ as well as the rotational Brownian motion that tend to deviate the MTB from the field direction. The velocity $\boldsymbol{v_0}$ can be divided into two components with respect to $\boldsymbol{H}$ as stated in [103]. Assume an angle of φ between the motion direction of the bacteria and the applied field $\boldsymbol{H}$, the velocity component parallel and perpendicular to $\boldsymbol{H}$ are given by

$$\upsilon_H = \upsilon_0 \cdot \cos\varphi \tag{3.1}$$

$$\upsilon_\perp = \upsilon_0 \cdot \sin\varphi \tag{3.2}$$

The nanoparticles inside the cell however are arranged in chain in order to maximize the magnetic moment ***m*** of the bacteria. The angle φ will depend on the ratio between the magnetic energy and the thermal energy such as its time averaged expression will equals a Langevin function as described in [104] and given by

$$\cos\varphi = L\left(\frac{mB}{KT}\right), \text{ where } B = \mu_0 H \tag{3.3}$$

where K is the Boltzmann constant and T the temperature, μ_0 is the permeability of free space, and ***B*** the magnetic field density.

Thus, the bacterial orientation with the magnetic field lines will be affected by the value of ***H*** as well as the temperature of the medium. The earth magnetic field of 0.5 Gauss exerts enough force on the magnetosomes chain to allow the overall motion of MTB to be in the direction of this field. However, at this field strength, the direction of MTB is greatly influenced by chemotaxis and aerotaxis. Considering a magnetic moment ***m*** of 10^{-16}(A.m^2) at room temperature (297.15K), the magnetic energy is 1.15 times the thermal energy when subjected to the earth's field. The magnetic energy becomes more important at higher field and we can expect that the bacterial direction will be specified by the magnetic field lines value greater than 4 Gauss, where the energy ratio is approximately 10.

3.2.3 MTB guidance

Different magnetic navigation methods can be used for MTB guidance. The simplest method consists on a three orthogonal Helmholtz pairs generating a homogenous magnetic field in 3D space. By powering the coils accordingly any field direction can be generated. While this method could be effective, it is evident that obstacles such that found in the anarchic arteriocapillar networks found in tumours are a limiting factor.

Another method using 3-axis Maxwell coils that is better suitable for tortuous paths could be used instead. The Maxwell configuration causes the MTB that follows the magnetic field lines to be trapped in the center of the coils. Controlling the motion of the bacteria is done by changing the current ratio between coils of the same pair. Since the current flowing in each coil of a Maxwell pair should be the same in order to have a linear gradient, having different current in each coil of the same pair will lead to a non-linear gradient. The relationship between the ratio of *I1* and *I2* (current in each coil of a Maxwell pair) and the position of the zero magnetic fields is plotted in Figure 3.1. We choose to change only one current value at a time. Therefore, depending on the displacement side, one current value is set to the maximum while the other is changed according to the desired position. The mathematical relationship between the zero field position and the current ratio is given by

$$I = \frac{I1}{I2} = \sqrt{\frac{r^2 + \left(z + \frac{d}{2}\right)^2}{r^2 + \left(z - \frac{d}{2}\right)^2}}^{3} \tag{3.4}$$

where *I1(A)* and *I2(A)* are current in each coil of the Maxwell pair, *r(m)* is the radius of the coil, *d(m)* is the distance between the coils and *z(m)* is the required position.

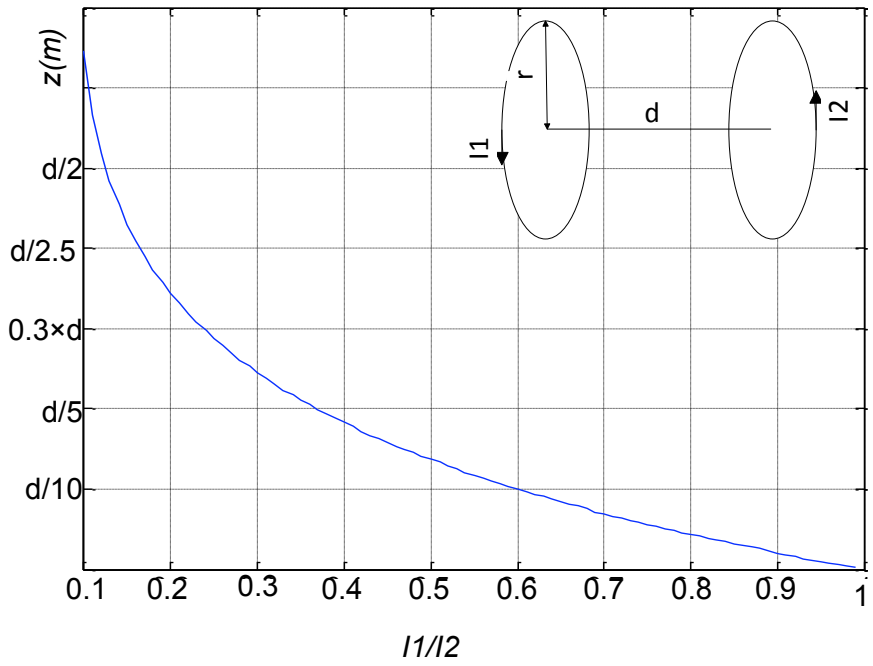

Figure 3.1. Changing the current value for one coil of a Maxwell pair causes the position of the zero fields to move from the center. However, the gradient linearity is no longer preserved.

3.2.4 Magnetic guidance system

A novel magnetic field strategy for efficient navigation of MTB is proposed. This method uses a combination of Helmholtz and Maxwell coils. It consists on 3-axis Helmholtz coils controlling the position of the magnetic field convergence point generated by a set of Maxwell coils. In fact, as depicted in Figure 3.2, a linear relationship stands between the current flowing in the Helmholtz coils and the position of the zero fields generated from the Maxwell pairs.

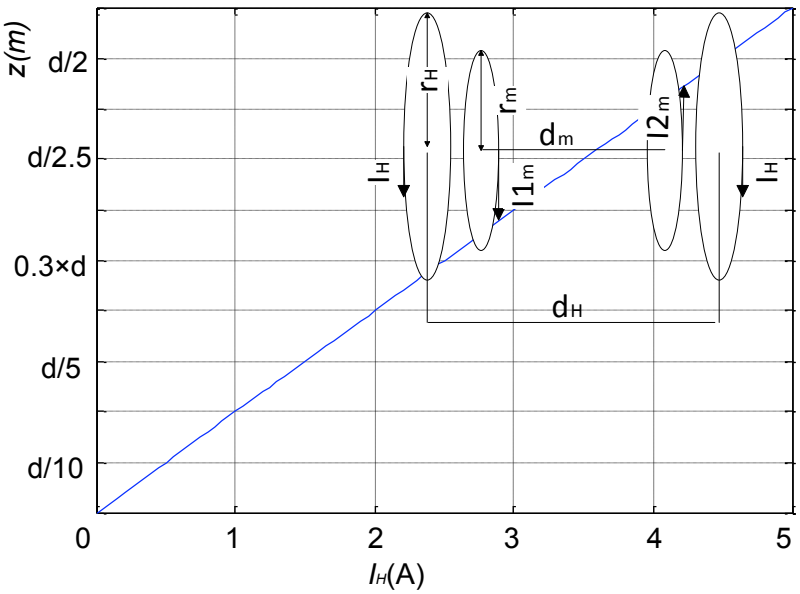

Figure 3.2. The relationship between the current I_H flowing in a Helmholtz pair and the displacement value of the Maxwell magnetic fields.

3.2.4.1 Helmholtz pairs

In this experiment we used 3-axis square Helmholtz coils having dimensions of 20×20×20cm. The coils have been spaced by 0.5445×L, where L is the length of one side. The maximum magnetic field that could be applied in continuous was 15 Gauss obtained with a current of 2A. We decided to use a cube frame for the Helmholtz coils in order to gain space since another set of coils is to be inserted inside. We achieve excellent homogeneity (field discrepancies < 2%) in approximately 10×10×10cm around the center. Furthermore, the cube frame allows the three coil pairs to be approximately the same size.

It is possible to develop an explicit form for the total magnetic field produced by a pair of square Helmholtz coils. For that, each side of the coil could be considered separately as a current carrying wire. Superposition of the contribution of each segment forming the pair of the square coils with appropriate rotation gives the final equation.

3.2.4.2 Maxwell pairs

A smaller 2-axis circular Maxwell coil set was used to generate a linear gradient. The first pair has a radius (*r*) of 6cm while the second was 8cm. The coils were spaced according to the optimal Maxwell relationship which is *r*×*sqrt*(*3*) and supplied with equal but opposed currents. The maximum gradient that we could continuously apply was 0.5 Gauss/mm. The Maxwell coils were connected in parallel and powered by one power supply while each Helmholtz coil was connected separately to a power supply. A software running on a computer allows to manipulate in real-time the current value of the power supplies using a GPIB controller (model) as depicted in Figure 3.3.

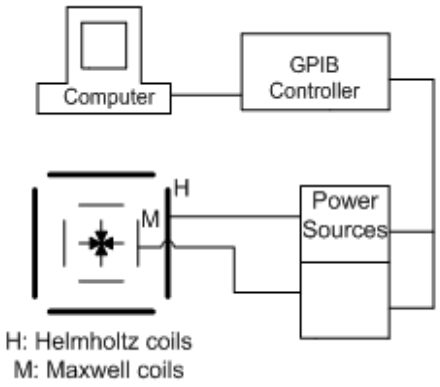

Figure 3.3. Automatic navigation of MTB is done using a computer controlling the power supplies through a GPIB interface.

The longitudinal component of the magnetic field and the magnetic field gradient produced by two electrical current loops are given by,

$$B(z) = N * \left(\frac{\mu_0 i a^2}{2\left(\left(\frac{1}{2}d - z\right)^2 + a^2\right)^{3/2}} - \frac{\mu_0 i a^2}{2\left(\left(\frac{1}{2}d + z\right)^2 + a^2\right)^{3/2}} \right) \tag{3.5}$$

$$\frac{dB(z)}{dz} = N * \left(-\frac{3\mu_0 i a^2 (-d + 2z)}{4\left(\left(\frac{1}{2}d - z\right)^2 + a^2\right)^{5/2}} + \frac{3\mu_0 i a^2 (d + 2z)}{4\left(\left(\frac{1}{2}d + z\right)^2 + a^2\right)^{5/2}} \right) \tag{3.6}$$

where, N is the number of loops in the coil, a is the radius of the loop, μ_0 is the vacuum permeability, i is the electrical current, d is the distance between the coils, and z is the position along the longitudinal axis of the loops.

3.3 Results

3.3.1 Magnetic field simulation

The resulting magnetic field from the Maxwell pairs is as depicted by Figure 3.4 a and b for two orthogonal pairs. Whatever the location of the bacteria before applying the magnetic field, they will all be directed to the center after the magnetic field is applied. This simulation is done for the 2D case; in order to apply the Maxwell magnetic field in 3D space a temporal multiplexing is required. In fact, each coil will have a longitudinal component of the magnetic field, the one required for MTB trapping, and a transversal magnetic field. The transversal field from one coil is opposite to the longitudinal component of the transversal coils. Since the longitudinal component has higher amplitude than the transversal one, the resulting magnetic field will be enough high for bacterial trapping. However, If three pairs are powered at the same moment, each direction will have a longitudinal component added to four transversal components, which will cause an almost cancellation of the longitudinal field. In order to apply a Maxwell field in 3D, the coils have to be powered by group of two pairs. Since there is 3 different combinations, each group of coils has to be powered 1/3 of the time period.

3.3.2 Magnetic field MTB sensitivity

The bacteria will be trapped between the Maxwell coils as depicted in Figure 3.5; the region extent where they accumulate depends on the gradient intensity as well as on their sensitivity to the magnetic fields. The MTB sensitivity to the magnetic field depends on their magnetic moment that depends on the number of magnetosomes in the cell. It is believed that mature cell contains twice as much magnetosome as a younger one. For that reason, when studied under microscope a different response and sensitivity to the magnetic field is observed. When submitted to a magnetic gradient of 0.5 Gauss/mm and observed at a macroscopic scale, the bacteria form a visible circle of 3.5 mm of diameter. Thus, we can conclude that most of the MC-1 MTB that we use are sensitive to a field as weak as 0.8 Gauss. As shown by the contour plot, the magnetic field

at the centre is null. When reaching this region of zero field, the MTB are free to move in every directions until it reach a magnetic field that will bring them to the zero field region again.

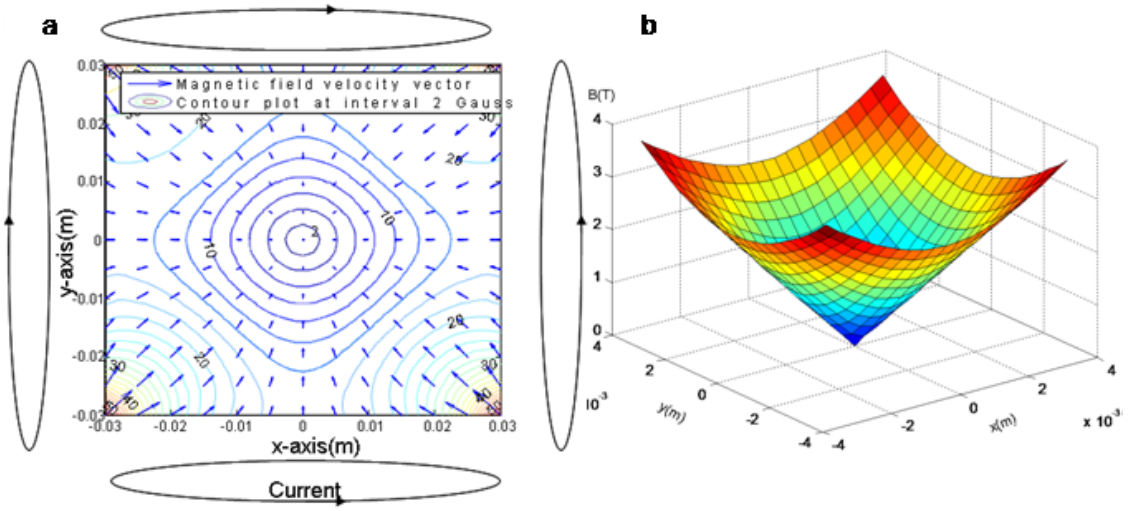

Figure 3.4. a) On the plane magnetic field velocity vector generated from 2D Maxwell pairs. b) Magnetic field absolute value as generated by a two Maxwell coil pairs in the x and y-axis. The magnetic field lines are directed toward the center where the field intensity is zero.

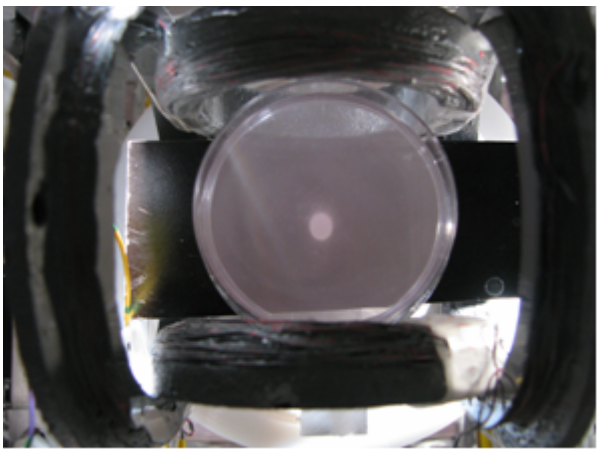

Figure 3.5. This figure shows an MTB sample under the influence of the Maxwell magnetic field. The bacteria from the entire sample are directed to the center of the container. The magnetic field gradient was 0.5Gauss/mm.

3.3.3 MTB guidance

The Helmholtz coils are able to offset the Maxwell magnetic field linearly in all directions of space. A demonstration for the guidance of MTB is shown in Figure 3.6. Two minutes after the Maxwell coils were powered, a bacterial accumulation becomes visible in the zero magnetic field regions as depicted by Figure 3.6 (a, b). The MTB continued to accumulate for three more minutes after which the set point was changed. The controller computed then the current to be applied to the Helmholtz coils and sent these values over a GPIB card to the power supplies. The MTB follow the new target, barring those stacked on the beaker surface as shown in Figure 3.6 (c, d, e, f).

3.4 Discussion

Trapping MTB by a gradient magnetic field in the target site may show many advantages over traditional MTB guidance. In fact, this method has the advantage to more likely uniformly distribute the drugs inside target region. In addition, the low magnetic field applied in the target region, which can be a tumoural lesion, gives freedom to the bacteria helping them to avoid obstacles that can encounter on their ways. In fact, a tumour forms a lot of capillaries through angiogenesis that have the characteristic to be leaky, irregular and misformed, with non-uniform blood flow preventing many drugs to attain the entire cancerous cells.

Gradient magnetic fields are also used to trap micro and nanomagnetic particles in a targeted region of the human body, which is commonly dubbed Magnetic Drug Targeting (MDT) [51, 52, 105, 106]. Because the magnetic force acting on the magnetic particles is proportional to the gradient fields as given by

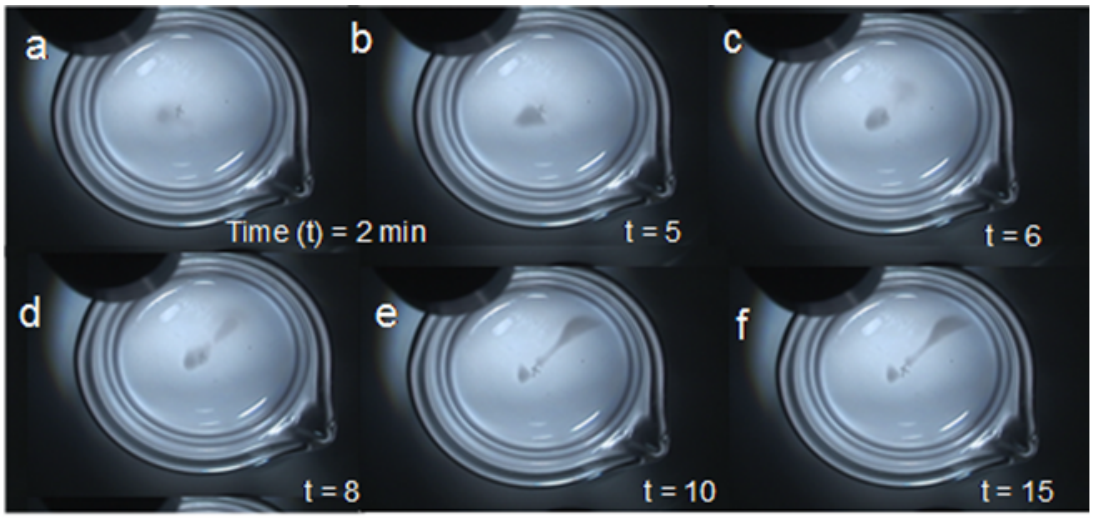

Figure 3.6. MTB guidance demonstration. In (a) and (b) a gradient was applied using the Maxwell coils. From c to f, the target location was changed which imply the activation of the Helmholtz coils.

$$\vec{F}_{mag} = \mu_0.(\vec{m}.\nabla)\vec{H} \qquad (3.7)$$

high values are required for efficient trapping. In Equation 3.7, $\boldsymbol{m}$ (A.m^2) is the magnetic moment, μ_0 (N.A^{-2}) is the permeability of vacuum, $\boldsymbol{H}$ (A·m^{-1}) is the magnetic field, and $\boldsymbol{F_{mag}}$ (N) is magnetic force. Table 3.1 summarizes the gradient field used in typical trapping applications involving MDT. For purpose of comparison the magnetic field gradient required to trap MC-1 MTB in a 1 mm diameter sphere area is also given. We notice that the gradient required to trap MTB is much less than that required for micro and nano magnetic particles trapping.

Table 3.1. Summary of some examples of the magnetic particles and the gradient required for their trapping

MAGNETIC PARTICLES	MEAN DIAMETER (μm)	MAGNETIC GRADIENT ($T \cdot m^{-1}$)	Reference
Magnetite	0.0156	10-30	[12]
Mn-Zn ferrite	2	26	[13]
Maghemite	0.03	4.5-18.8	[14]
Magnetite	0.25	5-70	[15]
Magnetite	10.9	0.443	[5]
MC-1 MTB	2	0.2*	-

*The gradient is calculated to trap the bacteria inside a spherical area having a 1mm diameter.

3.5 Conclusion

Bacterial tumour targeting has gained renewed interest these last years because of the ability of some bacteria to reach deep tumour region and induce a therapeutic effect [68, 70, 107]. However, we propose a new mechanism of drug delivery using magnetically controllable bacteria. We show the magnetic control of MTB using a novel magnetic navigation strategy adapted to operate close to an MRI system. Future works will be directed toward closing the loop of the magnetic control and MRI tracking in order to be able to navigate MTB through complex pathways and *in vivo* in real-time.

CHAPTER 4 MC-1 MAGNETOTACTIC BACTERIA NAVIGATION AND CONTROL WITHIN SMALL PHANTOM VESSELS: TOWARD BACTERIA TUMOUR TARGETING

4.1 Introduction

Anticancer therapy effectiveness depends mainly on two parameters; first, the intrinsic efficacy of the anti cancerous agent used, second, the quantity by which the agent reach the tumour [108]. The intensive research on cancer therapy of the past 20 years have led to a good understanding of the tumour biology and have brought many effective anticancer drugs up to the market. However, due to many physiological barriers that blood-borne agents encounter, the amount that reaches the tumour is often negligible compared to what was injected in the blood network [109-112].

The most common set of parameters affecting the delivery of blood-borne anticancer drugs to tumours are: The miss-formed angiogenesis capillaries supplying tumours, the high interstitial pressure inside solid tumours as well as the blood flow heterogeneity of vessels supplying the tumour. These parameters have as consequences the diminution of therapeutic reaching the target, the non-uniform distribution of drug inside the tumour and the increase of the time required for a drug or molecule to be in direct contact with the cancerous cells.

In order to overcome some of the limitations that have been just addressed, we propose to use living flagellated bacteria to target tumours. Magnetotactic bacteria (MTB) [46, 82, 83] have been chosen due to their ability to orient with an applied magnetic field and to swim persistently in that direction. MTB synthesize intracellular Fe_3O_4 nanoparticles, called magnetosomes, assembled in a chain acting as a compass to influence through magnetotaxis the swimming direction of the bacteria. Computer control of the motion direction of these microorganisms is then possible using a set of magnetic coils or permanent magnet. The MTB cell size ranging from 1 to 3μm in diameter gives them the ability to navigate in the smallest capillaries network, especially the malformed ones of a tumour. There are many MTB strains available in nature, but because of their high swimming speed, reaching 200 to 300μm, the MC-1 MTB was chosen as a potential candidate for this application.

Bacteria are believed to have a great potential in targeting the hypoxic zone of tumours, that other therapy fail to treat. According to [113] a set of criteria have been defined for a successful bacterial cancer therapy. MTB fulfill much of these requirements in order to be an efficient bacterial tumour targeting system. In fact, MTB do not have any known toxicity or related infection. Furthermore, they can selectively target tumours by direct navigation using controlled magnetic fields. Their active motility and high speed should help to uniformly invade the tumour and to access the quiescent and hypoxic region of it. However, unlike standard bacterial therapy approach, neither survival nor growth at the body temperature is expected from MTB. The overall MTB targeting procedure is limited to the time the bacteria remain active and alive at the body temperature, which is estimated to be between 30 to 45 minutes, unless a local temporal temperature decrease is apprehended.

Due to the little time frame available for MTB delivery to targets, efficient magnetic control is required. However, the major problem consists on the lack of knowledge on the internal tumour blood vessels architecture. Taking into account the bacteria speed, their magnetic sensitivity as well as their behavior at different field strength, the direction and intensity of the magnetic fields applied for guidance can be optimized.

4.2 Method

4.2.1 Magnetotactic bacteria characterization

We characterized the swimming of MTB *in vitro* by mimicking different situations that they could encounter in an *in vivo* environment. The characterization goal was to be able to predict the MTB behavior in a complex microvasculature network and to choose the correct magnetic field algorithm that has to be applied to obtain optimum targeting. In fact, as the MTB follow the magnetic field, they could be stuck easily into obstacles especially in a very complex capillary networks such as the tumour angiogenesis. As a consequence, changing the direction of the field is necessary to guide the bacteria. The problem is that there is no visual information on the route and obstacles that the bacteria are facing.

The bacteria motion speed and magnetic sensitivity are the two main factors that mostly affect the targeting procedure. These two factors however, do not follow exact science rules; they could

change from one sample to another as a consequence of changes in the growth or experimental conditions.

4.2.1.1 Growth condition

Magnetococcus sp. (MC-1) was grown in chemoheterolithotrophic liquid medium under microaerobic conditions. Iron-enrichment of the medium was done using 50µM of ferrous sulfate heptahydrate $FeSO_4 \cdot 7H_2O$ (F8048, Sigma-Aldrich).

4.2.1.2 Speed measurement

A sample containing MTB were deposited on a microscope slide, a cover slip placed over the drop using 450µm separators to form a pool in the center. The slide was then placed on a microscope stage (AxioImager Z1, Carl Zeiss Imaging solutions) under dark-field illumination. Image acquisition was made by AxioCamMr (Zeiss) using a 20× LD Ediplan lens magnifier. The exposure time was set to 200ms allowing the visualization of the trail left by bacterial motion. All measurements were made using the AxioVision v.4.6.0 software.

4.2.1.3 Magnetic field sensitivity

MTB population distribution under various magnetic field values generated using an orthogonal pair of magnetic coils was determined after image analysis. Magnetic sensitivity is estimated by counting the number of bacteria inside a given equipotential magnetic field. ImageJ v 1.42q software was used to count bacterial cell distribution.

4.2.2 Magnetotactic bacteria guidance

The experimental setup, for the in vitro MTB guidance, is composed of three parts. The first part is an optical system consisting on a Zeiss microscope (Stemi SV 11) with a Sony camera (DCR HC1000) connected to a computer through a firewire link. The second part is a tridimensional magnetic coils system (Resonance Research, Inc. Billerica, Massachusetts) powered by GPIB computer controlled power sources (Sorenson XG 1700, AMETEK Programmable Power, Inc. − San Diego, CA). The last part consists on a microfluidic channels where the bacteria are navigated and targeted.

4.2.2.1 Magnetic control system

Two pairs of the tridimensional magnetic control system served for navigation, while the third pair insured the magnetic field is less than 0.5 Gauss along the orthogonal direction. The reference system is as given by Figure 4.1. The coils, along the *x* and *z* directions, were powered with opposed current as in a Maxwell configuration as illustrated in Figure 4.1 (a). Changing the current ratio between coils of the same pair changes the zero field position along that axis. Since MC-1 MTB are unipolar and follow the magnetic field direction, they will be trapped in this zero field region. Automatic control of the position of the bacteria is granted through repositioning the zero field position. The mathematical relationship between the target position along one axis, and the current ratio is given by

$$\frac{I1}{I2} = \sqrt[3]{\frac{r^2 + \left(z + \frac{d}{2}\right)^2}{r^2 + \left(z - \frac{d}{2}\right)^2}} \tag{4.1}$$

where $I1$ *(A)* and $I2$ *(A)* are current in each coil of a pair, r *(m)* is the radius of the coil, d *(m)* is the distance between the coils and z *(m)* is the target position.

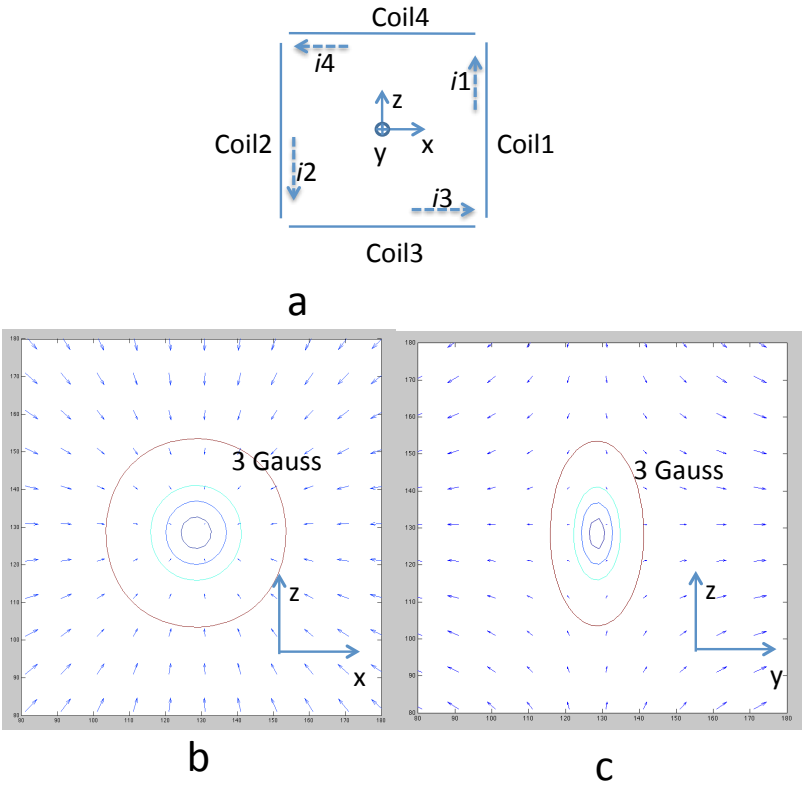

Figure 4.1. Magnetic field generated by two pairs of orthogonal magnetic coils, powered by opposite current as shown in (a). The in-plane magnetic field is shown in (b), while the magnetic field in the orthogonal direction is shown in (c). The magnetic field direction in (a) converges to the center of the coils, causing the bacteria to aggregate in this point. In the orthogonal direction, however, the magnetic fields direction diverges.

4.2.2.2 Micro-channels network

A design consisting on a multiple U-channels shape as depicted in Figure 4.2 was used for targeting experiment under microscope. The shape of the channels does not represent patterns that can be found in the microvasculature of a tumour, however, it does offer a pattern that can be reproduced precisely with computer simulation tools. The microchannel have a diameter of 100µm.

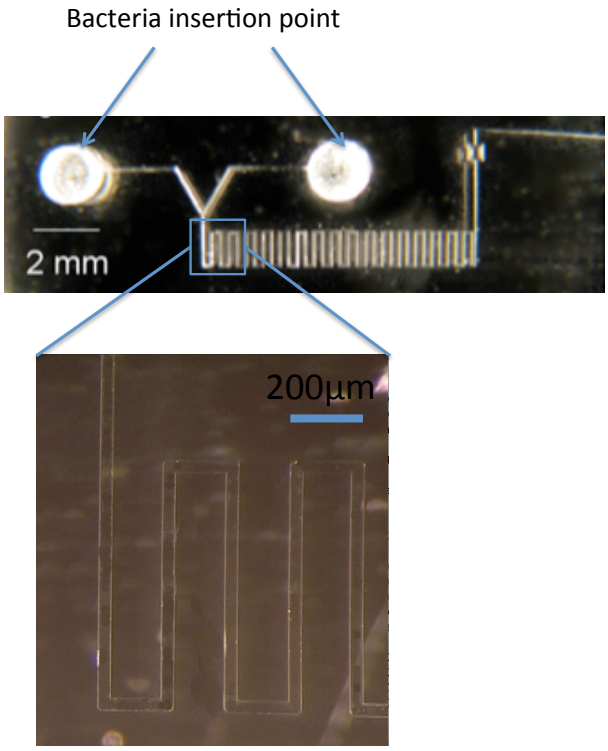

Figure 4.2. Microfluidic channel used for in vitro bacteria targeting. The channel have a diameter of 100µm. There is two entry points to the channel as well as two exits (not shown in the picture). The channel was filled with PBS (Phosphate Saline Buffer), prior to the deposition of the bacteria in the insertion points. The bacteria are inserted without any pressure to ensure that the ones reaching the target are under the action of the magnetic field.

4.2.2.3 Magnetic Field and bacteria targeting simulation

Equation 4.1 was numerically solved, for the two pair of coils, using MATLAB (The MathWorks, Natick, MA) and integrated in a computer program that generates a text file containing current to apply on each coils to create a given sequence of magnetic fields. The microchannels were simulated using a 2D matrix having zeros in the interior of the channels and ones otherwise. We used a simple model for a particle following the magnetic field to simulate a bacterium. When a simulated bacterium hits a wall, it follows the direction of the magnetic field that is orthogonal to that obstacle. Simulation served mainly as a visual aid and as illustrations purpose, however, the behaviour of bacteria is much more complex than our model especially when they hit obstacles.

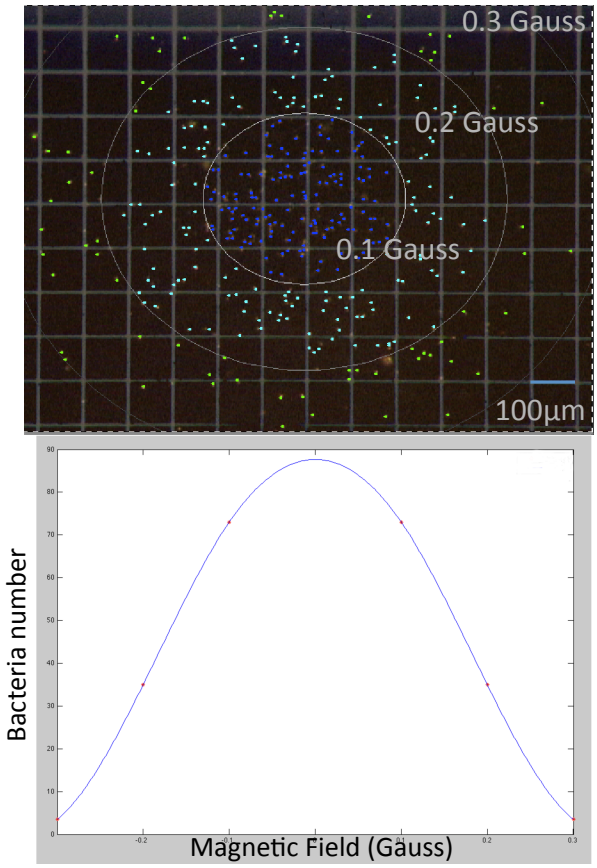

Figure 4.3. MTB distribution in a gradient magnetic field. The MTB lie inside the 0.3 Gauss magnetic equipotential circle, with more than half of them inside the 0.1 Gauss equipotential.

4.3 Results

4.3.1 Magnetotatic bacteria characterization

Figure 4.3 shows the MTB's distribution in a spatially varying magnetic field. The bacteria distribution map, thus obtained, can help to define the sensitivity range and the strength of the magnetic fields to be applied for navigation. The number of bacteria per equipotential is plotted in Figure 4.3. The MTB gather inside the 0.3 Gauss magnetic equipotential circle, with approximately 68% inside the 0.1 Gauss equipotential. The bacteria are in continual random motion in this zone since the magnetic field is very weak. The magnetic torque that is responsible for aligning the bacteria with the magnetic field is given by

$$N_m = \ m \times B = m \cdot B \cdot sin(\theta) \tag{4.2}$$

where m is the magnetic moment of a bacterium, B is the external field and θ is the angle between them. As soon as a bacterium reaches a certain field that causes the bacteria to realign with the magnetic field, it is sent back to the center of the magnetic fields. The magnetic moment m of a bacterium is given by the properties of its magnesomes chain, and more specifically, the number of nanoparticles and their size. According to these results, the 0.3 Gauss equipotential was chosen as boundaries limit for specifying the target region during the navigation experiment tests.

4.3.2 Magnetic Bacteria navigation in microfluidic channel

The bacteria are deposited on the insertion tank without applying pressure to insure that the bacteria do not attain the target under the action of flow. Furthermore, the shape of the microchannels is enough complex to make sure the bacteria do not reach the target following a random motion. These two facts were experimentally validated before conducting magnetic navigation experiments.

When the target location is set to the first U-shape channel the bacteria were able to reach the target, as depicted in Figure 4.4. In Figure 4.4 (a), we show the magnetic field applied as well as the target location. The circle denotes the magnetic field region where the field has an intensity of 0.3 Gauss. In Figure 4.4 (b) we show the microscope image of the bacteria submitted to the field presented in Figure 4.2 (a). Simulation as well as experiments showed that it is possible for the bacteria to exit through the insertion tanks and accumulate in the target zone. However, when the target location requires traveling through the microchannels maze, as it is the case shown in Figure 4.4 (c), no bacteria were able to reach the target. In fact the magnetic fields are orthogonal to the wall of the microchannels, and cause the bacteria to stick to the boundaries without being able to change direction. Furthermore, the intensity of the magnetic field is high far from the target and decrease to zero on the target spot. Since the swimming direction of MTB is given by a balance between the aligning magnetic energy ($m \cdot B$) and the thermal energy (K_bT), far from the target the bacteria are enforced to follow the direction of the magnetic field, while near the target their direction is loosely related to it. Due to the dimensions of the channels and their 90 degrees

angle, the imposed magnetic field makes the bacteria stuck as if they hit a wall especially when they are far from the target, as depicted in Figure 4.4 (c). This magnetic control method does not cope with micro-channels having very complex pattern especially the tortuous micro-fluidic network used for this experiment.

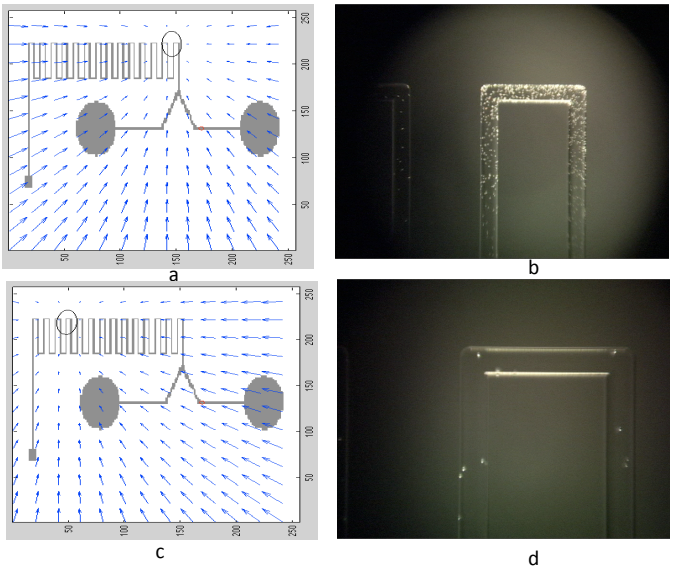

Figure 4.4. Targeting test in microfluidic channel. In (a) simulation of the magnetic field for a target location at the first U-shape occurrence in the channel. In (b) the corresponding MTB accumulation for the same magnetic field applied in a real channel with the same geometry. (c) When the converging field is set at another location, the bacteria are not able to bypass obstacle caused by the channel shape and to get to the target.

4.3.3 Magnetic control considering the microchannels geometry

Only when the applied magnetic field takes into account the phantom geometry that targeting becomes successful. In fact, Figure 4.5 shows what happen when the field translates around the target location instead of being static. The bacteria, in this case were able to go in the direction of the target without being stuck into obstacles. Figure 4.6 is a microscope image of the bacteria traveling the microchannels following the pattern shown in Figure 4.5. Magnetic field algorithm becomes very important in order to navigate accurately the bacteria, and can be generalized to complex geometries. Taking into account the geometry of the channels, the bacterial speeds and behavior for a given magnetic field, we can apply magnetic fields that optimize targeting.

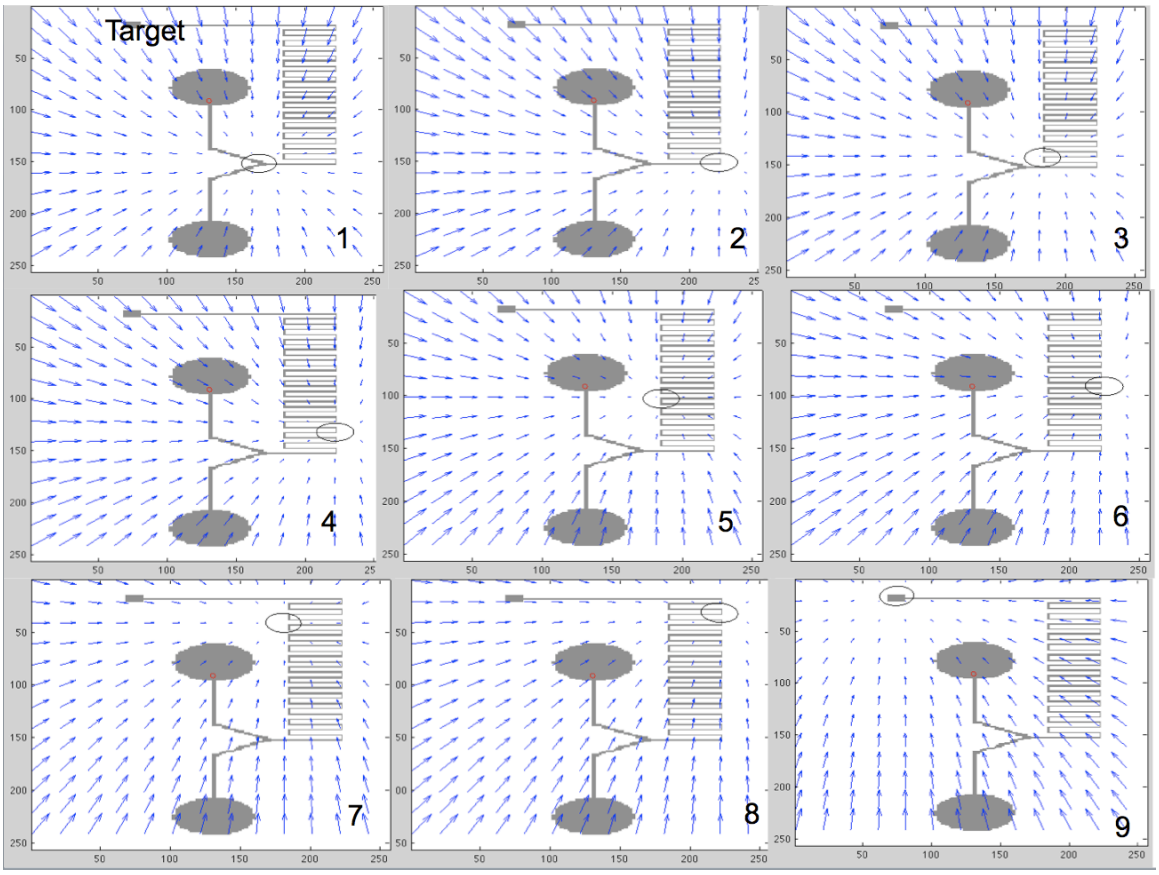

Figure 4.5. MTB magnetic control taking into account the geometry of the micro-fluidic channels.

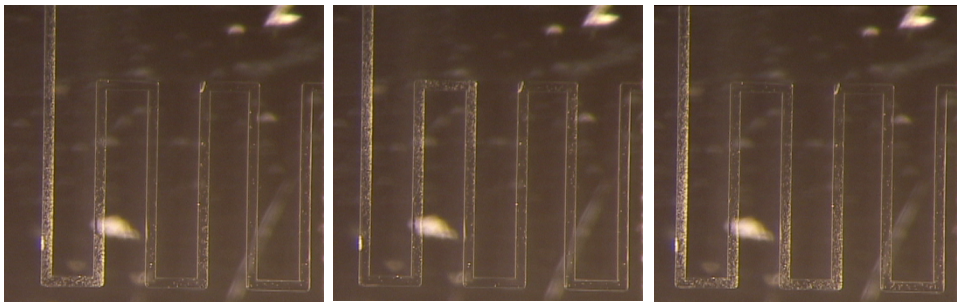

Figure 4.6. Optical microscope images sequence showing the MC-1 MTB traveling in a microchannel following a given pattern.

4.3.4 Magnetic control considering the microchannels geometry

The goal of this control method is to prevent the bacteria from being stuck in the microvasculature, while, automatically assign a target zone in order to cope with the lack of a road map. As depicted in Figure 4.7, modifying the shape of the target zone has as a consequence to change the direction by which bacteria attain the target without deviating the ones that already reached it. This is achieved through unbalanced current intensity between the two pairs of the coils system. Another approach would be to target smaller zones inside the target area that would be offset regarding the center as shown in Figure 4.8. Multiplexing in time several of these control methods can increase the outcome of the targeting procedure. In fact, targeting becomes possible even in complex microfluidic channels even if it takes more time. The bacteria navigate towards the target area in the U-channel using a two-time control method. As a matter of fact, having some knowledge of the architecture of the channel may help efficiently choose the control algorithm to employ. Even in the case of the tumour, several characteristic patterns exist and discussed in the literature.

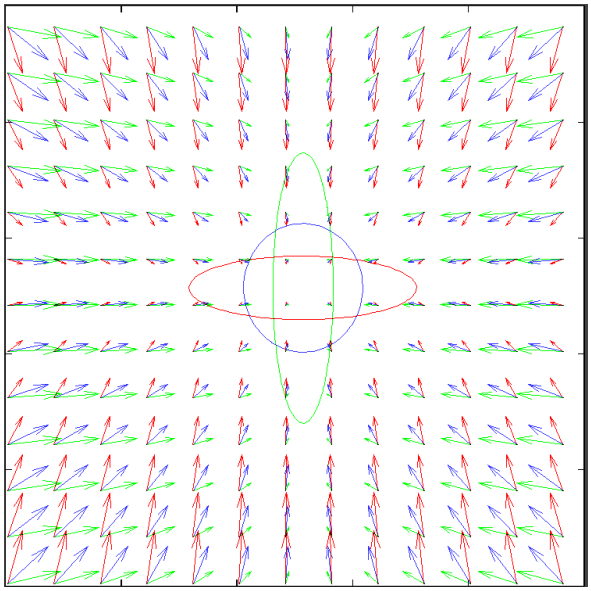

Figure 4.7. Unblanced gradient from the two pairs of coils changes the shape of the target zone, delimited by the 0.3 Gauss equipotential. Far from the target, the magnetic field specifying the direction of the MTB changes helping the bacteria to avoid obstacles.

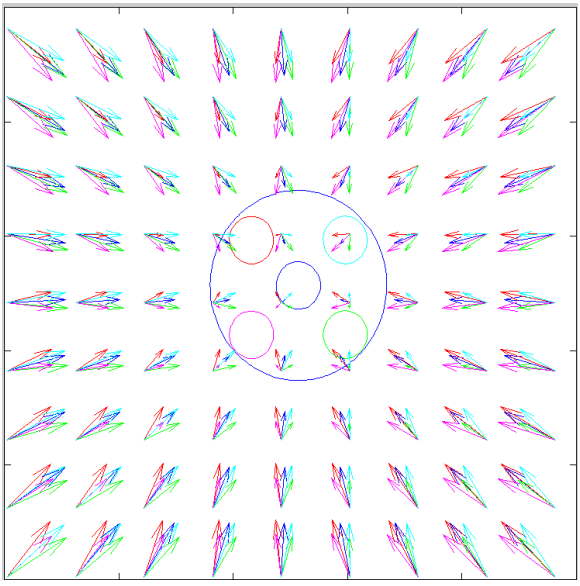

Figure 4.8. By using higher gradient, smaller targets inside the main one, can be specified, causing the far field to change direction. This technique can helo the bacteria to avoid obstacles.

4.4 Discussion and conclusion

The navigation approach we adopted consists of focusing a magnetic on the target. This strategy allows us to designate the target without imposing a specific way for the bacteria to reach it. This is especially pertinent for applications where a road map is not available. Modulating the intensity and the direction of the magnetic field lines, while keeping them directed toward the target, may prove to be advantageous in an in vivo targeting context.

The advantage of using bacteria to target tumours resides in their ability to target hypoxic zones that are characteristic of the center of solid tumours. Moreover, due to their active motility, bacteria can be an effective drug delivery agent by profiting from the leakages, reduced blood flow, and irregularities of the tumours vasculature. The commonly used bacteria belong to the *Clostridia*, *Salmonella* and *Bifidobacterium* strains. They can be genetically modified to express a certain gene that can have an antitumour effect or to suppress certain genes to strengthen the body's tolerance to them. The therapeutic effect comes from the bacteria thriving from consuming necrotic cancerous tissue, or from products such as endotoxins that can be used for the destruction of tumours. Bacteria can also be used as delivery agents for anticancer drugs and as vectors for gene therapy. When the bacteria is administered in combination with chemotherapy, extensive hemorrhagic necrosis of the tumours results in significant and

prolonged antitumor effects, which is best known as combination bacteriolytic therapy (COBALT).

Even though the preferential replication and accumulation of bacteria in tumours was proven, bacteria cancer therapy must face many challenges before it can become clinically effective. The first major limitation is the necessary high dose required to induce a significant therapeutic effect; this is often associated with severe toxicities. The inefficiency of bacteria to target small tumours, where a hypoxic zone has not yet been formed, constitutes the second major limitation. Also, combining bacterial therapy with other conventional methods, such as chemotherapy or radiotherapy, is mandatory in most cases for complete tumour consumption. Some of these limitations can be removed by using magnetotactic bacteria, the only living microorganisms to be proposed as a computer controllable drug delivery agent to solid tumours.

CHAPTER 5 A PLATFORM AND METHOD TO AGGREGATE AND CONTROL THE DISPLACEMENT OF MAGNETOTACTIC BACTERIA IN 3D VOLUME

5.1 Introduction

Magnetotactic bacteria (MTB) can be considered as self-propelled micro-bio-actuators or microcarriers in diverse applications where accurate computer directional control can be achieved by inducing a torque from a low intensity magnetic field. This torque acts on a chain of membrane-based nano-crystals known as magnetosomes, which operates like a magnetic nano-compass or nano-steering system embedded in each bacterial cell. MC-1 MTB also propel themselves with a flagella generating a thrust exceeding 4.0pN. Such features in this bacterial thus exhibit a highly advantageous mobility. This property, coupled with appropriately oriented computer-controlled magnetic fields of only a few Gausses, can be exploited for precise tasks on a nanometric scale. Notable examples to be cited are micromanipulation, microassembly and potentially, targeted drug delivery to tumoral sites in mice models, which has been demonstrated experimentally. In order to scale the force required to perform microassembly tasks, to propel future microrobots, or to increase the dose of therapeutic agents carried by the bacteria to a tumoral site, the ability of aggregating a required number of MTB within an adequate 3D volume and to move such aggregates in any desired directions becomes not only critical but essential. In this paper, a fundamental example of platforms referred to here as magnetotaxis systems is described. Such systems are based on a specific configuration of magnetic coils capable of producing a magnetic field environment to enable the formation of an aggregate within a given volume and to control its position in a 3D space using computer software.

5.2 Motile bacteria as micro-actuators

Over the last few years, motile bacteria have been considered as micro-actuators in engineered applications and systems to overcome the scaling limitation of previous methods of micro-actuation, including but not limited to the integration of an embedded miniature source of power. Yet, it is currently impossible to implement motor technology at such a microscale in accordance to existing modern engineering techniques. Initial applications relied on a system analogous to rafting, where an array of motile bacteria were attached to a flat surface, their flagella oriented in

such a way to collectively generate a fluid motion in microfluidic channels [114, 115]. However, the motility of flagellated bacteria was later exploited to propel or transport miniature objects [116] or as integral components in engineered micro-systems such as in micro-rotary motors [117] without directional control. But it was soon recognized that directional control was pivotal to fully exploit the capability of the bacteria to perform accurate tasks such as transporting a miniature object along a pre-planned trajectory. Although motile bacteria can respond to a variety of stimuli such as chemical gradients (chemotaxis), light (phototaxis), or oxygen gradients (aerotaxis), to name but a few examples, these stimuli cannot always be accurately controlled in a given space and may result in inaccurate directional control, such as run-and-tumble motions in chemotaxis gradients. Hence, the choice of an inappropriate stimulus would not only result in more difficult directional control if feasible, but would also limit their usage for applications requiring precision such as in micro-assembly that relies not only on an instant bacterial reaction but also on a continuous and accurate response to the directional control stimulus.

5.3 Bacterial transport application

The first bacterial transport application under directional control was reported in [46] where a single magnetotactic bacterium (MTB) [82, 83] (overall diameter of the cell between 1-2μm) under magnetotaxis [118] directional control was used to push a micro-bead along a planned trajectory. Later, other experiments proved that several flagellated bacteria could be used to move a larger microstructure using phototaxis [119] or as demonstrated in following experiments, electro-kinetic directional control [120]. Unlike electro-kinetic control that act on the microstructure and not on the bacteria, both phototaxis and magnetotaxis directional control have the advantage of directly influencing the bacteria while preserving its independent movement upon the specific properties of the object transported. Furthermore, although phototaxis and magnetotaxis modes of control are likely to be much more scalable — they can potentially operate on a larger working space due to the lower energy required for directional control, since no pulling force generated by an external source is involved — applications involving larger working volumes can be more easily supported.

5.4 The magnetotaxis advantage

Nonetheless, magnetotaxis directional control can prove to be advantageous over phototaxis control in particular applications, including but not limited to the delivery of therapeutic loads to targeted tumoral regions in the human body [44]. Indeed, not only could phototaxis control be limited by the effective depth of light penetration into the body, but also by not being able to allow the formation of an aggregate of bacteria within a tridimensional space. Such capability of aggregating the bacteria within a tridimensional volume could prove to be critical in enhancing targeted drug delivery through hard to access and unpredicteable microvasculature, while allowing the adjustment of therapeutic dosages by forming aggregates with a specific number of drug-loaded bacteria. The formation of such aggregates and its displacement control could also enlarge the range of applications in micromanipulation and microassembly tasks. Scaling the propelling force when attaching bacteria to a microscale object, such as a microstructure or a microrobot, is limited by geometrical features. For instance, the bacteria must be attached to the exposed surface and oriented in order to allow motion in the desired direction as it was the case in all previously mentioned examples. However, more flexibility in scaling force can be achieved without attaching the bacteria to an object by using instead an aggregate possessing the required number of bacteria aligned according to magnetotaxis directional control. Their flagella can then be oriented in order to collectively generate a fluid motion that would exert a displacement force on the manipulated micro-object while retaining the possibility to dispatch the same aggregate in order to perform more complex microassembly tasks. This principle was validated experimentally in [121] where an aggregate of approximately 5000 MC-1 MTB was controlled to assemble micro-bricks as a miniature replica of an Egyptian Step pyramid in less than 15 minutes. The experimental data gathered showed that a larger aggregate could actually push a micro-object faster, suggesting that bacteria at a certain distance from the manipulated object could also have an effect on its displacement. Preliminary analyses suggest that this long-range interaction between the bacteria and the micro-object happens through the surrounding fluid and could be related to the phenomenon of bioconvection.

5.5 Aggregation platform

In all cases, the workspace in which magnetotaxis control is exerted to force the MTB to aggregate and to move them in any directions must be within a proper magnetic environment

generated and controlled by what is referred to here as a magnetotaxis system or platform. For directional control of the MC-1 MTB for instance, such magnetotaxis platform generates a magnetic field to induce a directional torque on a chain of Fe_3O_4 magnetic nanoparticles known as magnetosomes that each MTB synthesizes during the growth phase. This magnetic torque aligns the bacteria along the direction of the external field while the bacterial flagella propel the cell forward. Although there can be variations in system's implementations, the fundamental magnetotaxis platform described here relies on three orthogonal pairs of magnetic coils. Each coil is separately powered by a programmable power supply enabling us to generate either a homogenous or a gradient magnetic field. A gradient field is used to aggregate the MTB while a homogenous field controls the motion of the aggregate.

5.5.1 Bacteria swarm formation

The gradient field shown in Figure 5.1 (a) is generated by two pairs of identical magnetic coils powered with the same electrical current amplitude but flowing in opposite direction (Maxwell configuration). In this particular example, this magnetic field configuration causes the bacteria swimming over a substrate to be constrained in a region referred to here as the aggregation zone where the magnetic field lines converge towards a zero Gauss location as illustrated by the arrows length in Figure 5.1 (a). The periphery of the aggregation zone is not at zero Gauss but at the higher magnitude of magnetic field that is unable to induce a sufficient torque on the chain of magnetosomes of the MC-1 cells in this particular case for directional control purpose for unconstrained aggregation zone, i.e. without obstacle preventing the migration of the MTB. Indeed, when gathered in the aggregation zone as depicted by Figure 5.1 (b) the MTB follow a continuous free circular motion as shown on the figure. Hence, once aggregated, the motion of the MTB is restrained inside the aggregation zone delimitated by a boundary where the magnetic field is less than a threshold that results in magnetotaxis directional control to be no more effective. Experiments estimate this threshold to be 0.3 Gauss for the MC-1 MTB with approximately 50% of the bacteria in the sample being inside the magnetic field equipotential of 0.1 Gauss.

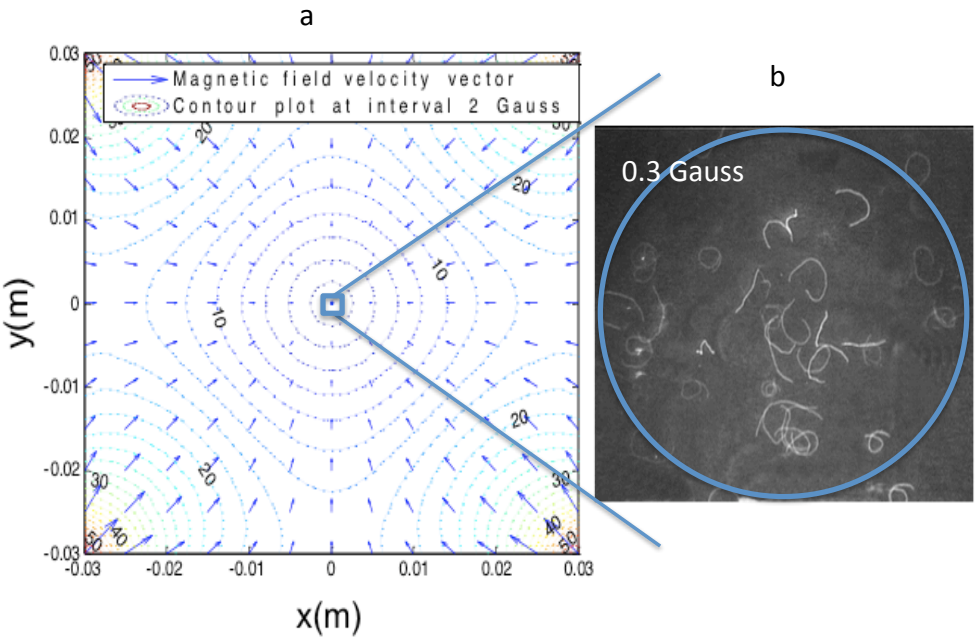

Figure 5.1. Magnetic gradient field used for MTB aggregation and swarm formation. Once the bacteria enter the area where the magnetic field is less than 0.3 Gauss, they begin to move in circle.

5.5.2 Bacteria swarm directional control

The size of the aggregate can be controlled by the magnitude of the gradient magnetic field where increasing the magnitude of the electrical current flowing in each coil result in a denser and smaller diameter aggregate. Changing the current ratio between the coils of the same pair shifts the aggregation zone position along the axis joining both coils. Therefore, moving the aggregate of MTB from one location to another can be done by repositioning the aggregation zone. The mathematical relationship between the target position along one axis, and the current ratio powering two coils of the same pair is given by

$$\frac{I1}{I2} = \sqrt[3]{\frac{r^2 + \left(z + \frac{d}{2}\right)^2}{r^2 + \left(z - \frac{d}{2}\right)^2}} \tag{5.1}$$

where *I1* and *I2* are the currents powering each coil, *r* (m) is the radius of the coils, *z* (m) is the position of the aggregation zone and *d* (m) is the distance separating the coils.

A simple method to move an aggregate of MC-1 MTB is presented in Figure 5.2 where the aggregate's initial position (represented by a circle in the center of the field) and the final position (represented by a dotted circle) are depicted. In order to form the initial aggregate in the center all the power supplies become active and are set with the same current amplitude flowing through the coils (if the initial position of the aggregation zone is set in the center of the pairs of coils) previously fabricated with the same specifications. For the aggregate to reach the targeted final location, a focused field setting a new aggregation zone is directed toward the new targeted location and is applied for a minimum period of time that is sufficient to allow the bacteria to reach the destination. The digital timing diagram below the figure shows the activity of each power supply and the relative current amplitude delivered to each coil. Then, after orienting the magnetic field lines towards the next location of the aggregation zone in order to avoid the MTB to diffuse too far from the axe separating the initial position to the next position of the aggregate, the aggregation zone is then set on the new target by activating all the power supplies using unbalanced current magnitudes in each coil to offset and localize the zero Gauss magnetic field in the new aggregation site. This method although simple will avoid MTB to be diffused outside the regions separating the two successive locations of the aggregation zone but would result in a distortion in the shape of the aggregate.

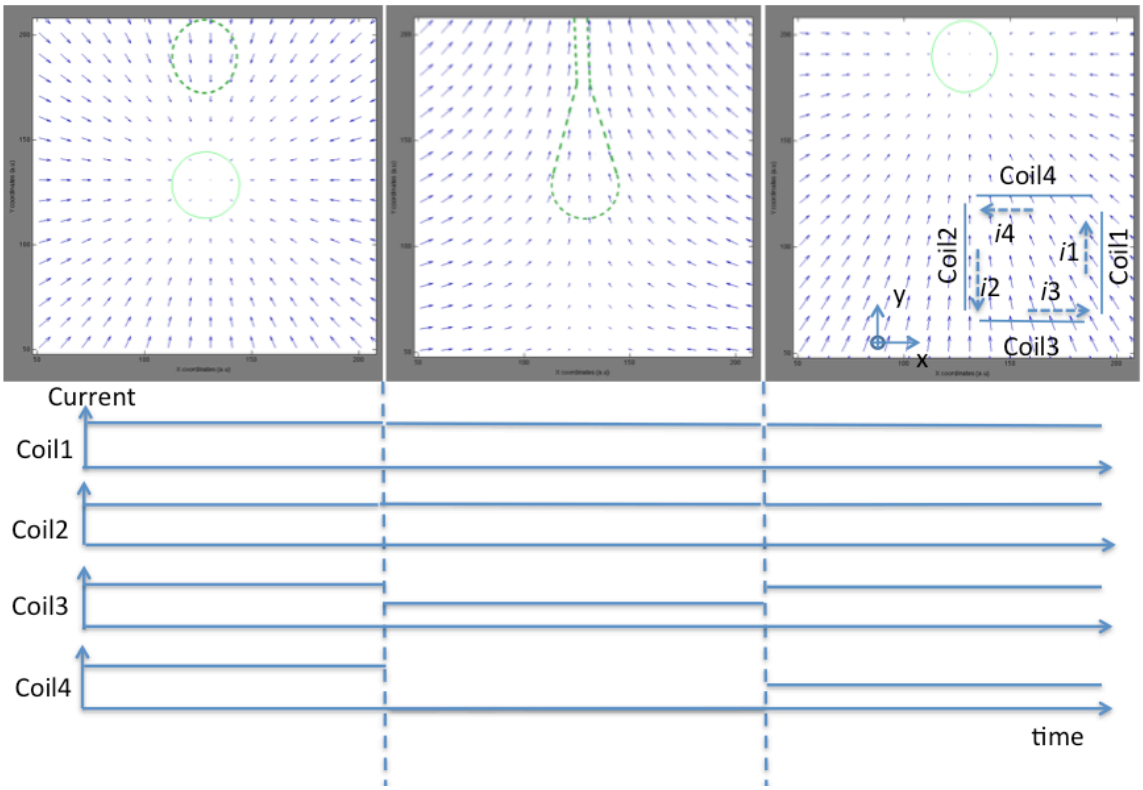

Figure 5.2. Bacteria aggregate motion control along a pre-planned path. The circle with continuous line is the actual position of the bacteria, while the dotted-line circle represent the target position or the bacteria in the move. Aggregate formation is assured by the application of a gradient magnetic field. Shutting down the power for the coil4 result in displacement of the bacteria swarm along a funnel path. Considering the distance between the two positions and the mean bacteria speed, the time required for application of this field is determined. Once the time is up, the gradient field configuration is reapplied with unbalanced currents that cause the bacteria to aggregate in this new position.

5.5.3 Tridimensional swarming

The formation of the aggregate as described previously is facilitated by the presence of a planar obstacle such as a microscopic slide, which would most likely be the case for microassembly tasks. It should be noted also that the zero Gauss location could be set below the microscope slide at the constrained aggregation zone in order to provide sufficient directional magnetic field magnitude to align the MTB to achieve enhanced fluid motion for micromanipulation and microassembly tasks. But for other applications such as interventions

inside the human body, aggregate's formation and controlled motion within a tridimensional space may be required. In such a case, the method described previously will not be applicable because the magnetic field would diverge in the z-direction (i.e. the axe previously constrained by the microscope slide). To overcome this limitation, a virtual magnetic barrier has to substitute this physical obstacle on which the MTB could accumulate. A solution to this issue is to generate a magnetic monopole. However, in a static magnetic field, such monopole cannot be achieved in a 3D volume as magnetic fields that converge from one direction will exit from the other direction. This limitation can be solved simply by multiplexing over time the strength and orientation of the magnetic field configurations to create a delimited zone in which the bacteria are constrained within a given aggregation zone. Figure 5.3 (a) shows the magnetic fields obtained when activating 5 coils, two pairs along the x- and y-axis, as well as one coil along the z-axis. In this configuration, the magnetic field converges towards the center of the x-y plane, while it diverges in only one direction along the z-axe. Figure 5.3 (b) shows the second magnetic field configuration when the other coil along the z-axe is activated while the first is turned off. Multiplexing these to magnetic field configurations in time allows the formation of an aggregate of MTB. Considering that the MTB are only sensitive to the direction of the magnetic field, when we normalize the magnetic field intensity of these two configurations at regular intervals in space and add them together, we obtain the configuration shown in Figure 5.3 (c). In fact, we can notice that some time after activating the magnetic field sequence, the bacteria will accumulate to form an aggregate.

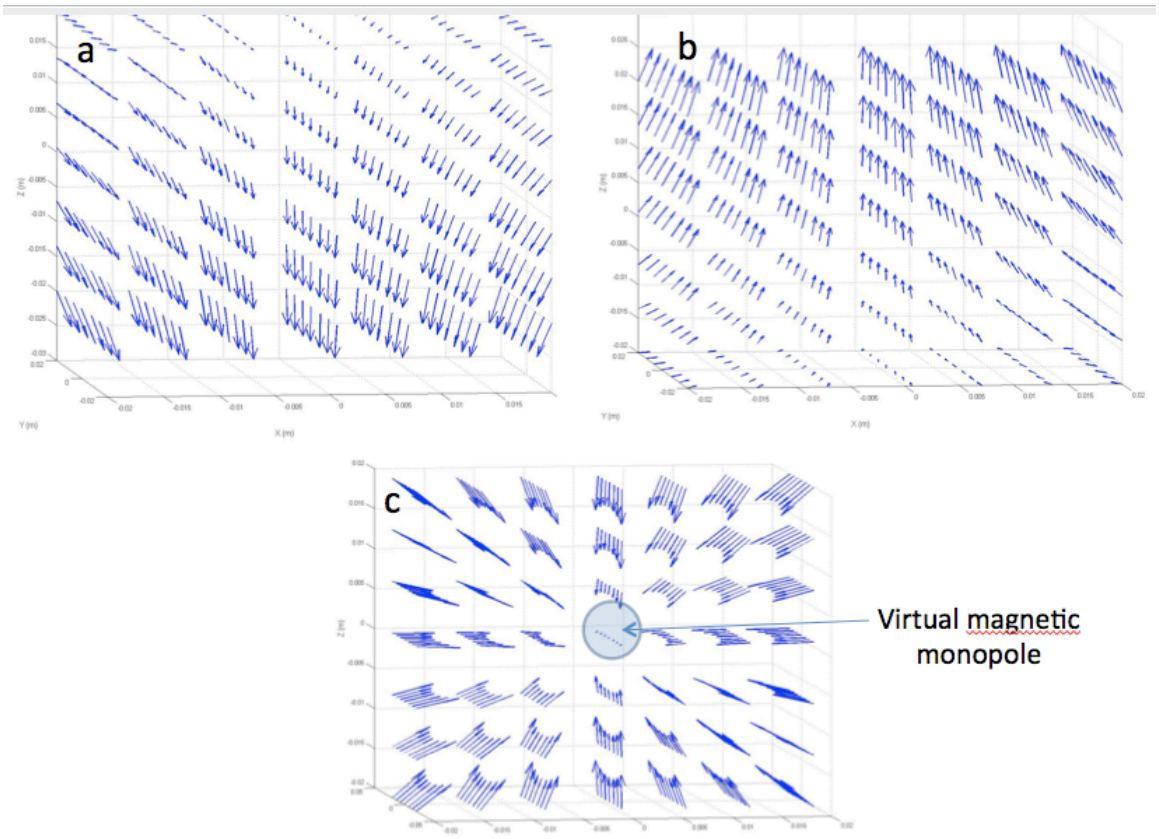

Figure 5.3. Applying a magnetic field generated by 5 coils at a time multiplexed in order to cover all possible permutation resulted in a mean bacteria displacement toward the center of the coils. The time required for the aggregate formation using this control method is higher than formation of an aggregate in a 2D surface, because the applied magnetic field does not provide a direct path to the target for each instant of time. Again, powering the coils with unbalanced currents, cause the aggregate zone to be shifted.

5.6 Tridimensional swarm control

Figure 5.4 shows the tridimensional magnetic control of an aggregate of MTB. The aggregate is visible to the naked eye because of the increase in density of MTB. The MTB are first guided to the central plane of the sample as shown in Figure 5.4 (1) by activating both coils in the z-axis. The aggregate is then produced following the technique described in the previous section. The aggregate can then be moved along any orthogonal direction by using 5 coils. Again, one can observe the distortion of the aggregate caused by variations of the swimming velocities

among MTB in the aggregate. Such distortion can be minimized by replacing a single longer transition path by several shorter segments.

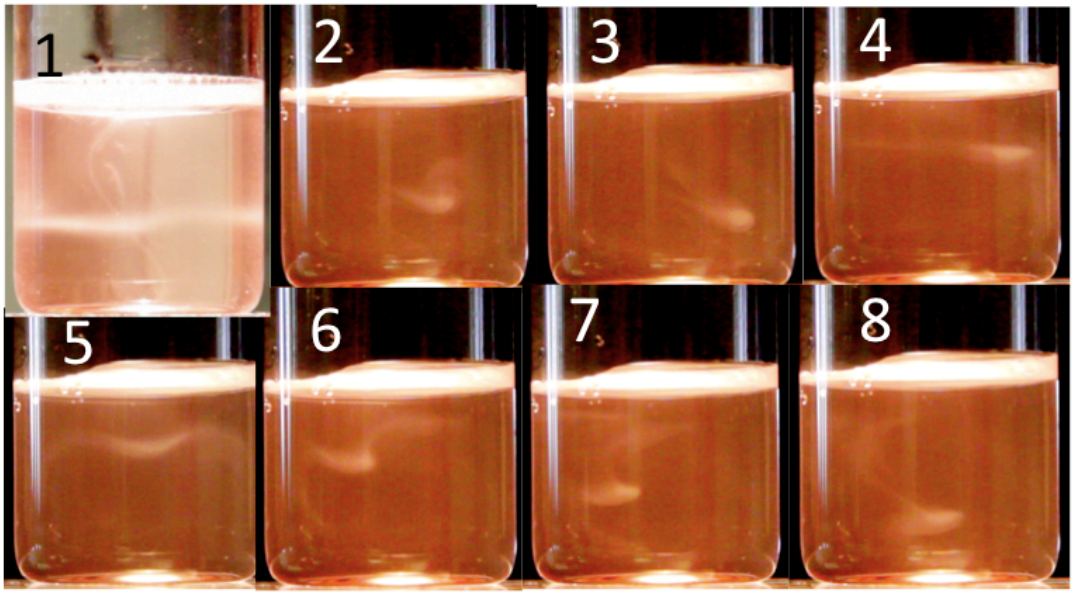

Figure 5.4. A demonstration of bacteria control in 3D by multiplexing the power supplies over time. Powering only one pair of coils in a Maxwell configuration restrains the bacteria motion to a plane as depicted in (1). Photos (2) to (8) shows 3D control of a bacteria aggregate using the control method described in the text.

CHAPTER 6 TUMOUR TARGETING BY COMPUTER CONTROLLED GUIDANCE OF MAGNETOTACTIC BACTERIA ACTING LIKE AUTONOMOUS MICROROBOTS

6.1 Introduction

Improvement of the outcome of cancer therapy could be granted by overcoming the physiological barriers that a drug encounters on its way to the site of administration [9-20]. Solid tumours, which account for 85% of all tumours, contain heterogeneous blood vessels, which cause a non-uniform drug distribution, and involve a high interstitial pressure that prevents drug molecules, particles, or cells from easily diffusing inside the tumour. Furthermore, systemically injected drugs are prone to bind non-specifically to healthy tissues or to be cleared by the body before a therapeutic effect takes place. Thus, as significant dosage of the active agent is needed in order to induce therapeutic effects, systemic cancer therapies cause many side effects, which are associated with higher systemic exposure. Existing therapies are continually improved to make systemic therapies more effective on tumours and less harmful to the body. The most significant advances are the use of active targeting [4] to ensure higher binding of encapsulated drug molecules on tumour cells.

Direct drug delivery aims to restrain the cytotoxic drug effect to the tumour site. It is often associated with the use of drug encapsulated in magnetic particles that are steered inside the vasculature and delivered to the tumour using magnetic gradients [48-52]. An external power source in this case is required to induce a force on magnetic micro or nano-particles. Magnetic drug targeting is also possible using gradients field generated from a clinical magnetic resonance imaging (MRI) system, profiting from its imaging capabilities and integrated hardware and software for deep tumour targeting [58-64]. However, an autonomous microsystem capable of direct-targeted delivery to a specific location in the body is beyond today's technological achievements. Such autonomous microsystem, if made available one day, could be similar to bacteria since they do have essential components for such application. Bacteria possess the ability to swim in low Reynolds number hydrodynamics such as the human blood flow and own a bench of sensors allowing them to react to specific stimuli in addition to their ability to produce and synthesize molecules and toxins.

Many sorts of bacteria, like *Clostridia*, *Salmonella* and *Bifid bacterium*, accumulate preferentially in tumours [67-74]. They have been considered as potential candidates to fight cancer because of their ability to reach hypoxic regions of solid tumours, which are hard to target with conventional therapies. *Clostridium novyi*, obligate anaerobic bacteria, causes significant xenograft tumour regression in mice when administered in combination with chemotherapy and an antivascular agent [69]. They are found to successfully germinate in the hypoxic parts of the tumour. While *C. novyi* have been depleted from their lethal toxin prior to intravenous injection, *Salmonella typhimurium* are proven to be better tolerated by the body at high dose as demonstrated by initial clinical trials [81]. Presence of quiescent and necrotic cells is found necessary for the accumulation of *S. typhimurium* in the central region of cylindroid polycarbonate lids, which suggests a minimum tumour size is required for bacterial therapy usability. *Bifidobacterium adolescentis*, normal inhabitants of healthy human and animal intestinal tracts, have also been used as the delivery system to transport endostatin genes to solid tumours. Once more, trials on tumour bearing mice revealed the presence of this bacillus only in the tumour, sparing normal tissues.

The foundation of the bacterial cancer therapy goes back to the pioneering work of Dr. Coley who was among the first to deliberately induce a bacterial infection in final stage patients to treat cancer [66]. Even though the preferential replication and accumulation of many bacteria in tumours was proven since then, bacteria cancer therapy faces many challenges before it becomes clinically effective. The first major limitation is the necessary high dose required to induce a significant therapeutic effect, which is most of the time associated to severe toxicities. The inefficiency of bacteria to target small tumours, where a hypoxic zone is not formed yet, constitutes the second major limitation. Also, combining bacterial therapy with other conventional methods, such as chemotherapy or radiotherapy, is mandatory in most cases for complete tumour consumption.

In order to take profit from the capability of the bacteria to reach the hypoxic zone of tumours, systemic administration and bacterial attraction to the tumour must be optimized. We propose to use magnetic fields to guide the bacteria to tumours instead of chemotaxis and aerotaxis, which are the conventional ways bacteria use to invade the tumour. Magnetotactic bacteria (MTB) orient and swim following the direction of an applied magnetic field [46, 82-84]. We propose to use them as remotely computer-controlled drug transporters. We demonstrate in this paper that a

significant tumour invasion and penetration can be achieved through direct navigation by magnetic fields of MTB.

6.2 Materials and methods

6.2.1 MC-1 magnetotactic bacteria

MC-1 strain was chosen for the in vivo experiment due to its high motility speed, appropriate size and its magnetotactic ability. At the difference of the bacteria that proliferate in the tumour, the MC-1 cannot reproduce and grow at 37 degrees. In fact, at 37 degrees, its speed decreases from $180\mu ms^{-1}$ to $20\mu ms^{-1}$, 40 minutes after its exposure, time after which the bacteria die. Not only the temperature affects MC-1 MTB swimming speed, the channel diameter also has an effect. It is found experimentally that the speed of MC-1 MTB goes from $180\mu ms^{-1}$ in open space to $120\mu ms^{-1}$ inside a 4µm channel. MC-1 synthesizes Fe_3O_4 magnetic nanoparticles, called magnetosomes that it assembles into a chain that acts as a compass forcing the bacteria to align with an applied magnetic field. When the magnetosomes size is optimized for maximum magnetic field sensitivity, MC-1 becomes sensitive to magnetic fields as low as 0.3 Gauss.

6.2.2 Animal tumour model

MDA-MB-231, a breast cancer human cell line, was injected s.c. on each flank of nu/nu 7 CD1 female mice. After tumours growth, MTB navigation experiments started. A 100µl of $1x10^8$ MTB/ml in PBS was injected in the trail vein of the animal. Depending on the magnetic treatment and the MC-1 injection, four groups were discerned. The first group (group I) was a control that lacked a MTB injection and an applied magnetic field. The second group (group II) was also a control group that received a MC-1 injection but lacked the applied magnetic field. The third group (group III) was an experimental group that received a MC-1 injection and a where a magnetic field was applied to target the tumour. An electromagnet was used for MC-1 guidance for group III.A, while 3D coils were used for group III.B. The magnetic field was applied for 30 minutes, then the animal was sacrificed and the tumours, liver, spleen, and kidney were extracted for immunohistochemistry analysis.

Two tumours, one on each flank, were grown in mice belonging to the group III. One tumour served as a target, while the second was a control. Comparisons between tumours from the

different groups and tumours belonging to the same mouse were done in order to assess the magnetic advantage over passive targeting. Table 6.1 presents a summary of the experimental and control groups used for the experiments.

Table 6.1. Description of the groups used in the in vivo experiments.

GROUPS	MC-1 INJECTION	Magnetic field application	NUMBER OF TUMOURS PER MOUSE	DESCRIPTION
Group I (1 mouse)	No	No	1	Control group used to assess the validity of the immunohistochemistry coloration. In the text we refer to this group as a negative control group.
Group II (2 mice)	Yes	No	1	Control group used to estimate the magnetic advantage over passive targeting. In the text we refer to this group as a positif control group.
Group III.A (2 mice)	Yes	Yes	2	Experimental group. Magnetic field generated with an electromagnet (similar to a permanent magnet). The magnet was placed externally to the tumour.
Group III.B (2 mice)	Yes	Yes	2	Experimental group. Magnetic field generated with a tridimensional coils system. The magnetic field was focused on the center of the tumour.

6.2.3 Magnetic setups

Two different magnetic setups are used; the first one consists on an electromagnet placed on the targeted tumour and powered by a current source delivering a magnetic field of 20 Gauss on its tip. The magnetic field is estimated to be 15 Gauss in the center of the targeted (primary) tumour and 3 Gauss in the center of the secondary tumour. The second setup consists on three orthogonal magnetic pairs of coils capable of generating a focused magnetic field on the target, as shown in Figure 6.1. In this case, the magnetic field is zero in the center of the targeted tumour. The non-targeted tumour was positioned inside the setup so that there is less magnetic targeting, which was not the case with the electromagnet since a guiding magnetic field on the secondary tumour was present but having lower intensity.

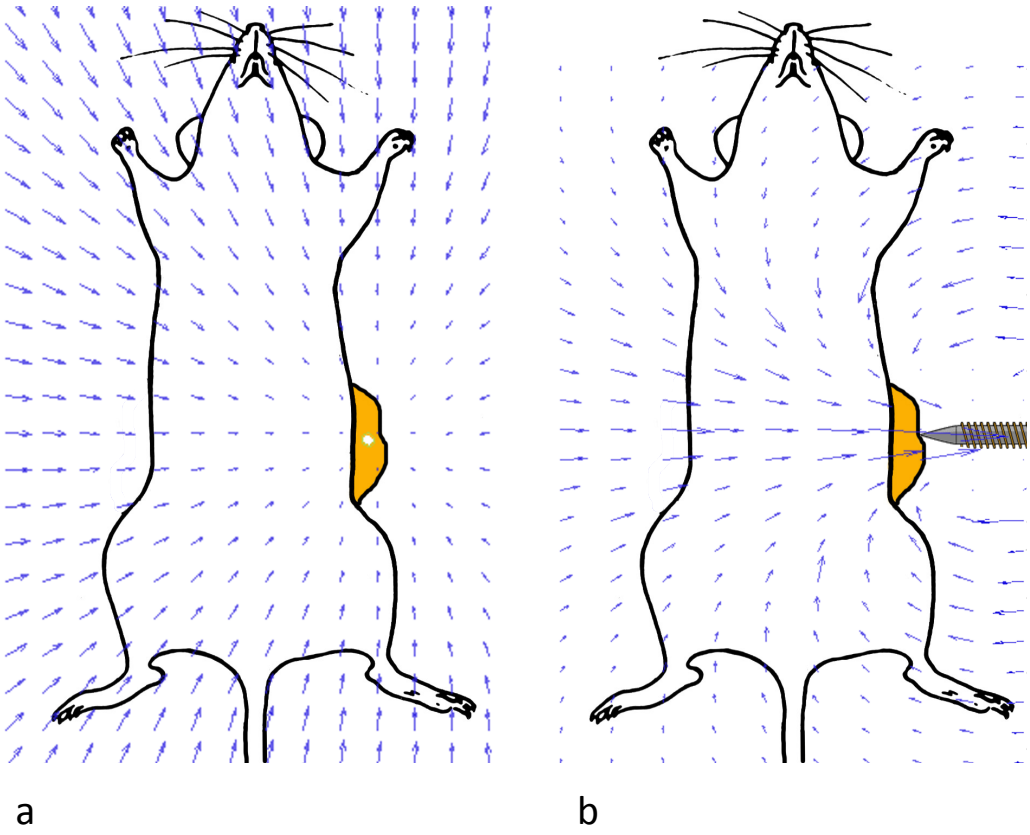

Figure 6.1. Magnetic field simulation showing the magnetic field lines as generated by (a) a 3D magnetic coils system and (b) an electromagnet or a permanent magnet. The magnetic field in (a) is focused on the target, and thus the bacteria will be attracted to the center of the tumour. However, in (b), the bacteria are attracted to the electromagnet tip.

6.2.4 Immunohistochemistry and images analysis

Tumours and collected organs were fixed in a 10% formalin solution for immunohistochemistry analysis. A longitudinal section of each tumour was coloured to highlight the MC-1 distribution. In the immunohistochemistry slides, we could identify a MC-1 bacterium as a 1 to 2µm-sized coccus with a yellow to brown color. Bacteria were counted using the Cell Counter plugins of the ImageJ software (Wayne Rasband, National Institutes of Health, USA).

6.3 Results

6.3.1 Organs and blood analysis

Following the i.v. injection, we found MC-1 bacteria in the liver, the spleen, the tumour, and the blood. Figure 6.2 shows two histology slides of the spleen and the liver. The bacteria are recognized by their brown color, circular shape and characteristic size. They have been found to accumulate in the liver and the spleen but we did not find any in the kidney. Analysis of blood samples at the end of the experiment revealed the presence of MC-1 in a normal motile state. In fact, because the animal was under anesthesia, the temperature of the body decreased which increased in its turn the in vivo lifetime of the bacteria.

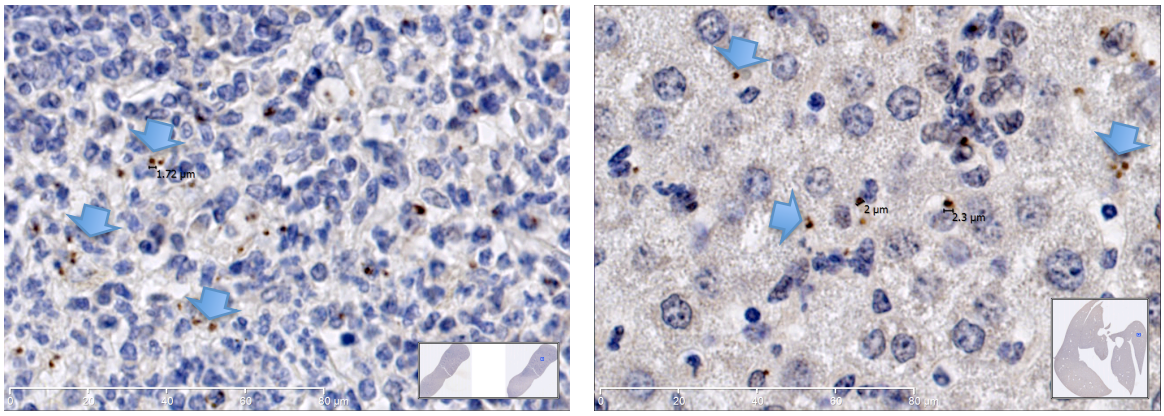

Figure 6.2. Immunohistochemistry coloration of a section of the spleen and the liver displaying the presence of MC-1.

6.3.2 Comparison between the control groups and the experimental groups

The group I tumour that did not receive any treatment was analysed in order to confirm the specificity of the antibody used for the immunohistochemistry. Very few unspecific reactions were noticed for the group I, which can be explained by antibodies binding to some cellular debris. Meanwhile, when compared to groups where a bacteria injection was carried out, the number of wrong signals found was up to 38 times less. Table 6.2 summarizes some key data for

the in vivo experiments. We counted the number of bacteria in two histology slides for each tumour. Table 6.2 also displays the higher density of the bacteria that was observed inside a FOV of 100μm^2, and the invaded surface of the tumour with more than 20 MC-1 cells per area of 100μm^2. Figure 6.3 shows in a graphic bar the number of MC-1 cells found in tumours for each of the 4 groups. Tumours of the group III.B were the most targeted showing the highest number of bacteria in the histology slide. Also, this group exhibited the highest observed bacteria density. In fact, the area, containing a cell density of more than 20 MC-1 per 100μm^2, was more than twice as big as the one observed for the groups II and III.A.

A color map graphic showing the distribution of the MC-1 cells in the tumour is depicted by Figure 6.4. We notice a higher presence of MC-1 in the center of the tumour for the group III.B where the bacteria accumulated in large quantity. A histology portion shows an example of a highly invaded section of the tumour's centre belonging to the group III.B.

Table 6.2. Summary of the key data obtained after histology slide analysis for the control and the experimental tumours.

TUMOUR	TUMOUR SURFACE (mm^2)	MEAN NUMBER OF BACTERIA	MAXIMUM DENSITY (NUMBER OF MC-1 IN 100 μm^2)	INVADED SURFACE* (mm^2)
Group I	182	24	4	0
Group II	124.5	205	40	0.41
	105.5	618	37	0.88
Group III.A	150	312	55	0.53
	72.1	344	70	0.80
Group III.B	85	905	95	2.28
	185	914	54	1.47

* Only a density of more than 20 MC-1 in 100 μm^2 was considered

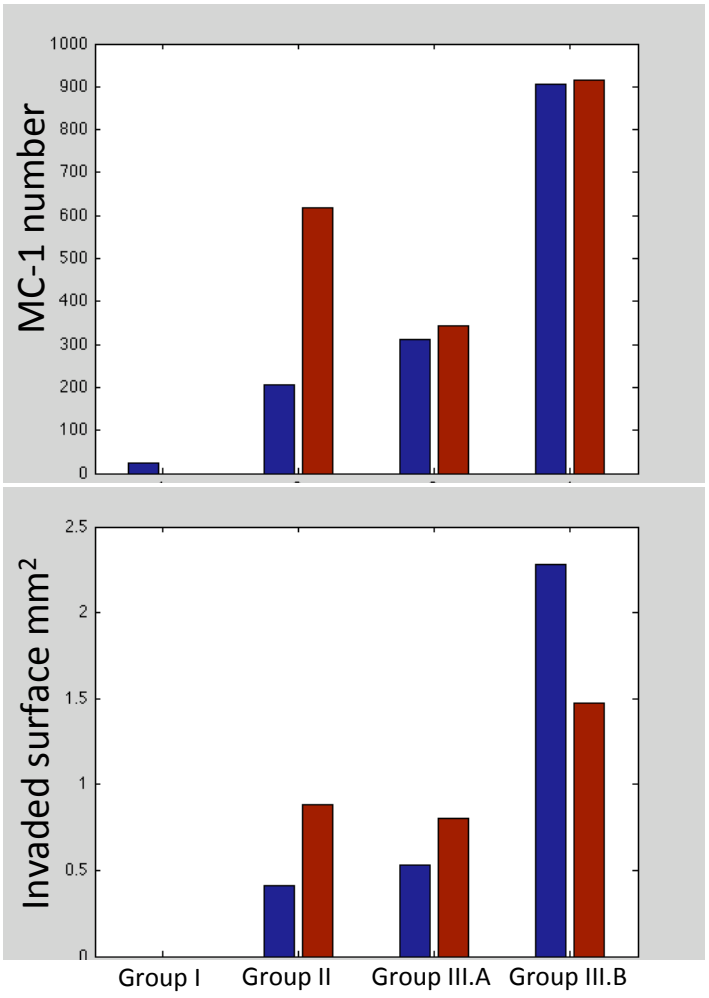

Figure 6.3. Graphic bar showing (up) the number of bacteria found in tumours for the 4 groups and (down) the invaded surface where a density of more than 20 MC-1 cells per 100µm^2 was found.

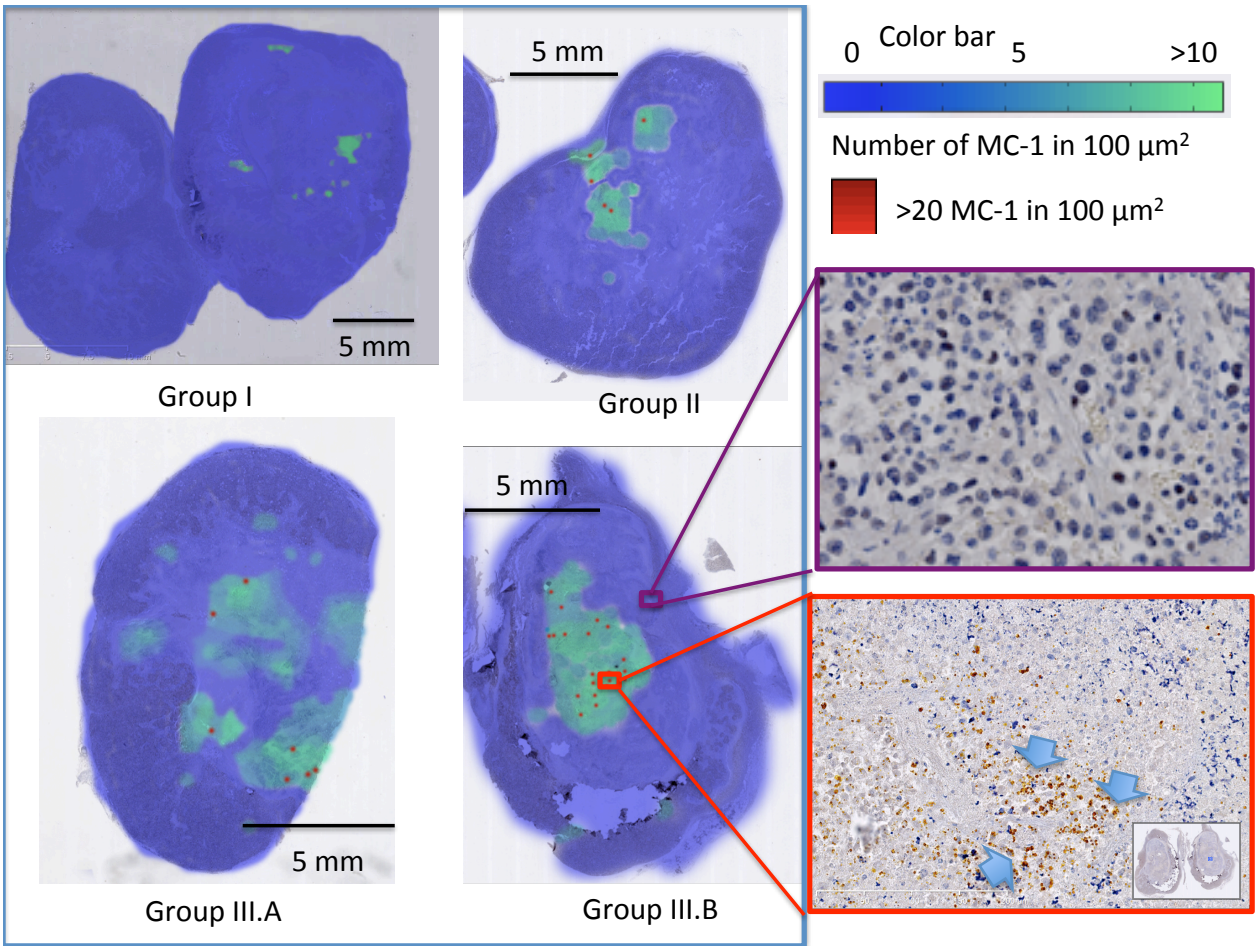

Figure 6.4. In vivo MTB targeting experiment. MDAMB-231 tumour cells were grown in the flanks of nu/nu CD1 female mice. After MTB intravenous injection, a magnetic targeting procedure using an electromagnet (group III.A) and a 3D coils system (group III.B) was applied. An immunohistology analysis of the tumours reveals the presence of MTB in the necrotic region. The MTB exhibit a particular color as well as a characteristic size and shape which allow their differentiation it from the xenograft cells. A color map of the four experimental tumours groups is shown. The color corresponds to the bacterial count inside a FOV of 100µm^2. We notice a wider distribution of MTB in the group III.A and group III.B compared to the group II. In fact, in group III.A and group III.B a magnetic guidance was imposed while for the group II only the blood flow is responsible for the delivery of MTB to the tumour.

6.3.3 Comparison between tumours from the same mouse

The experiment that most highlights the magnetic advantage over passive bacteria transport is the one involving comparison between tumours implanted in the same mouse with the magnetic field focused on one tumour but not on the other. Table 6.3 presents the surface of the tumour's section

and the number of bacteria that were found. Tumours belonging to the group III.B, which received a magnetic control using the 3D coils system, depict a number of bacteria in the targeted tumour that is 10 times larger than its counterpart in the non-targeted one. However, there is no clear indication whether or not there is a magnetic advantage in using the electromagnet for MTB delivery to tumours. Figure 6.5 shows the number of bacteria in the targeted and in the non-targeted tumours in a graphic bar for groups III.A and III.B.

Table 6.3. Summary of the key data obtained after histology slide analysis for the tumours implanted on the same mouse.

TUMOUR GROUP		TUMOUR SURFACE (mm^2)	NUMBER OF BACTERIA
Group III.A	*Targeted Tumour*	150	312
	Non-targeted Tumour	53.9	34
	Targeted Tumour	72.1	344
	Non-targeted Tumour	93.5	700
Group III.B	*Targeted Tumour*	85	905
	Non-targeted Tumour	105	28
	Targeted Tumour	185	914
	Non-targeted Tumour	70.4	145

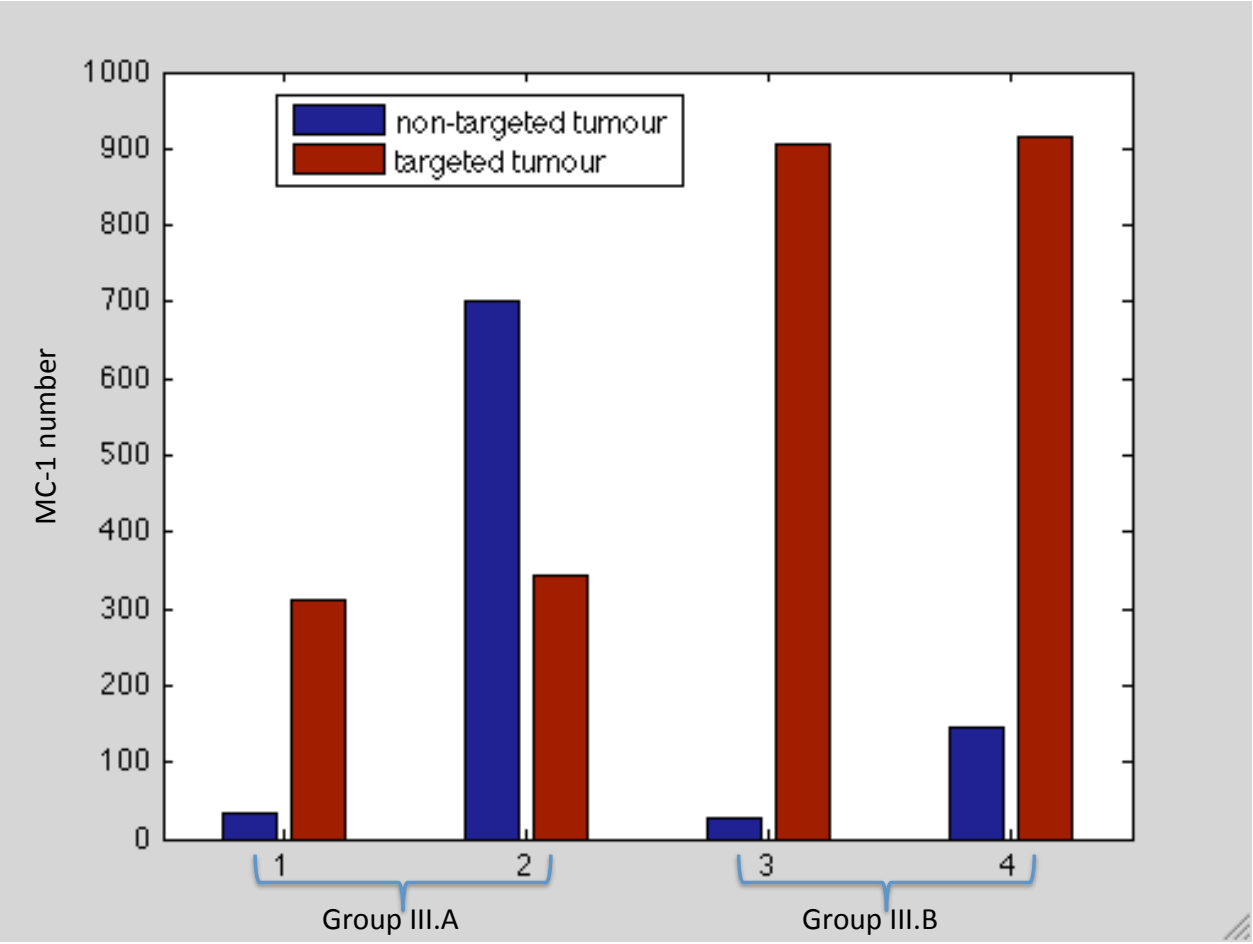

Figure 6.5. Graphic bar showing the number of MC-1 cells for the tumours implanted on the same mouse. Each pair of bars represents respectively the non-targeted and the targeted tumour for one mouse. This experiment has been conducted only for the group III.A and group III.B. A higher magnetic targeting specificity is obtained with the 3D magnetic coil systems rather than the electromagnet.

6.4 Discussion

The in vivo results presented in this paper constitute a preliminary investigation on using magnetotactic bacteria to target tumours. As it was reported in the past with other bacteria types, the magnetotactic bacteria were able to reach deep tumour regions often characterized by necrosis and hypoxia. A special magnetic system, which was designed and built especially for these in vivo experiments, helped the accumulation of the bacteria in the tumour through the application of a focused magnetic field on the target. In this paper, we report on average twice the number of bacteria found in the tumour when a magnetic field was applied using the 3D magnetic coils

system over passive transport with the blood flow in the absence of any magnetic field. A second experience based on the comparison of tumours implanted in the same animal reported 10 times more bacteria in the targeted tumour over the non-targeted tumour. This result suggests that the applied magnetic field may also be used to avoid a specific zone in the body.

After being injected in the blood stream, the bacteria are transported by the flow, and since the tumour is highly vascularized, especially in the periphery, we naturally expected to find bacteria without the application of a magnetic field. In fact, finding bacteria in deep tumour regions highlights the advantage of the bacteria active motility and its effective molecular motor over passive targeting.

To avoid systemic circulation, magnetotactic bacteria can be used for localised delivery of therapeutic drugs to solid tumours. However, small animal tests do not allow the reproduction of a localised delivery experiment, as projected in the future. Ideally, the bacteria have to be injected as near as possible to the tumour site, or in its periphery. In this case, tumours that are accessible through natural means, such as colorectal cancer, become more attractive candidates for this kind of drug delivery.

CHAPTER 7 DESIGN OF A MTB-BASED SYSTEM FOR HUMAN CANCER TREATMENT

7.1 Introduction

This section presents the overall robotic platform responsible for MTB drug delivery. Aside from the computer controlled magnetic coils system responsible for MTB navigation, magnetic resonance imaging will be used for operation monitoring and road map evaluation.

7.2 Platform design

The future robotic platform that will encompass MTB drug delivery is built around a modified magnetic resonance imaging (MRI) system that will provide MTB navigation, body imaging, and emboli particle steering. The MTB navigation is granted by a set of magnetic coils, similarly described in chapters 4 and 5, that will be placed outside of the MRI bore. In fact, the high static magnetic field of the MRI prevents the use of the MRI as well as its gradients for MTB navigation because it is not possible to change the direction of the magnetic field inside the MRI. The 3D Steering Magnetic Coils (SMC), represented in Figure 7.1, will be connected to the MRI bore through the patient table. This table will be placed inside the MRI for imaging and inside the SMC for MTB navigation. The imaging capabilities of the MRI will be used for the road map sketch, target imaging as well as quantification of targeting success at the end of the procedure. The procedure will theoretically end when the bacteria are considered dead, about after 30-45 minutes after MTB injection). The MTB targeting methodology is as follows:

- Tumour imaging and road map sketch. (Using MRI)
- Injection of the MTB loaded drug and guidance to the tumour site based on a vasculature model of the tumour (outside the MRI, inside the magnetic field control coils).
- Imaging and quantification of targeting success using MRI images by comparing them to the ones taken before injection. The percentage of MTB reaching the tumour can be obtained using calibration curves representing the MR-relaxation rate for different MTB concentration.

Although the bacteria approach would perform better than any other in the low Reynolds hydrodynamic environment of the capillary network, their limited thrust would not be able to counteract the greater flow rates encountered in larger diameter blood vessels. For this reason, emboli particles can be used to obstruct the blood vessels supplying the tumour with a technique known as Magnetic Resonance Propulsion (MRP) discussed in the first chapter of the literature review. The coils responsible for the navigation and steering of the magnetic emboli particles are denoted as SGC on the Figure 7.1.

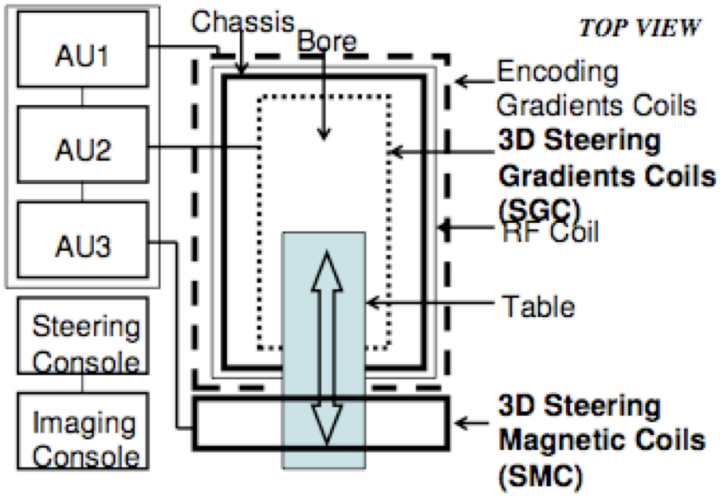

Figure 7.1. Robotic platform depicting the MRI bore in which lies 3D Steering Gradient Coils (SGC) aimed to propel emboli magnetic particles. Facing the MRI bore, the 3D Steering Magnetic Coils (SMC) are responsible for MTB guidance and delivery to the tumour. The MRI table moves the patient from the inside of the MRI to the SMC. The magnetosomes inside the MTB cause signal loss on MR-images that allows, with the help of a proper calibration curve, the evaluation of the percentage of bacteria that reach the target.

7.3 Magnetic Resonance Imaging of MTB

Magnetic nanoparticles have been used for a long time as contrast agents for Magnetic Resonance Imaging (MRI). Depending on the size of the nanoparticles, the contrast agents are classified as SPIO (superparamagnetic iron oxides) for nanoparticles of diameters greater than 50nm or USPIO (ultra-small superparamagnetic iron oxide) for those of diameters less than 50nm [122-124]. Even though their effect on the MR-image is different, both SPIO and USPIO rely on the magnetic susceptibility difference to their surroundings to create strong local magnetic field heterogeneities.

Besides their usage as contrast agents, superparamagnetic nanoparticles are used for cell-labeling prior to in vivo injection [125]. In fact, nanoparticles used for labeling are uniformly distributed and are attached to the cells via antibody binding. These nanoparticles alter the MR-signal because of their effect on the magnetic field. In the case of MTB, the nanoparticles are embedded in the bacterial cells rather than being attached to the cell membrane.

7.3.1 Magnetosomes effect on MR-signal

MTB synthesize magnetosomes in a permanent single domain size range. The particles are then uniformly magnetized with maximum magnetic dipole moment per unit volume [100]. The induced magnetic field from a single magnetosome can be approximated by the field of a dipole as described by Equation 7.1 where $\mu_0 = 4\pi 10^{-7}$ H·m^{-1} is the permeability of free space.

$$\vec{B}'(P) = \frac{\mu_0}{4\pi}\left(3\frac{(\vec{m}.\vec{r})\vec{r}}{r^5} - \frac{\vec{m}}{r^3}\right) \tag{7.1}$$

For a uniformly magnetized object, the dipolar magnetic moment $\vec{m}$ (A·m^2) is given by

$$\vec{m} = \frac{4}{3}\pi a^3 \vec{M}_{SAT} \tag{7.2}$$

where $\vec{M}_{SAT}$ is the saturation magnetization of the object, and a, its radius (m) if its shape is approximated as a sphere. Not only does the size of the magnetosomes contribute to the total magnetic dipole moment (the sum of the moment of the individual particles), but their arrangement along a chain does as well. Figure 7.2 shows a numerical simulation of the magnetic field lines induced by a magnetosome chain superimposed on top of an image of a MC-1 magnetotactic bacterium. Typically, there are 5 to 14 magnetosomes per cell with sizes averaging between 70 and 100nm. For our simulation, we consider a chain of 11 magnetosomes in length with a mean magnetosome diameter of 80nm. The saturation magnetization of magnetite is 0.6 Tesla.

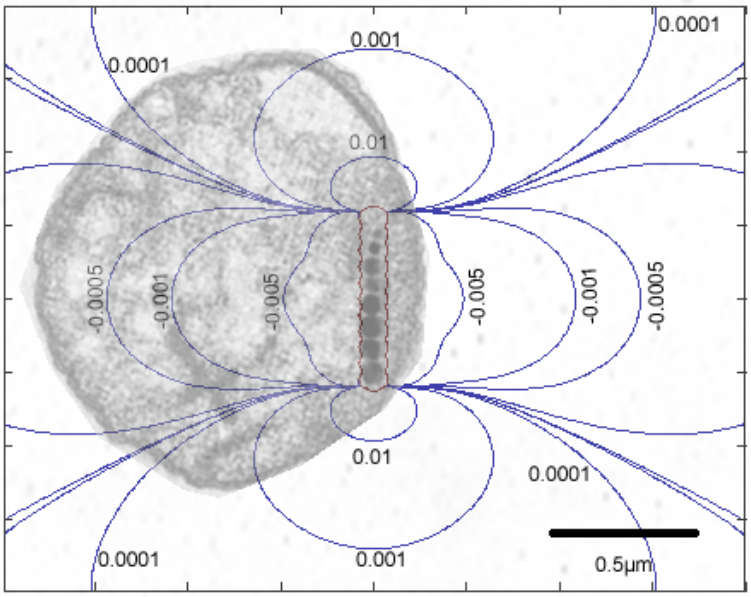

Figure 7.2. Magnetic field lines generated by a magnetosome chain superimposed on top of an image of a magnetotactic bacterium. In this simulation, we consider the presence of 11 magnetosomes with a mean diameter of 70nm. The distance between the magnetosomes is of 20nm. The saturation magnetazation for magntite (0.6 Tesla) is considered since at the MRI field of 1.5 Tesla, the magnetite chain is saturated.

The magnetosome chain will significantly disturb the local magnetic field. As depicted in Figure 7.3, the magnetic field perturbation is significant near the bacterium surpassing 100ppm and decreases farther away from the bacterium. This is quite significant for our application considering that an accepted homogeneity level of modern MRI clinical scanner is approximately 5ppm over a 50cm diameter spherical volume at 1.5Tesla. On a macroscopic scale, these perturbations will cause geometric as well as intensity-based artifacts. However, on a microscopic scale, these perturbations will affect the spin-lattice (T_1) and spin-spin (T_2) relaxation times as given by

$$\frac{1}{T_i} = \frac{1}{T_{i,0}} + \alpha_i \left[MTB\right], \qquad i = 1,2 \tag{7.3}$$

where $T_{i,0}$ is the relaxation rate of the medium, $\left[MTB\right]$ is the concentration of the magnetotactic bacteria (cells/ml) and α_i is the relaxivity expressed in $(\frac{ml}{cells \cdot s})$ a property specific to the effect

of MTB on the NMR signal. Equation 7.3 is generally used to characterize contrast agents in an MRI.

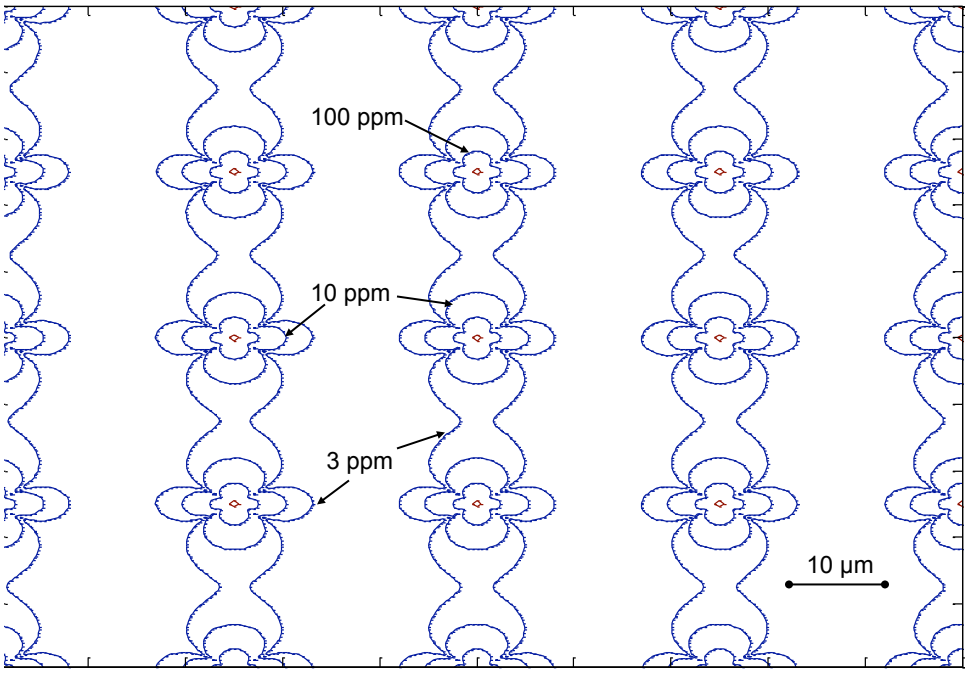

Figure 7.3. Simulation of a local magnetic field perturbation for a uniformly distributed concentration of MTB. The distance between MTB is taken to be 25µm, which corresponds to a concentration of approximately 10^7 bacteria/ml.

7.3.2 Relaxation times

Several concentrations of MTB were prepared by centrifugation. Qualitative observation of bacterial motility and response to a magnetic field before and after concentrations through centrifugation was performed using a Zeiss Imager Z1 microscope. Each concentration of the bacteria samples was determined by direct counting and by optical density measurements as presented in Table 7.1. Each 1ml MTB sample used for the experiments was inserted into a 2ml Progene microtube.

Table 7.1. Bacterial concentration and T_2-relaxation values for different MTB concentrations calculated from signal ratio measurements.

	Concentration $\times 10^7$ (bacteria/ml)	T2 (ms)
Sample 1 (medium)	0	646
Sample 2	2.2	305
Sample 3	3.5	203
Sample 4	4.8	172
Sample 5	6.2	156
Sample 6	6.7	114

Images were run under a Siemens Avanto 1.5Tesla scanner using a wrist antenna. T_1-weighted spin echo sequence parameters were: T_E = 11ms with three different T_R = 450/550/700ms, slice thickness of 20mm, and pixel spacing of 0.586 mm. T_2-weighted fast spin echo sequence parameters were: T_E = 96/125/135ms, T_R = 5096ms and pixel spacing of 0.293mm.

Samples containing MTB show signal enhancement compared to the medium in T_1-weighted images as depicted in Figure 7.4. However, this signal enhancement does not change much with higher MTB concentrations. The effect of the concentration of MTB is more evident on T_2-weighted images as depicted in Figure 7.5. As the concentration of bacteria increases, the signal decay becomes important. Table 7.1 presents T_2-relaxation values calculated from signal ratio measurement with different T_E values. Figure 7.6 shows the signal variation as a function of the bacteria concentration for different T_E values. As the T_E value increases, the difference in signal between different concentrations increases as well. Using Equation 7.3, we can calculate the T_2-relaxivity for MTB, this value is found to be $\alpha_2 = 7.448 \cdot 10^{-8} (\frac{ml}{cells \cdot s})$. Once the relaxivity of an

agent is known, the concentration of the MTB can be obtained on a voxel basis by direct measurement of the T_2-relaxation value and inversion of Equation 7.3.

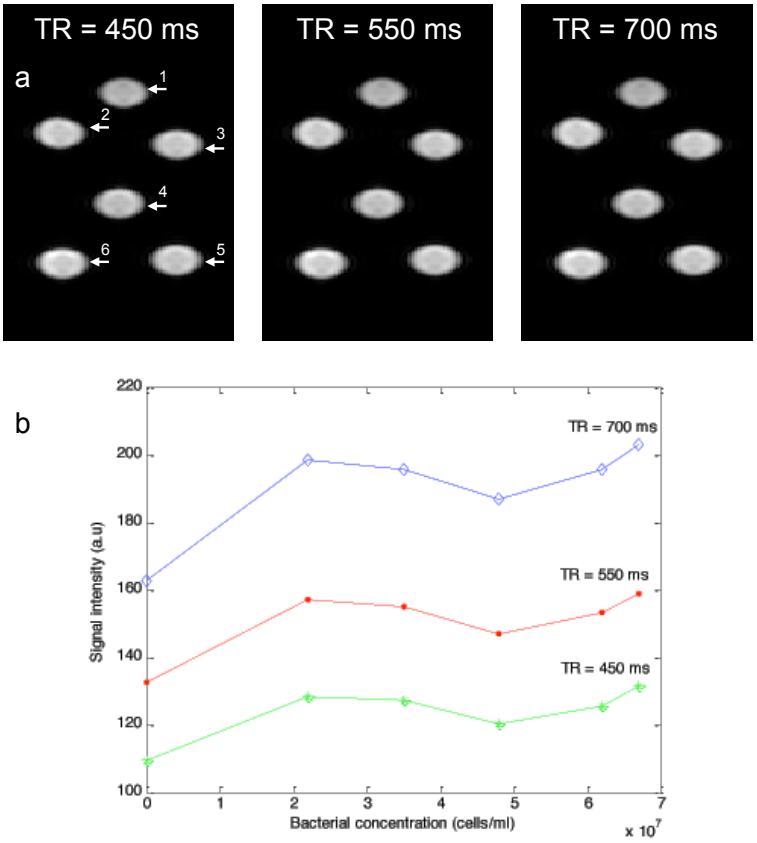

Figure 7.4. T_1 images of several concentrations of magnetotactic bacteria (MTB) samples. Samples 1 to 6 (as numbered in a) show increasing concentrations starting with a medium without MTB (sample 1). T_1-weighted spin echo sequence with T_E = 11 ms, three different T_R = 450/550/700 ms, a slice thickness of 20mm, and a pixel spacing of 0.586mm. (b) Signal intensity as a function of bacterial concentration for a T_1-weighted acquisition with three different Repetition Time (T_R) values. Notice that the signal contrast between samples of different concentrations is not important.

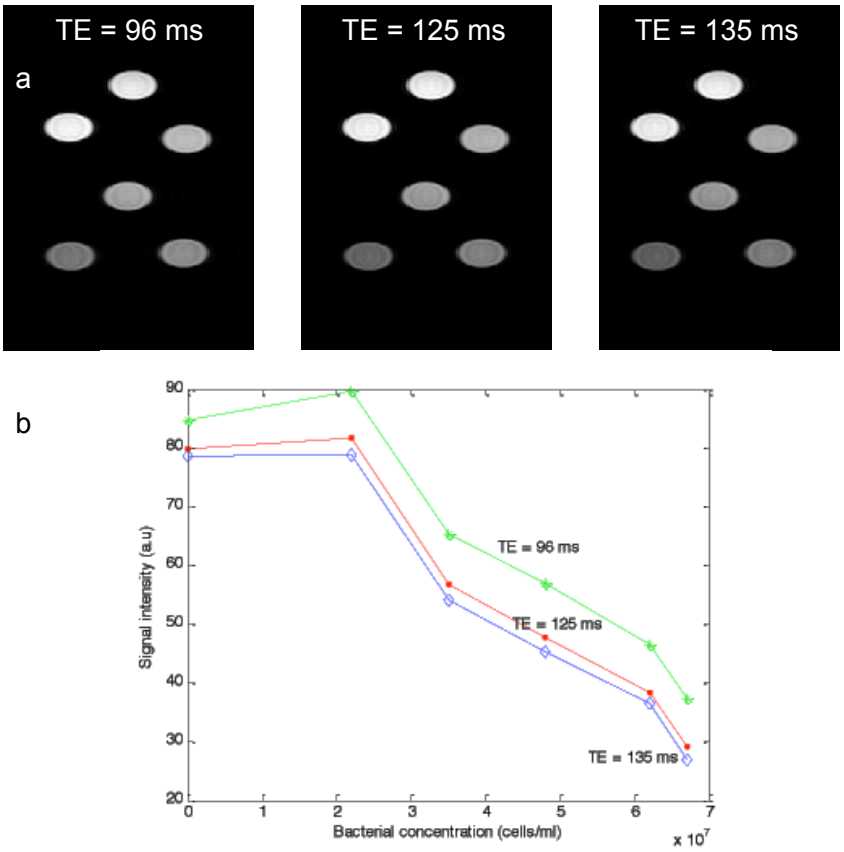

Figure 7.5. T_2-images of several concentrations of magnetotactic bacteria (MTB) samples. Samples 1 to 6 (as numbered in a) show increasing concentrations starting with a medium without MTB (sample 1). T_2-weighted fast spin echo sequence with T_R = 5096ms, three different T_E = 96/125/135ms, a slice thickness of 20mm, and a pixel spacing of 0.293mm. (b) Signal intensity as a function of bacterial concentration for a T_2-weighted acquisition with three different Echo Time (T_E) values. Notice that the signal contrast between samples of different bacterial concentrations is important.

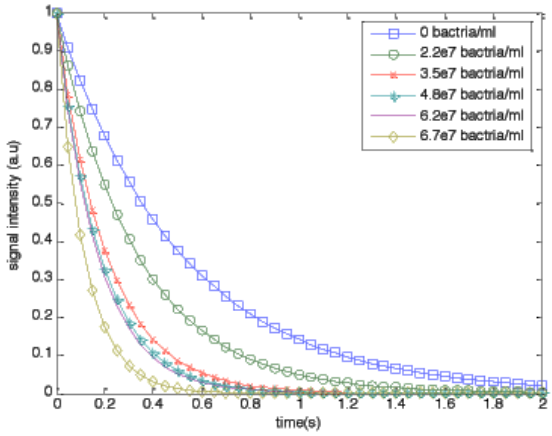

Figure 7.6. T_2-relaxation curves for different MTB concentrations.

Hence, MTB cause a decrease in both T_1 and T_2 values in a manner inversely proportional to their concentration; however, the effect on T_2 is found to be greater than the effect on T_1 as is the case with superparamagnetic MRI contrast agents. In fact, the magnetosome chain will cause in this case a decrease in signal intensity and rapid signal decay through T_2 enhancement. This attenuation of the signal is proportional to the concentration of bacteria and allows for quantification and guiding of MTB by magnetic control. Previous studies on bacterial analysis and quantification in MRI have reported the possibility to detect concentrations of 10^8-10^9 cells/mL of magnetically labeled bacteria [123]. We were able to detect MTB at a concentration as low as 2.2×10^7cells/mL using a clinical MRI scanner in a field of 1.5 Tesla.

7.3.3 Separation and evaluation of different sources of contrast

In order to verify and prove that the magnetosomes are the main source of the contrast seen on T_2 MR-images, we separately investigate the influence of the magnetosome's chain, the motility, and the cell of MC-1 magnetotactic bacteria (MTB) on the Magnetic Resonance imaging (MRI) contrast. Three samples were used. The first sample is made up of magnetic bacteria that successfully synthesize magnetic nanoparticles. MC-1 bacteria that do not synthesize magnetosomes form the second sample while the third sample is composed of dead MC-1 magnetic bacteria. T_2-weighted magnetic resonance images were obtained for multiple echo times.

The MC-1 cell itself, when no magnetosomes are synthesized, seems not to have any noticeable effect on MR-images. In fact, Figure 7.7 shows T_2 experimental relaxation curves for magnetic and

non-magnetic MC-1 cells as well as the medium. As T_E values are increased, the signal intensity for the magnetic MC-1 dropped while the one for non-magnetic MC-1 did not change when compared to the medium. While the T_2 value for the magnetic MC-1 was estimated to be 203ms for a bacterial concentration of $5 \cdot 10^7$ MTB per ml, it was found to be 725ms for the non-magnetic MC-1. The PBS medium has an experimental T_2 equal to 1072ms. Experimental T_2 relaxation curves for motile and non-motile magnetic MC-1 show very slight differences as depicted in Figure 7.8. At the same bacterial concentration of $1 \cdot 10^8$ MC-1 per ml, the T_2 value for the motile MC-1 was estimated to be 162ms while it was estimated to be 148ms for the non-motile MC-1.

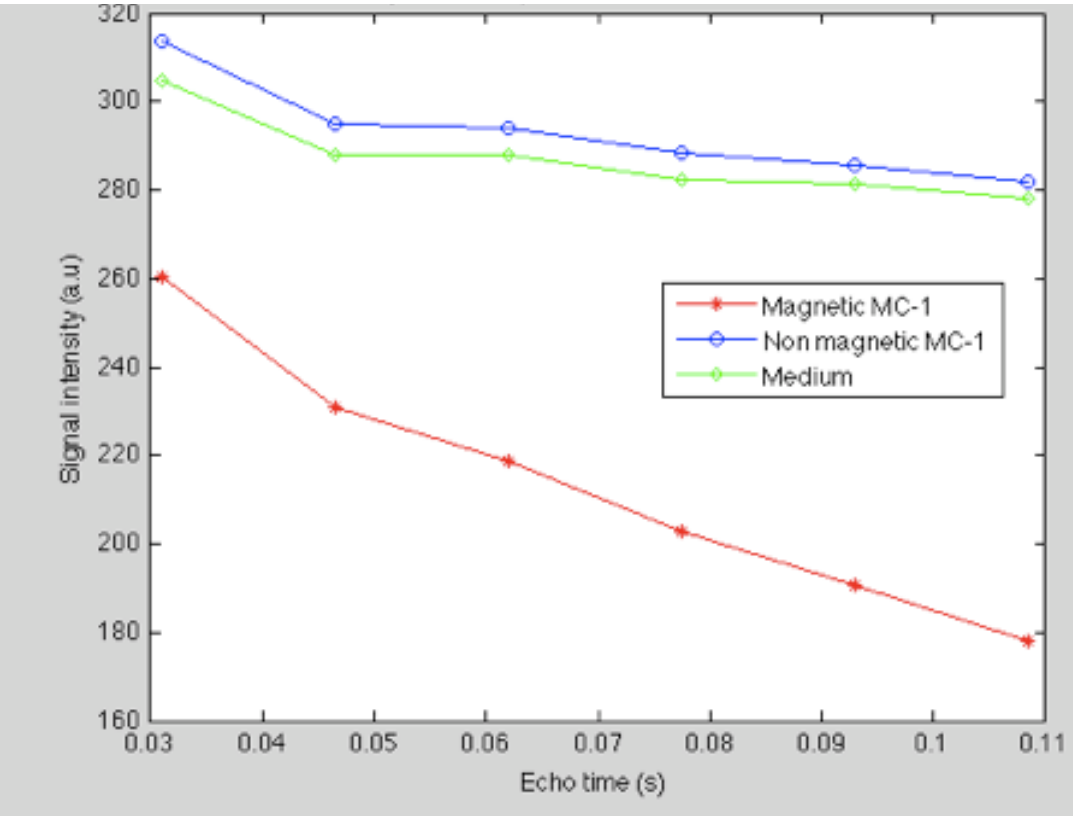

Figure 7.7. Experimental T_2 relaxation curves for magnetic and non-magnetic MC-1. The signal variation of the non-magnetic MC-1 is very similar to the medium. While the T_2 value for the magnetic MC-1 was estimated to be 203ms for a bacterial concentration of $5 \cdot 10^7$, it was found to be 725ms for the non-magnetic MC-1. The PBS medium has an experimental T_2 equal 1072ms. T_2 was estimated by fitting the signal intensity data for different T_E values to a monoexponential decay curve.

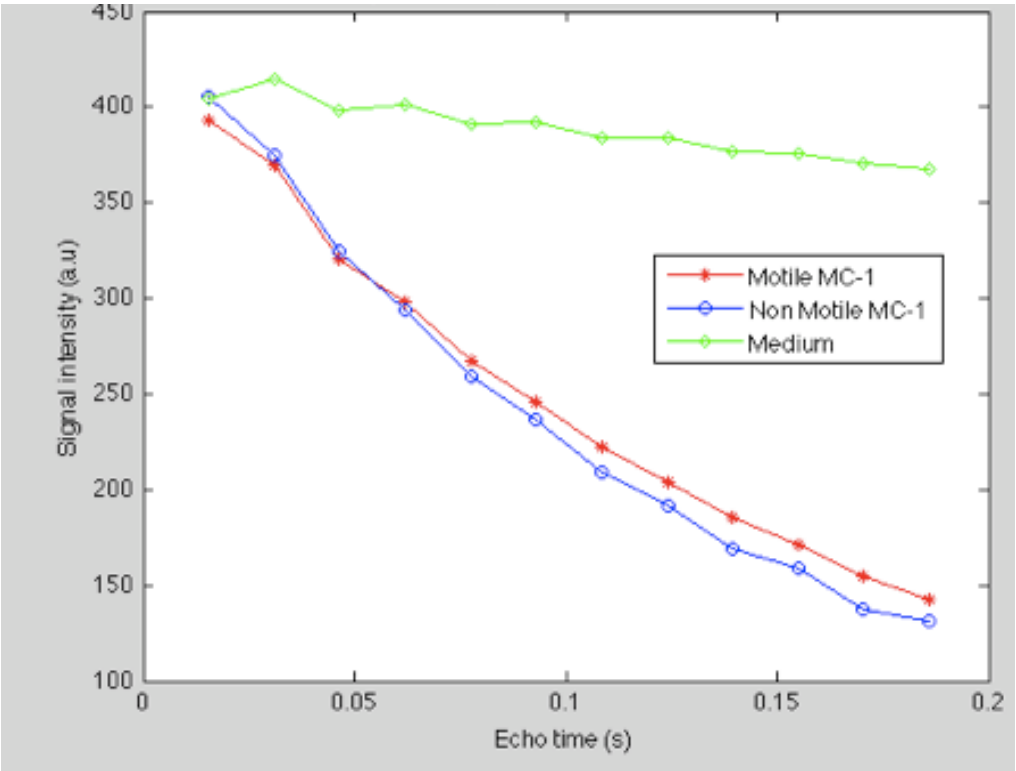

Figure 7.8. Experimental T_2 relaxation curves for motile and non-motile MC-1. Both samples show similar relaxation curves. An identical bacterial concentration of $1 \cdot 10^8$ MC-1 per ml was used for both samples. The T_2 value for the motile MC-1 was 162ms while it was 148ms for the non-motile MC-1. T_2 was estimated by fitting the signal intensity data for different T_E values to a monoexponential decay curve.

From Figure 7.7 and Figure 7.8, we conclude that the MR-contrast obtained in the presence of MC-1 is mainly due to the presence of magnetic nanoparticles inside the cell body. The cell constituent and the motion add very little to the MR-contrast.

CHAPTER 8 GENERAL DISCUSSION

The use of magnetotactic bacteria, in particular MC-1 cells, can enhance tumour-targeting efficacy compared to the use of magnetic microparticles when traveling through the smallest diameter capillaries found in the human microvasculature. On the other hand, the use of magnetic microparticles, especially with materials of relatively high magnetization saturation, becomes more effective in larger diameter capillaries when compared to the use of the MC-1 cell as microcarriers for targeted drug delivery.

The discussion section comprises a comparison of targeting efficiency with magnetic microparticles and with MTB, emphasizing the particularities of each method.

8.1 MTB vs magnetic microparticles: yield comparison in drug delivery to tumours

Prior to comparing drug delivery to tumours using MTB and magnetic microparticles, an understanding of the fundamental theoretical equations used to compute the efficiency of each approach is necessary. In fact, the mathematical laws governing motion of magnetic microparticles in the microvasculature differ from those for magnetotactic bacteria.

8.1.1 Magnetic force on a magnetized particle

A magnetic particle being transported by the blood flow in the microvasculature still needs to be steered at vessel bifurcations for enhanced targeting. Steering in this particular case is accomplished using a magnetic force $\boldsymbol{F_{mag}}$ (N) that acts on a magnetized body and that is induced by a gradient field $\boldsymbol{H}$ ($A \cdot m^{-1}$). Such force is computed as

$$\vec{F}_{mag} = \mu_0 . (\vec{m} . \nabla) \vec{H} \tag{8.1}$$

where $\boldsymbol{m}$ ($A.m^2$) is the magnetic moment and μ_0 ($N.A^{-2}$) is the permeability of vacuum. A spherical magnetic particle with a radius R *(m)* subject to a magnetic force will move with a velocity

$$\upsilon = \frac{\mu_0}{6\pi\eta R}.(\vec{m}.\nabla)\vec{H} \tag{8.2}$$

where η (Kg.s^{-1}.m^{-1}) is the viscosity of the medium.

Magnetic microparticles compete well against MC-1 cells if the velocity computed in Equation 8.2 is equivalent or greater than the swimming velocity of MTB in human blood as recorded experimentally. Although our group has recorded average and peak swimming velocities of approximately 200 and 300μm·s^{-1} respectively in human blood at room temperature, we considered, for the sake of comparison, an average swimming speed of υ_0 = 100μm·s^{-1}. This decision was taken in consideration of our experimental results, which showed that the velocity of the MC-1 cells decrease continuously when operating at the human internal temperature of 37^{o}C and reach a maximum operational time of approximately 40 minutes.

8.1.2 MTB alignment with an external magnetic field

The chain of magnetosomes inside the cell will contribute to maximize the magnetic moment of each bacterium where the ratio between the thermal energy and the magnetic potential energy can be expressed as

$$\Lambda = \frac{mB}{KT}, \text{ where } B = \mu_0 H \tag{8.3}$$

We notice here that a higher value of ***H*** is required to maintain the orientation of the MC-1 cell in order to correct displacement error. This error is caused by an increase of Brownian motion due to the higher temperature level in the microvasculature. Hence, as given in [83], the average value of cos φ is found to be

$$\langle \cos\varphi \rangle = L(\Lambda) \tag{8.4}$$

For a cell with a magnetic moment ***m*** of 10^{-16}(A.m^2) at room temperature (297.15^{o}K), the magnetic energy is 1.15 times the thermal energy when subjected to the geomagnetic field of 0.5Gauss. However, an increase of the magnetic field to 4 Gauss will yield very accurate displacement with an energy ratio of approximately 10.

If we neglect thermal fluctuations and a high enough external magnetic field $\boldsymbol{H}$, the dynamics of the orientation of the bacterial magnetic moment with the magnetic field can be determined using Equation 8.5 [104].

$$-\alpha\frac{d\theta}{dt}+mB\sin\beta=0 \tag{8.5}$$

In Equation 8.5, α is the rotational friction coefficient, θ is the particle orientation with respect to a fixed direction, and β is the angle between the magnetic field and the magnetic moment of the cell.

This comparative study includes several morphotypes of MTB that exist in nature. Commonly observed morphotypes include spherical cells (cocci), rod-shaped, curved bacteria (vibrio), multi-cellular MTB (a group of cells arranged as a sphere), and helical (spirillum) of various dimensions and swimming velocities.

8.2 Comparative study contextualize

Even though many factors influence the motion of microparticles and MTB in the microvasculature as described in [49], we only consider here the most predominant factors: the magnetic and fluidic forces. The fluidic force is caused by the blood flow and is equal to

$$F_f=-6\pi\eta R_P\left(\upsilon_P-\upsilon_f\right) \tag{8.6}$$

Equation 8.6 considers a laminar flow and a spherical particle having a hydrodynamic radius of R_P. In Equation 8.6, η and υ_f are the blood viscosity and velocity respectively. Here, equilibrium of forces between magnetic force and Stokes law of fluid friction weighted by a wall effect correlation [126] allows us to calculate the theoretical particle magnetophoretic terminal velocity [127] inside a microchannel.

Considering a simple navigation case consisting on a Y-shaped microvascular channel as depicted by Figure 8.1, the targeting efficiency is assessed for different steering parameters for both magnetic microparticles and MTB involving various flow rates and sizes of microchannels as to reflect real conditions in the human vasculature.

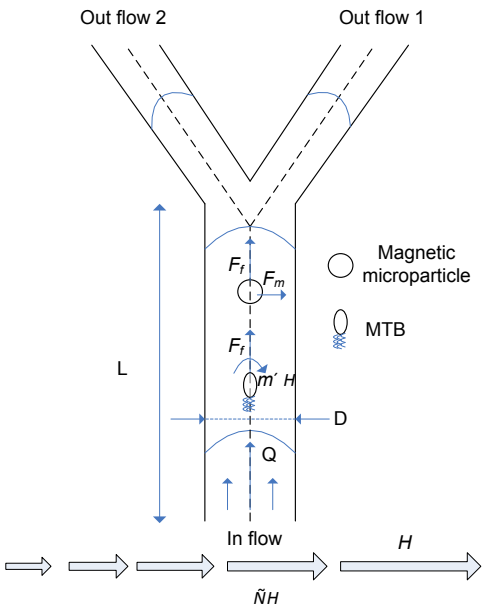

Figure 8.1. *Y-shaped* microvascular channel used for navigation simulation of steering efficiency. D represents the channel diameter and L its length; we consider L = D × 100. Even if magnetic particle steering involves many forces, we consider only the most important, which are the magnetic and fluidic forces. MTB are subject to magnetic torque, but their motion is governed by flagella, which allow the bacteria to move at constant speed along the direction of the magnetic field.

In this study, the velocity of MC-1 cells is compared to the velocity of a 2μm magnetite sphere steered by magnetic gradients in the blood. Magnetite is a well-known material with a relatively high magnetization saturation and proven biocompatibility. This material is widely used as a safe contrast agent for MR-imaging.

Table 8.1. Summary characteristics of some MTB and calculation of the required gradient necessary to have a magnetophoretic speed equivalent to the MTB speed giving a spherical magneitte microparticle with the same size range as the MTB.

MTB NAME	CELL MORPHOLOGY	Mean Speed ($\mu m \cdot s^{-1}$)	WIDTH (OR DIAMETER) (μm)	LENGTH (μm)	MAGNETIC MICROPARTICLE	
					DIAMETER (μm)	MAGNETIC GRADIENT ($mT \cdot m^{-1}$)
MC-1 [44]	Coccoid	200	2	-	2	7.6×10^3
Magnetospirillum gryphiswaldense [85]	Helical	50	0.2–0.7	1-20	10	91
AMB-1 [86]	Helical	49	0.5	3-10	5	320
MV-1 and MV-2 [87]	Vibroid to Helical	-*	0.2–0.5	1-5	2	1.9×10^3
MMP (Many celled Magnetotactic bacteria)[87]	Sphere (a cluster of 10-30 Coccoid cells)	105	3-12	-	8	287
Magnetobacterium bavaricum [87]	Rod-shaped	40	1–1.5	6–9	7	139
RS-1[87]	Helical to Rod-shaped	-*	0.9–1.5	3-5	4	326
Magnetospirillum magnetotacticum (MS–1) [88]	Spirillum	40	0.5	5	2.5	989

* For MTB speed missing data we considered a value of 50 $\mu m \cdot s^{-1}$ for the calculation of the magnetic gradient

The channel taken from realistic conditions has a length-diameter ratio of 100 or in other words, $L = D \times 100$ where L is the channel length and D is the diameter. For every channel diameter, we calculated the maximum blood flow that allows for 100% steering efficiency. In order for a microparticle or MTB to be steered toward the targeted channel at the bifurcation, it was assumed that half the diameter of the main channel had to be traveled before reaching the bifurcation. This was considered as a worst-case scenario since all the microparticles located on the same side of the centerline of the channel prior to the Y-bifurcation were to exit through the targeted outlet.

8.3 Comparative study simulation results

Table 8.1 summarizes the main MTB characteristics such as their cell morphology, respective swimming velocity and dimension. It also displays the magnetic gradient required to move a magnetite microparticle of similar size at the same velocity as the corresponding cell type's velocity. The smaller the cell is, the higher the required magnetic field must be in order to achieve the same velocity (specify). In fact, for some cases like those of MC-1, MV-1, MV-2 and MS-1 cells, the magnetic gradient required to achieve an equivalent speed is extremely high and may even be impractical for deep targets in the human body. For smaller MTB with relatively low swimming speeds, the required magnetic gradient is reasonable and could easily be implemented. However, these smaller MTB would not necessary be good candidates to target tumoural lesions. The use of molecular motors embedded in MC-1 magnetotactic bacteria for drug targeting is an efficient method since it does not require an external energy source. On the other hand, despite its limitations in the smallest diameter capillaries, magnetic drug targeting represents a more flexible approach where steering parameters can be customized depending upon the application needs and the geometry of the targeted vessels. Another interesting feature in the use of MTB is the fact that they do not require blood flow to move. This facet allows them to swim in larger diameter vessels if complemented by another method, such as the use of a balloon catheter or larger magnetic embolization particles to temporarily stop blood flow. These cells can also be very effective in enhancing the uniform distribution of drugs inside the tumour, which is a key component to the eradication of the tumour. Furthermore, MTB can increase the time required for drugs to be in direct contact with cancerous cells because of the high interstitial pressure inside the tumour. Without the use of MTB, the diffusion of drugs would otherwise be very slow.

High gradient amplitudes are required to achieve 100% steering efficiency with moderate flow velocities. For instance, the MC-1 cell can theoretically sustain a flow rate of $10mm \cdot s^{-1}$, which would require gradient amplitudes as high as $2T \cdot m^{-1}$ for a magnetite microparticle of the same diameter as the MC-1 cell. Hence, to reach a higher magnetophoretic velocity, a smaller particle must be submitted to a much higher magnetic gradient than a larger particle containing a higher effective volume of the same magnetic material. The magnetic force in this case is greatly affected by the size of a spherical magnetic core since such force will be proportional to the cube of the radius of the core itself.

In fact, larger magnetic cores with diameters of 5μm or higher can be used not only for targeting in the tumour itself, but for embolization of small capillaries near the tumoural lesion in order to stop blood supply to the tumour. The maximum flow velocity within which 100% steering efficiency of microparticles of 5μm can be achieved is much higher than that required for 2μm-wide magnetic microparticles, even with relatively moderate magnetic gradients ($<0.5 T \cdot m^{-1}$). We notice that in this case, MC-1 MTB is no more efficient a solution compared to magnetic microparticles that can sustain a large flow velocity with reasonable magnetic gradients. In addition to an increase in particle size, other magnetic components that present higher magnetization values than magnetite, such as Cobalt-Iron, could also be used to increase the magnetic force and achieve higher magnetophoretic velocities. Such models are possible provided that the design prevents the release of toxic Cobalt ions in the blood.

CONCLUSION

Magnetotactic bacteria were investigated as drug delivery vehicles to solid tumours. They exhibit the advantage of being controllable by magnetic field, which in its turn, can be generated by a computer program.

In order to develop this new concept, fundamental studies on the bacteria's motion, its response to different magnetic field values and relaxation parameters in MRI were conducted. Then, magnetic navigation was investigated keeping the main final application of active delivery of drug to tumours in mind. Designing a magnetic setup that is adapted to a human body was also an issue that influenced the final platform design. Finally, the real question was to see if the MC-1 bacteria could indeed target deep inside tumours in a live animal. We validated that the MTB could target tumour cell xenografts grown in the flanks of nu/nu CD1 mice. After administering an intravenous injection of the bacterial sample, a magnetic guidance was applied toward the right flank xenograft. Even in a worse case experiment where the MTB were injected far from the targeted tumour sites (injection performed at the tail), efficient targeting at a pre-defined zone was achieved. The experimental results also show that applying a lower intensity magnetic pole as depicted inside the other xenograft can control a dose.

While metastatic cancers most often require systemic therapy, there are specific contexts in which more effective localized therapy would have major impact on both quality of life and survival. Navigation the MTB to the tumours is a first step toward building a new localized therapeutic vector for cancer therapy. However, the MTB alone do not have any therapeutic effects and their surface has to be functionalized in order to make them a transporter of drugs to tumours. Combining existing treatment such as radiotherapy with the MTB could enhance the final therapy outcome through sensitizing the tumours to the radiation.

To date, there is no magic way to treat cancer. Doctors dispose of many tools that they apply depending on the disease location, advancement, and the patient tolerance to the side effects of the therapy. The concept of magnetotactic bacteria targeting tumour is not the missing magic way to treat cancer, however, it can be an additional tool for doctors to help patients that are inadmissible to other treatments.

REFERENCES

[1] D. M. Brizel, G. L. Rosner, L. R. Prosnitz, and M. W. Dewhirst, "Patterns and variability of tumor oxygenation in human soft tissue sarcomas, cervical carcinomas, and lymph node metastases," *Int J Radiat Oncol Biol Phys.,* vol. 32, pp. 1121-5, 1995.

[2] E. K. Rofstad, K. Sundfør, H. Lyng, and C. G. Tropé, "Hypoxia-induced treatment failure in advanced squamous cell carcinoma of the uterine cervix is primarily due to hypoxia-induced radiation resistance rather than hypoxia-induced metastasis," *Br J Cancer,* vol. 83, pp. 354-359, 2000.

[3] J. P. Cosse and C. Michiels, "Tumour hypoxia affects the responsiveness of cancer cells to chemotherapy and promotes cancer progression," *Anticancer Agents Med Chem.,* vol. 8, pp. 790-7, 2008.

[4] K. Maruyama, O. Ishida, T. Takizawa, and K. Moribe, "Possibility of active targeting to tumor tissues with liposomes," *Advanced Drug Delivery Reviews,* vol. 40, pp. 89-102, 1999.

[5] Q. Yang, M. E. Hokland, J. L. Bryant, Y. Zhang, U. Nannmark, S. C. Watkins, R. H. Goldfarb, R. B. Herberman, and P. H. Basse, "Tumor-localization by adoptively transferred, interleukin-2-activated NK cells leads to destruction of well-established lung metastases," *International Journal of Cancer,* vol. 105, pp. 512-9, 2003.

[6] R. Gardlik, M. Behuliak, R. Palffy, P. Celec, and C. J. Li1, "Gene therapy for cancer: bacteria-mediated anti-angiogenesis therapy," *Gene Therapy,* vol. 18, pp. 425-431, 2011.

[7] C. L. Erickson-Miller, R. D. May, J. Tomaszewski, B. Osborn, M. J. Murphy, J. G. Page, and R. E. Parchment, "Differential toxicity of camptothecin, topotecan and 9-aminocamptothecin to human, canine, and murine myeloid progenitors (CFU-GM) in vitro," *Cancer Chemotherapy and Pharmacology,* vol. 39, pp. 467-472, 1997.

[8] R. S. Sidhu and A. P. Bollon, "Tumor necrosis factor activities and cancer therapy -- A perspective," *Pharmacology & Therapeutics,* vol. 57, pp. 79-128, 1993.

[9] R. K. Jain, "Transport of Molecules in the Tumor Interstitium: A Review," *Cancer Research,* vol. 47, pp. 3039-3051, 1987.

[10] R. K. Jain, "Determinants of Tumor Blood Flow: A Review," *Cancer Research,* vol. 48, pp. 2641-2658, 1988.

[11] R. K. Jain, "Delivery of Molecular and Cellular Medicine to Solid Tumors," *Microcirculation,* vol. 4, pp. 1-23, 1997.

[12] R. K. Jain, "Transport of Molecules, Particles, and Cells in Solid Tumors," *Annual Review of Biomedical Engineering,* vol. 1, pp. 241-263, 1999.

[13] R. K. Jain and K. A. Ward-Hartley, "Dynamics of cancer cell interactions with microvasculature and interstitium," *Biorheology,* vol. 24, pp. 117-25, 1987.

[14] F. Yuan, Y. Chen, M. Dellian, N. Safabakhsh, N. Ferrara, and R. K. Jain, "Time-dependent vascular regression and permeability changes in established human tumor

xenografts induced by an anti-vascular endothelial growth factor/vascular permeability factor antibody," *Proceedings of the National Academy of Sciences,* vol. 93, pp. 14765-14770, 1996.

[15] F. Yuan, M. Leunig, S. K. Huang, D. A. Berk, D. Papahadjopoulos, and R. K. Jain, "Mirovascular Permeability and Interstitial Penetration of Sterically Stabilized (Stealth) Liposomes in a Human Tumor Xenograft," *Cancer Research,* vol. 54, pp. 3352-3356, 1994.

[16] K. B. Bischoff, R. L. Dedrick, D. S. Zaharko, and J. A. Longstreth, "Methotrexate pharmacokinetics," *Journal of Pharmaceutical Sciences,* vol. 60, pp. 1128-1133, 1971.

[17] B. Endrich, H. Reinhold, J. Gross, and M. Intaglietta, "Tissue perfusion inhomogeneity during early tumor growth in rats," *J Natl Cancer Inst.,* vol. 62, pp. 387-95, 1979.

[18] C. J. Gulledge and M. W. Dewhirst, "Tumor oxygenation: a matter of supply and demand," *Anticancer Res.,* vol. 16, pp. 741-749, 1996.

[19] N. Z. Wu, R. D. Braun, M. H. Gaber, G. M. Lin, E. T. Ong, S. Shan, D. Papahadjopoulos, and M. W. Dewhirst, "Simultaneous Measurement of Liposome Extravasation and Content Release in Tumors," *Microcirculation,* vol. 4, pp. 83-101, 1997.

[20] N. Z. Wu, D. Da, T. L. Rudoll, D. Needham, A. R. Whorton, and M. W. Dewhirst, "Increased Microvascular Permeability Contributes to Preferential Accumulation of Stealth Liposomes in Tumor Tissue," *Cancer Research,* vol. 53, pp. 3765-3770, August 15 1993.

[21] J. Folkman and M. Klagsbrun, "Angiogenic factors," *Science,* vol. 235, pp. 442-447, January 23 1987.

[22] W. Risau, "Mechanisms of angiogenesis," *Nature,* vol. 386, pp. 671-674, 1997.

[23] A. Dvorak, S. Kohn, E. Morgan, P. Fox, J. Nagy, and H. Dvorak, "The vesiculo-vacuolar organelle (VVO): a distinct endothelial cell structure that provides a transcellular pathway for macromolecular extravasation," *Journal of Leukocyte Biology,* vol. 59, pp. 100-115, 1996.

[24] H. F. Dvorak, J. A. Nagy, J. T. Dvorak, and A. M. Dvorak, "Identification and characterization of the blood vessels of solid tumors that are leaky to circulating macromolecules," *The American journal of pathology,* vol. 133, pp. 95-109, 1988.

[25] W. G. Roberts and G. E. Palade, "Neovasculature Induced by Vascular Endothelial Growth Factor Is Fenestrated," *Cancer Research,* vol. 57, pp. 765-772, 1997.

[26] H. Hashizume, P. Baluk, S. Morikawa, J. W. McLean, G. Thurston, S. Roberge, R. K. Jain, and D. M. McDonald, "Openings between Defective Endothelial Cells Explain Tumor Vessel Leakiness," *American Journal of Pathology,* vol. 156, pp. 1363-80, 2000.

[27] F. Yuan, H. A. Salehi, Y. Boucher, U. S. Vasthare, R. F. Tuma, and R. K. Jain, "Vascular permeability and microcirculation of gliomas and mammary carcinomas transplanted in rat and mouse cranial windows," *Cancer Research,* vol. 54, pp. 4564-4568, 1994.

[28] S. K. Hobbs, F. Yuan, L. Griffith, and al., "Pore cutoff size of tumor microvessels: Effect of tumor type, treatment, and host microenvironment," in *Proceedings of the 88th Anmial*

Meeting of American Association for Cancer Research, San Diego, Ca, USA, 1997, p. 263.

[29] P. Rubin and G. Casarett, "Microcirculation of tumors. I. Anatomy, function, and necrosis," *Clin. Radiol.,* vol. 17, pp. 220-229, 1966.

[30] J. M. Brown and A. J. Giaccia, "The unique physiology of solid tumors: opportunities (and problems) for cancer therapy," *Cancer Research,* vol. 58, pp. 1408-16, 1998.

[31] P. A. Netti, S. Roberge, Y. Boucher, L. T. Baxter, and R. K. Jain, "Effect of transvascular fluid exchange on arterio-venous pressure relationship: implication for temporal and spatial heterogeneities in tumor blood flow," *Microvasc. Res.,* vol. 52, pp. 27-46, 1996.

[32] L. J. Nugent and R. K. Jain, "Extravascular diffusion in normal and neoplastic tissues," *Cancer Res.,* vol. 44, pp. 238-244, 1984.

[33] E. A. Swabb, J. Wei, and P. M. Gullino, "Diffusion and convection in normal and neoplastic tissues," *Cancer Res.,* vol. 34, pp. 2814-2822, 1974.

[34] E. M. Sevick and R. K. Jain, "Measurement of Capillary Filtration Coefficient in a Solid Tumor," *Cancer Research,* vol. 51, pp. 1352-1355, 1991.

[35] T. P. Butler, F. H. Grantham, and P. M. Gullino, "Bulk Transfer of Fluid in the Interstitial Compartment of Mammary Tumors," *Cancer Research,* vol. 35, pp. 3084-3088, 1975.

[36] L. Zhang, J. J. Abbott, L. X. Dong, B. E. Kratochvil, D. J. Bell, and B. J. Nelson, "Artificial Bacterial Flagella: Fabrication and Magnetic Control," *Applied Physics Letters,* vol. 94, pp. 064107-9, 2009.

[37] T. Honda, K. I. Arai, and K. Ishiyama, "Micro swimming mechanisms propelled by external magnetic fields," *IEEE Transactions on Magnetics,* vol. 32, pp. 5085-5087, 1996.

[38] J. J. Abbott, K. E. Peyer, M. C. Lagomarsino, L. Zhang, L. X. Dong, I. K. Kaliakatsos, and B. J. Nelson, "How Should Microrobots Swim?," *International Journal of Robotics Research,* vol. 28, pp. 1434-1447, 2009.

[39] L. Zhang, L. X. Abbott, L. X. Dong, K. E. Peyer, B. E. Kratochvil, H. X. Zhang, C. Bergeles, and B. J. Nelson, "Characterizing the Swimming Properties of Artificial Bacterial Flagella," *Nano Letters,* vol. 9, pp. 3663-3667, 2009.

[40] B. Behkam and M. Sitti, "E. Coli Inspired Propulsion for Swimming Microrobots," in *Proceedings of 2004 ASME International Mechanical Engineering Conference and Exposition*, Anaheim, CA, 2004.

[41] B. Behkam and M. Sitti, "Modeling and Testing of a Biomimetic Flagellar Propulsion Method for Microscale Biomedical Swimming Robots," in *Proceeding of 2005 IEEE/ASME International Conference on Advanced Intelligent Mechatronics*, Monterey, California, USA, 2005, pp. 37-42.

[42] B. Behkam and M. Sitti, "Design Methodology for Biomimetic Propulsion of Miniature Swimming Robots," *Journal of Dynamic Systems, Measurement, and Control,* vol. 128, pp. 36-43, 2006.

[43] S. Martel, "Nanorobots for microfactories to operations in the human body and robots propelled by bacteria," *Journal Facta Universitatis Series Mechanics, Automatic Control & Robotics (FU-MCAR),* vol. 7, pp. 1-8, 2009.

[44] S. Martel, M. Mohammadi, O. Felfoul, Z. Lu, and P. Pouponneau, "Flagellated magnetotactic bacteria as controlled MRI-trackable propulsion and steering systems for medical nanorobots operating in the human microvasculature," *International Journal of Robotics Research,* vol. 28, pp. 571-582 2009.

[45] B. Behkam and M. Sitti, "Bacterial Flagella-Based Propulsion and On/Off Motion Control of Microscale Objects," *Applied Physics Letters,* vol. 90, pp. 023902-4, 2007.

[46] S. Martel, C. Tremblay, S. Ngakeng, and G. Langlois, "Controlled manipulation and actuation of micro-objects with magnetotactic bacteria," *Applied Physics Letters,* vol. 89, pp. 233904-6, 2006.

[47] S. Martel and M. Mohammadi, "A robotic micro-assembly process inspired by the construction of the ancient pyramids and relying on several thousand flagellated bacteria acting as micro-workers," in *IROS'09 Proceedings of the 2009 IEEE/RSJ international conference on Intelligent robots and systems* St. Louis, MO, USA, 2009.

[48] Z. G. Forbes, B. B. Yellen, K. A. Barbee, and G. Friedman, "An approach to targeted drug delivery based on uniform magnetic fields," *IEEE Transactions on Magnetics,* vol. 39, pp. 3372-3377, 2003.

[49] E. J. Furlani and E. P. Furlani, "A model for predicting magnetic targeting of multifunctional particles in the microvasculature," *Journal of Magnetism and Magnetic Materials,* vol. 312, pp. 187-193, 2007.

[50] E. P. Furlani and K. C. Ng, "Analytical model of magnetic nanoparticle transport and capture in the microvasculature," *Physical Review E,* vol. 73, pp. 61919-1-10, 2006.

[51] F. Mishima, S. Takeda, Y. Izumi, and S. Nishijima, "Three dimensional motion control system of ferromagnetic particles for magnetically targeted drug delivery systems," *IEEE Transactions on Applied Superconductivity,* vol. 16, pp. 1539-1542, 2006.

[52] L. E. Udrea, N. J. C. Strachan, V. Badescu, and O. Rotariu, "An in vitro study of magnetic particle targeting in small blood vessels," *Physics in Medicine and Biology,* vol. 51, pp. 4869–4881, 2006.

[53] C. Alexiou, R. J. Schmid, R. Jurgons, M. Kremer, G. Wanner, C. B. E. Huenges, T. Nawroth, W. Arnold, and F. G. Parak, "Targeting cancer cells: magnetic nanoparticles as drug carriers," *European Biophysics Journal,* vol. 35, pp. 446-450, 2006.

[54] Z. G. Forbes, B. B. Yellen, D. S. Halverson, G. Fridman, K. A. Barbee, and G. Friedman, "Validation of high gradient magnetic field based drug delivery to magnetizable implants under flow," *IEEE Transactions On Biomedical Engineering,* vol. 55, pp. 643-649, 2008.

[55] G. Iacob, O. Rotariu, N. J. C. Strachan, and U. O. Häfeli, "Magnetizable needles and wires - modeling an efficient way to target magnetic microspheres in vivo," *Biorheology,* vol. 41, pp. 599-612, 2004.

[56] B. B. Yellen, Z. G. Forbes, D. S. Halverson, G. Fridman, K. A. Barbee, M. Chorny, R. Levy, and G. Friedman, "Targeted drug delivery to magnetic implants for therapeutic

applications," *Journal of Magnetism and Magnetic Materials,* vol. 293, pp. 647-654, 2005.

[57] . *Small Times*. Available: http://www.smalltimes.com/

[58] A. Chanu, O. Felfoul, G. Beaudoin, and S. Martel, "Adapting the software platform of MRI for the real-time navigation of endovascular untethered ferromagnetic devices," *Magnetic Resonance in Medicine,* vol. 59, pp. 1287-97, 2008.

[59] O. Felfoul, J.-B. Mathieu, G. Beaudoin, and S. Martel, "In vivo MR-tracking based on magnetic signature selective excitation," *IEEE Transactions on Medical Imaging,* vol. 27, pp. 28-35, 2008.

[60] S. Martel, O. Felfoul, J.-B. Mathieu, A. Chanu, S. Tamaz, M. Mohammadi, M. Mankiewicz, and N. T. N., "MRI-based nanorobotic platform for the control of magnetic nanoparticles and flagellated bacteria for target interventions in human capillaries," *International Journal of Robotics Research,* vol. 28, pp. 1169-1182, 2009.

[61] S. Martel, J.-B. Mathieu, O. Felfoul, A. Chanu, E. Aboussouan, S. Tamaz, P. Pouponneau, L. Yahia, G. Beaudoin, G. Soulez, and M. Mankiewicz, "A computer-assisted protocol for endovascular target interventions using a clinical MRI system for controlling untethered microdevices and future nanorobots," *Computer Aided Surgery,* vol. 13, pp. 340-52, 2008.

[62] J.-B. Mathieu and S. Martel, "Aggregation of magnetic microparticles in the context of targeted therapies actuated by a magnetic resonance imaging system," *Journal of Applied Physics. Materials.,* vol. 106, pp. 044904-1 to 7, 2009.

[63] J.-B. Mathieu and S. Martel, "MRI Steering of Aggregating Magnetic Microparticles for Enhanced Therapeutic Efficacy in Cancer Targeting," *Magnetic Resonance in Medicine,* vol. 63, pp. 1336 -1345, 2010.

[64] P. Pouponneau, J.-C. Leroux, G. Soulez, L. Gaboury, and S. Martel, "Co-encapsulation of magnetic nanoparticles and doxorubicin into biodegradable microcarriers for deep tissue targeting by vascular MRI navigation," *Biomaterials,* vol. 32, pp. 3481-6, 2011.

[65] R. D. Berg, "The indigenous gastrointestinal microflora," *Trends in Microbiology,* vol. 4, pp. 430-435, 1996.

[66] W. B. COLEY, "Contribution To the Knowledge of Sarcoma," *Annals of Surgery,* vol. 14, pp. 199-220, 1891.

[67] K. B. Chwanrow, M. Cronin, D. O'Hanlon, G. C. O'Sullivan, and M. Tangney, "Bacteria as vectors for gene therapy of cancer," *Bioengineered Bugs,* vol. 1, pp. 385-394, 2010.

[68] C. Bettegowda, L. H. Dang, R. Abrams, D. L. Huso, L. Dillehay, I. Cheong, N. Agrawal, S. Borzillary, J. M. McCaffery, E. L. Watson, K.-S. Lin, F. Bunz, K. Baidoo, M. G. Pomper, K. W. Kinzler, B. Vogelstein, and S. Zhou, "Overcoming the hypoxic barrier to radiation therapy with anaerobic bacteria," *Proceedings of the National Academy of Sciences,* vol. 100, pp. 15083-15088, 2003.

[69] L. H. Dang, C. Bettegowda, D. L. Huso, K. W. Kinzler, and B. Vogelstein, "Combination bacteriolytic therapy for the treatment of experimental tumors," *Proceedings of the National Academy of Sciences,* vol. 98, pp. 15155-15160, 2001.

[70] R. W. Kasinskas and N. S. Forbes, "Salmonella typhimurium specifically chemotax and proliferate in heterogeneous tumor tissue in vitro," *Biotechnology and Bioengineering,* vol. 94, pp. 710-721, 2006.

[71] N. T. Kimura, S. Taniguchi, K. Aoki, and T. Baba, "Selective Localization and Growth of Bifidobacterium bifidum in Mouse Tumors following Intravenous Administration," *Cancer Research,* vol. 40, pp. 2061-2068, 1980.

[72] S. C. Liu, N. P. Minton, A. J. Giaccia, and J. M. Brown, "Anticancer efficacy of systemically delivered anaerobic bacteria as gene therapy vectors targeting tumor hypoxia/necrosis," *Gene therapy,* vol. 9, pp. 291-6, 2002.

[73] H. C. Nauts, W. E. Swift, and B. L. Coley, "The Treatment of Malignant Tumors by Bacterial Toxins as Developed by the Late William B. Coley, M.D., Reviewed in the Light of Modern Research," *Cancer Research,* vol. 6, pp. 205-216, 1946.

[74] J. M. Pawelek, K. B. Low, and D. Bermudes, "Bacteria as tumour-targeting vectors," *Lancet Oncol.,* vol. 4, pp. 548-56, 2003.

[75] S. Patyar, R. Joshi, D. S. P. Byrav, A. Prakash, B. Medhi, and B. K. Das, "Bacteria in cancer therapy: a novel experimental strategy," *J Biomed Sci.,* vol. 17, pp. 21-29, 2010.

[76] R. A. Malmgren and C. C. Flanigan, "Localization of the vegetative form of Clostridium tetani in mouse tumors following intravenous spore administration," *Cancer Res.,* vol. 15, pp. 473-477, 1955.

[77] N. P. Minton, "Clostridia in cancer therapy," *Nat. Rev. Microbiol.,* vol. 1, pp. 237-242, 2003.

[78] R. Carey, J. Holland, H. Whang, E. Neter, and B. Bryant, "Clostridial oncolysis in man," *Eur J Cancer.,* vol. 3, pp. 37-42, 1967.

[79] I. Cheong, X. Huang, C. Bettegowda, L. A. J. Diaz, K. W. Kinzler, S. Zhou, and B. Vogelstein, "A bacterial protein enhances the release and efficacy of liposomal cancer drugs," *Science,* vol. 314, pp. 1308-1311, 2006.

[80] M. Q. Wei, K. A. O. Ellem, P. Dunn, M. J. West, C. X. Bai, and B. Vogelstein, "Facultative or obligate anaerobic bacteria have the potential for multimodality therapy of solid tumours," *Eur J Cancer.,* vol. 43, pp. 490-6, 2007.

[81] J. F. Toso, V. J. Gill, P. Hwu, F. M. Marincola, N. P. Restifo, D. J. Schwartzentruber, R. M. Sherry, S. L. Topalian, J. C. Yang, F. Stock, L. J. Freezer, K. E. Morton, C. Seipp, L. Haworth, S. Mavroukakis, D. White, S. MacDonald, J. Mao, M. Sznol, and S. A. Rosenberg, "Phase I study of the intravenous administration of attenuated Salmonella typhimurium to patients with metastatic melanoma," *J Clin Oncol.,* vol. 20, pp. 142-52, 2002.

[82] R. Blakemore, "Magnetotactic bacteria," *Science,* vol. 190, pp. 377-379, 1975.

[83] R. B. Frankel, "Magnetic guidance of organisms," *Annual review of biophysics and bioengineering,* vol. 13, pp. 85-103, 1984.

[84] D. Schuler, "Formation of Magnetosomes in Magnetotactic Bacteria," *J. Molec. Microbiol. Biotechnol.,* vol. 1, pp. 79-86, 1999.

[85] M. Arnoldi, C. M. Kacher, E. Bäuerlein, M. Radmacher, and M. Fritz, "Elastic properties of the cell wall of Magnetospirillum gryphiswaldense investigated by atomic force microscopy," *Applied Physics A: Materials Science & Processing,* vol. 66, pp. S613-S617, 1998.

[86] A. S. Bahaj, P. A. B. James, and I. W. Croudace, "Metal uptake and separation using magnetotactic bacteria," *IEEE Transactions on Magnetics,* vol. 30, pp. 4707-4709, 1994.

[87] S. Seong and T. H. Park, "Swimming characteristics of magnetic bacterium, Magnetospirillum sp. AMB-1, and implications as toxicity measurement," *Biotechnology and Bioengineering,* vol. 76, pp. 11-16, 2001.

[88] S. Spring and D. A. Bazylinski, "Ecophysiology and Biochemistry," in *The Prokaryotes, Volume 2*, S. N. York, Ed., ed, 2006, pp. 842-862.

[89] L. Yanli, G. Meiying, D. Shunying, P. Kefang, and J. Rongfen, "Characterization of magnetotactic bacteria and their magnetosomes isolated from Tieshan iron ore in Hubei Province of China," *Materials Science and Engineering,* vol. 26, pp. 597-601, 2006.

[90] W. André and S. Martel, "Micro-photovoltaic cells designed for magnetotaxis-based controlled bacterial microrobots," *Transactions of the Institute of Electronics, Information and Communication Engineers (IEICE),* vol. 5, pp. 101-106, 2008.

[91] M. R. Benoit, D. Mayer, Y. Barak, I. Y. Chen, W. Hu, Z. Cheng, S. X. Wang, D. M. Spielman, S. S. Gambhir, and A. Matin, "Visualizing Implanted Tumors in Mice with Magnetic Resonance Imaging Using Magnetotactic Bacteria," *Clin Cancer Res,* vol. 15, pp. 5170-5177, 2009.

[92] P. Yongxin, W. Lin, L. Jinhua, T. Lanxiang, D. Chenglong, L. Qingsong, Z. Rixiang, M. Winklhofer, and N. Petersen., "Reduced Efficiency of Magnetotaxis in Magnetotactic Coccoid Bacteria in Higher than Geomagnetic Fields," *Biophysical Journal,* vol. 97, pp. 986-991, 2009.

[93] J. Wittborn, K. V. Rao, R. Proksch, I. Revenko, E. D. Dahlberg, and D. A. Bazylinski, "Magnetization reversal observation and manipulation of chains of nanoscale magnetic particles using the magnetic force microscope," *Nanostructured Materials,* vol. 12, pp. 1149-1152, 1999.

[94] M. Greenberg, K. Canter, I. Mahler, and A. Tornheim, "Observation of magnetoreceptive behavior in a multicellular magnetotactic prokaryote in higher than geomagnetic fields," *Biophysical Journal,* vol. 88, pp. 1496-1499, 2005.

[95] I. S. Jacobs and C. P. Bean, "An approach to elongated fine-particle magnets," *Physical Review E,* vol. 100, pp. 1060-1067, 1955.

[96] F. S. Nogueira and H. G. P. Lins de Barros, "Study of the motion of magnetotactic bacteria," *Eur. Biophys. J. Biophys. Lett. ,* vol. 90, pp. 400-412, 1995.

[97] T. Van, U. Zimmermann, and H. Löwen, "Clockwise-directional circle swimmer moves counter-clockwise in Petri dish- and ring-like confinements," *Soft Matter.,* vol. 5, pp. 4510-4519, 2009.

[98] E. Lauga, W. R. DiLuzio, W. G. M., and H. A. Stone, "Swimming in circles: motion of bacteria near solid boundaries," *Biophysical Journal,* vol. 90, pp. 400-412, 2006.

[99] W. R. DiLuzio, L. Tuner, M. M., P. Garstecki, W. D. B., H. C. Berg, and G. M. Whitesides, "Escherichia coli swim on the right-hand side," *Nature,* vol. 435, pp. 1271-1274, 2005.

[100] R. B. Frankel, D. A. Bazylinski, M. S. Johnson, and B. L. Taylor, "Magneto-aerotaxis in marine coccoid bacteria," *Biophysical Journal,* vol. 73, pp. 994-1000, 1997.

[101] O. Felfoul and S. Martel, "Tracking magnetotactic bacteria using an MRI system for future in-vivo therapeutic targeting," presented at the International Society of Magnetic Resonance in Medicine Annual Meeting Proceedings (ISMRM), 2008.

[102] K. S. Rhode, M. Sermesant, D. Brogan, S. Hegde, J. Hipwell, P. Lambiase, E. Rosenthal, C. Bucknall, S. A. Qureshi, J. S. Gill, R. Razavi, and D. L. Hill, "A system for real-time XMR guided cardiovascular intervention," *IEEE transaction on medical imaging,* vol. 31, pp. 1428-1440, 2005.

[103] G. Harasko, H. Pfutzner, and K. Futschik, "Domain analysis by means of magnetotactic bacteria," *IEEE Transactions on Magnetics,* vol. 31, pp. 938-949, 1995.

[104] A. Cebers and M. Ozols, "Dynamics of an active magnetic particle in a rotating magnetic field," *Physical Review E (Statistical, Nonlinear, and Soft Matter Physics),* vol. 73, pp. 21505-1-5, 2006.

[105] Y. Yoshida, S. Fukui, S. Fujimoto, F. Mishima, S. Takeda, Y. Izumi, S. Ohtani, Y. Fujitani, and S. Nishijima, "Ex vivo investigation of magnetically targeted drug delivery system," *Journal of Magnetism and Magnetic Materials,* vol. 310, pp. 2880-2882, 2007.

[106] B. Gleich, N. Hellwig, H. Bridell, R. Jurgons, C. Seliger, C. Alexiou, B. Wolf, and T. Weyh, "Design and evaluation of magnetic fields for nanoparticle drug targeting in cancer," *IEEE Transactions on Nanotechnology,* vol. 6, pp. 164-170, 2007.

[107] N. S. Forbes, L. L. Munn, D. Fukumura, and R. K. Jain, "Sparse Initial Entrapment of Systemically Injected Salmonella typhimurium Leads to Heterogeneous Accumulation within Tumors," *Cancer Research,* vol. 63, pp. 5188-5193, September 1, 2003 2003.

[108] R. K. Jain, "Delivery of molecular and cellular medicine to solid tumors," *Journal of Controlled Release,* vol. 53, p. 49, 1998.

[109] P. Vaupel, F. Kallinowski, and P. Okunieff, "Blood flow, oxygen and nutrient supply, and metabolic microenvironment of human tumors: A review," *Cancer Res.,* vol. 49, pp. 6449–6465, 1989.

[110] R. K. Jain, "Barriers to drug delivery in solid tumors," *Sci. Am,* vol. 271, pp. 58–65, 1994.

[111] R. K. Jain, "Transport phenomena in tumors," *Adv. Chem. Eng.,* vol. 20, pp. 129–200, 1994.

[112] G. Helmlinger, F. Yuan, M. Dellian, and R. K. Jain, "Interstitial pH and pO2 gradients in solid tumors in vivo: High-resolution measurements reveal a lack of correlation," *Nature Medecine,* vol. 3, pp. 177–182., 1997.

[113] A. T. St Jean, M. Zhang, and N. S. Forbes, "Bacterial therapies: completing the cancer treatment toolbox," *Current Opinion in Biotechnology,* vol. 19, pp. 511-517, 2008.

[114] M. J. Kim and K. S. Breuer, "Microfluidic pump powered by self-organizing bacteria," *Small,* vol. 4, pp. 111-118, 2008.

[115] N. Darnton, L. Turner, K. Breuer, and H. C. Berg, "Moving fluid with bacterial carpets," *Biophysical Journal,* vol. 86, pp. 1863-1870, 2004.

[116] D. B. Weibel, P. Garstecki, D. Ryan, W. R. DiLuzio, M. Mayer, J. E. Seto, and G. M. Whitesides, "Microoxen: Microorganisms to move microscale loads," *Proceedings of the National Academy of Sciences,* vol. 102, pp. 11963-11967, 2005.

[117] Y. Hiratsuka, M. Miyata, T. Tada, and T. Q. P. Uyeda, "A microrotary motor powered by bacteria," *Proceedings of the National Academy of Sciences,* vol. 103, pp. 13618-13623, 2006.

[118] H. Debarros, D. M. S. Esquivel, and M. Farina, "Magnetotaxis," *Sci. Progr.,* vol. 74, pp. 347-359, 1990.

[119] E. Steager, C. B. Kim, J. Patel, S. Bith, C. Naik, L. Reber, and M. N. Kim, "Control of microfabricated structures powered by flagellated bacteria using phototaxis," *Applied Physics Letters,* vol. 90, pp. 263901-3, 2007.

[120] M. S. Sakar, E. B. Steager, A. A. Julius, V. M. K. Kumar, and G. J. Pappas, "Biosensing and actuation for microrobots," presented at the Int. Conf. on Robotics and Automation (ICRA), Anchorage, USA, 2010.

[121] S. Martel and M. Mohammadi, "Using a swarm of self-propelled natural microrobots in the form of flagellated bacteria to perform complex micro-assembly tasks," presented at the Int. Conf. on Robotics and Automation (ICRA), Anchorage, USA, 2010.

[122] C. F. G. C. Geraldes and S. Laurent, "Classification and basic properties of contrast agents for magnetic resonance imaging," *Contrast Media & Molecular Imaging,* vol. 4, pp. 1-23, 2009.

[123] M. S. Olson, R. M. Ford, J. A. Smith, and E. J. Fernandez, "Analysis of Column Tortuosity for MnCl2 and Bacterial Diffusion Using Magnetic Resonance Imaging," *Environmental Science & Technology,* vol. 39, pp. 149-154, 2004.

[124] É. Tóth, L. Helm, and A. Merbach, "Relaxivity of MRI Contrast Agents," in *Contrast Agents I*. vol. 221, W. Krause, Ed., ed: Springer Berlin / Heidelberg, 2002, pp. 61-101.

[125] K. A. Hinds, J. M. Hill, E. M. Shapiro, M. O. Laukkanen, A. C. Silva, C. A. Combs, T. R. Varney, R. S. Balaban, A. P. Koretsky, and C. E. Dunbar, "Highly efficient endosomal labeling of progenitor and stem cells with large magnetic particles allows magnetic resonance imaging of single cells," *Blood,* vol. 102, pp. 867-72, 2003.

[126] R. Kehlenbeck and R. D. Felice, "Empirical relationships for the terminal settling velocity of spheres in cylindrical columns," *Chemical Engineering and Technology,* vol. 22, pp. 303-308, 1999.

[127] V. Fidleris and R. L. Whitmore, "Experimental determination of the wall effect for spheres falling axially in cylindrical vessels," *British Journal of Applied Physics,* vol. 12, pp. 490-4, 1961.